

# **Advanced Test Reactor Core Modeling Update Project Annual Report for Fiscal Year 2010**

**Rahmat Aryaeinejad  
Douglas S. Crawford  
Mark D. DeHart  
George W. Griffith  
Brian J. Gross  
D. Scott Lucas  
Joseph W. Nielsen  
David W. Nigg  
Jorge Navarro  
James R. Parry  
Josh Peterson  
Kevin A. Steuhm  
David W. Nigg**

**September 2010**



The INL is a U.S. Department of Energy National Laboratory  
operated by Battelle Energy Alliance

# **Advanced Test Reactor Core Modeling Update Project Annual Report for Fiscal Year 2010**

Rahmat Aryaeinejad  
Douglas S. Crawford  
Mark D. DeHart  
George W. Griffith  
Brian J. Gross  
D. Scott Lucas  
Joseph W. Nielsen  
David W. Nigg  
Jorge Navarro  
James R. Parry  
Josh Peterson  
Kevin A. Steuhm  
David W. Nigg

**September 2010**

**Idaho National Laboratory  
Nuclear Science and Technology Directorate  
Idaho Falls, Idaho 83415**

**<http://www.inl.gov>**

**Prepared for the  
U.S. Department of Energy  
Office of Nuclear Energy  
Under DOE Idaho Operations Office  
Contract DE-AC07-05ID14517**

#### **DISCLAIMER**

This information was prepared as an account of work sponsored by an agency of the U.S. Government. Neither the U.S. Government nor any agency thereof, nor any of their employees, makes any warranty, expressed or implied, or assumes any legal liability or responsibility for the accuracy, completeness, or usefulness, of any information, apparatus, product, or process disclosed, or represents that its use would not infringe privately owned rights. References herein to any specific commercial product, process, or service by trade name, trade mark, manufacturer, or otherwise, does not necessarily constitute or imply its endorsement, recommendation, or favoring by the U.S. Government or any agency thereof. The views and opinions of authors expressed herein do not necessarily state or reflect those of the U.S. Government or any agency thereof.



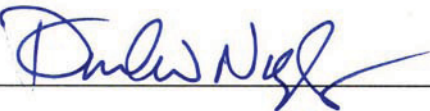


**Nuclear Science and Technology Directorate**

**Advanced Test Reactor Core Modeling Update Project  
Annual Report for Fiscal Year 2010**

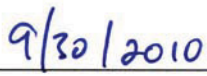
**INL/EXT-19940  
September 2010**

**Approved by:**



---

David W. Nigg  
Principal Investigator



---

September 30, 2010



## SUMMARY

Legacy computational reactor physics software tools and protocols currently used for support of Advanced Test Reactor (ATR) core fuel management and safety assurance and, to some extent, experiment management are obsolete, inconsistent with the state of modern nuclear engineering practice, and are becoming increasingly difficult to properly verify and validate (V&V). Furthermore, the legacy staff knowledge required for application of these tools and protocols from the 1960s and 1970s is rapidly being lost due to staff turnover and retirements. In 2009 the Idaho National Laboratory (INL) initiated a focused effort to address this situation through the introduction of modern high-fidelity computational software and protocols, with appropriate V&V, within the next 3-4 years via the ATR Core Modeling and Simulation and V&V Update (or “Core Modeling Update”) Project. This aggressive computational and experimental campaign will have a broad strategic impact on the operation of the ATR, both in terms of improved computational efficiency and accuracy for support of ongoing DOE programs as well as in terms of national and international recognition of the ATR National Scientific User Facility (NSUF).

The ATR Core Modeling Update Project, targeted for full implementation in phase with the anticipated ATR Core Internals Changeout (CIC) in the 2014 time frame, began during the last quarter of Fiscal Year 2009, and has just completed its first full year. Key accomplishments so far have encompassed both computational as well as experimental work. A new suite of stochastic and deterministic transport theory based reactor physics codes and their supporting nuclear data libraries (SCALE, KENO-6, HELIOS, NEWT, and ATTILA) have been installed at the INL under various permanent sitewide license agreements and corresponding baseline models of the ATR and ATRC are now operational, demonstrating the basic feasibility of these code packages for their intended purpose. Furthermore, a capability for rigorous sensitivity analysis and uncertainty quantification based on the TSUNAMI system is being implemented and initial computational results have been obtained. This capability will have many applications in 2011 and beyond as a tool for understanding the margins of uncertainty in the new models as well as for validation experiment design and interpretation.

On the experimental side, new hardware was fabricated, measurement protocols were approved, and the first two of several planned sets of flux validation measurements based on neutron activation spectrometry were then conducted at the ATRC facility in collaboration with a separate online reactor instrumentation evaluation project associated with the ATR NSUF. These measurements will continue through much of 2011, and will include the fabrication and introduction of additional new experimental hardware to broaden the scope of the planned validation protocols. Further opportunities to collaborate with various planned experimental campaigns in the ATRC and ATR will be identified as the Core Modeling Update Project proceeds, with a particular emphasis on collaboration with U-Mo fuel qualification experiments being conducted in connection with the DOE Reduced Enrichment for Research and Training Reactors (RERTR) Program. Such opportunities are expected to include RERTR-related experiments in the ATRC and possibly a so-called “depressurized” low-power run of the ATR itself.

A second component of the experimental validation campaign involves the possible construction of a system for non-invasive measurement of the burnup of ATR fuel elements *in-situ* in the ATR canal. Post-irradiation ATR fuel burnup measurements will serve as a key fuel depletion model validation tool and also as an aid in improved fuel management. Initial in-canal feasibility measurements to identify appropriate engineering parameters and radiation measurement instrumentation for such a system were completed in June 2010. These studies have already produced some original scientific results, publishable in the pertinent refereed literature. Data analysis will continue through the first part of 2011. A proposal for construction of a permanent system will be then prepared and transmitted to the Department of Energy for consideration.

It is also important to recognize that the ATR Core Modeling Update Project represents not only an investment in new technology. It also represents a key investment in people – an investment in the new generation of INL scientific and engineering staff who will, by demographic necessity, assume leadership roles in the overall ATR enterprise over the next several years. Accordingly, several students and early-career INL Scientific and Engineering staff members are being proactively integrated into the effort and this will accelerate in 2011 and beyond. In addition, we also significantly augmented our senior staff capabilities in computational reactor physics for ATR via two external new hires.

Finally we note that although full implementation of the new computational models and protocols will extend over a period 3-4 years as noted above, interim applications in the much nearer term have already been demonstrated. In particular, these demonstrations included an analysis that was useful for understanding the cause of some issues in December 2009 that were triggered by a larger than acceptable discrepancy between the measured excess core reactivity and a calculated value that was based on the legacy computational methods. As the Modeling Update project proceeds we anticipate further such interim, informal, applications in parallel with formal qualification of the system under the applicable INL Quality Assurance procedures and standards.

# CONTENTS

SUMMARY,.....	v
ACRONYMS .....	viii
1.0 INTRODUCTION .....	1
2.0 HIGH-FIDELITY TRANSPORT THEORY MODELS OF THE ATR .....	11
3.0 HIGH-FIDELITY TRANSPORT THEORY MODELS OF THE ATRC .....	52
4.0 VALIDATION EXPERIMENTS IN THE ATRC.....	68
5.0 FEASIBILITY TESTING FOR ATR FUEL BURNUP MEASUREMENT SYSTEM .....	86
6.0 REFERENCES .....	115

## ACRONYMS

AGR	Advanced Gas Reactor
ATR	Advanced Test Reactor
CFD	Computational Fluid Dynamics
CIC	Core Internals Changeout
CSAP	Core Safety Assurance Package
ENDF	Evaluated Nuclear Data File
NST	Nuclear Science and Technology
NSUF	National Scientific User Facility
RERTR	Reduced Enrichment for Research and Test Reactors
V&V	Verification and Validation

## 1.0 INTRODUCTION

This report documents the accomplishments of the ATR Core Modeling, Simulation and V&V Update (or “ATR Core Modeling Update”) Project during the Fiscal Year 2010. This section provides a brief overview of the background, rationale, organizational structure, and a basic summary of progress to-date for the project. Later sections cover additional detail on specific technical accomplishments during the year.

### 1.1 Description of the Advanced Test Reactor

The Advanced Test Reactor (ATR), located at the Idaho National Laboratory (INL), is one of only a few high-power research reactors of its type in the world, with a variety of missions involving accelerated testing of nuclear fuel and other materials in a very high neutron flux environment, medical and industrial isotope production, and other applications. Along with its companion critical mockup (ATRC), the ATR is one of the key nuclear engineering research and testing facilities within the US Department of Energy (DOE) National Laboratory Complex. The ATR and ATRC also serve as the centerpieces of the recently-formed ATR National Scientific User Facility (NSUF), whose purpose is to facilitate the current trend toward broadening the applications of the ATR beyond its traditional base.

The ATR (Figures 1-1 and 1-2) is a highly-heterogeneous light-water and beryllium moderated, beryllium reflected, light-water cooled system with fully enriched (93%  $^{235}\text{U}$ ) plate-type fuel elements arranged in a serpentine pattern. Gross reactivity and power distribution control during operation is achieved through the use of eight pairs of rotating control drums with hafnium neutron absorber plates on one side as can be seen in Figure 1. There are several design features incorporated into the ATR core and hence the ATRC core (Figures 1-3 and 1-4) as well, to optimize experimental capabilities. These features include, a) the use of flux traps to provide high thermal neutron fluxes for irradiation or experiments in nine regions, b) incorporation of special control shim design to retain axial flux symmetry throughout an ATR fuel cycle; and c) regional power control to provide capability for power shifting between core lobes and thereby optimize neutron flux for a wide range of simultaneous uses, studies and experiments. The ATR can be operated at powers as high as 250 MW although most routine applications do not require the maximum power. Typical thermal neutron fluxes in the flux traps can be as high as  $5.0 \times 10^{14}$  n/cm<sup>2</sup>-s. Typical operating cycle lengths are in the range of 45–60 days. The core fuel configuration and the experiment loadings are usually rearranged between cycles and each fuel element is typically burned for two or three cycles during its useful lifetime.

The ATRC core is an open-pool nuclear mock-up of the ATR core that typically operates at approximately 600 W, producing a thermal neutron flux in the traps that is in the range of  $1.0 \times 10^9$  n/cm<sup>2</sup>-s. As is the case for the ATR itself, the core consists of a 4-ft-high (122 cm), uniform-width, vertical 40-element fuel annulus shaped in a serpentine fashion between and around nine flux-trap areas located in a three-by-three square array. The cruciform fixture inside the serpentine is called the neck shim housing. The reactivity of the core is controlled by: (a) five vertically withdrawn safety rods that use cadmium as the poison material; (b) 24 vertically withdrawn hafnium neck shim rods; and (c) eight pairs of rotating outer shim control cylinders (OSCCs) that use hafnium poison plates.

ATRC criticality can normally be stably attained at a power as low as 0.25 mW and the maximum rated power is in the range of 5 kW. The ATRC facility is typically used with prototype experiments to characterize in advance, with precision and accuracy, the expected changes in core reactivity to be expected for the same experiments in the ATR. Useful physics data can also be obtained for evaluating the worth and calibration of control elements as well as thermal and fast neutron distributions.

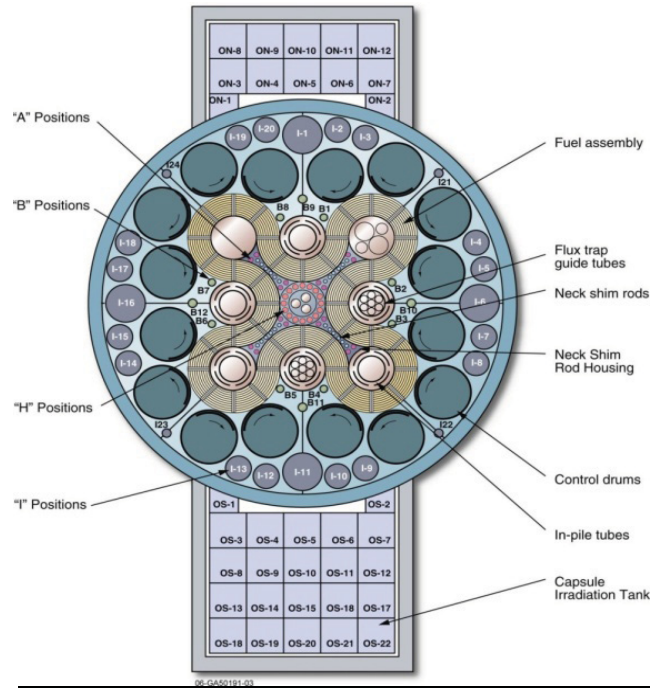


Figure 1-1. Core and reflector geometry of the Advanced Test Reactor.

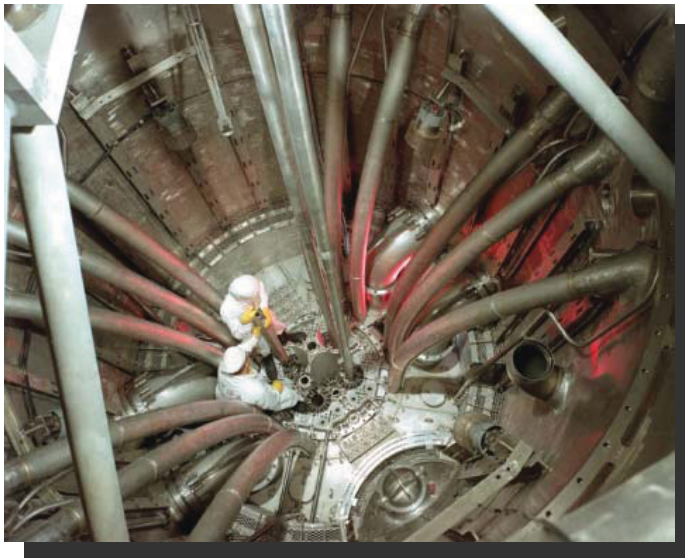


Figure 1-2. View into the ATR pressure vessel.



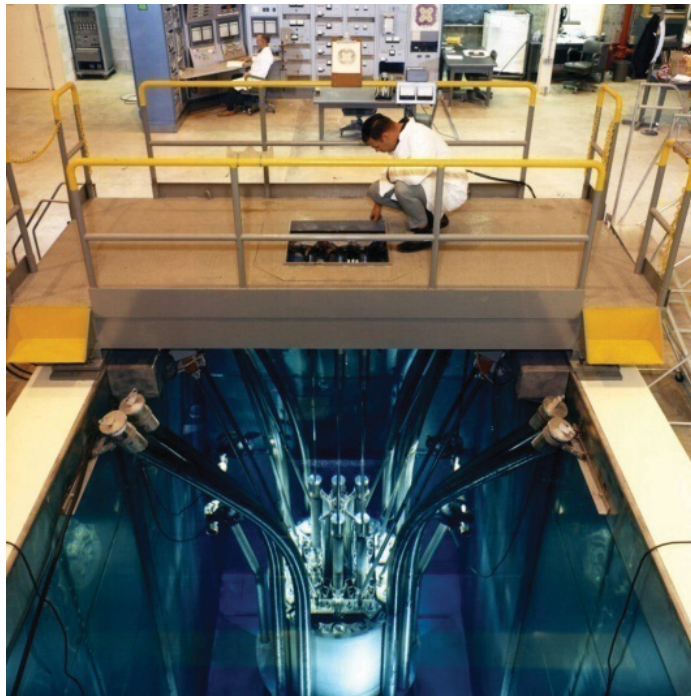


Figure 1-3. The Advanced Test Reactor Critical Facility.

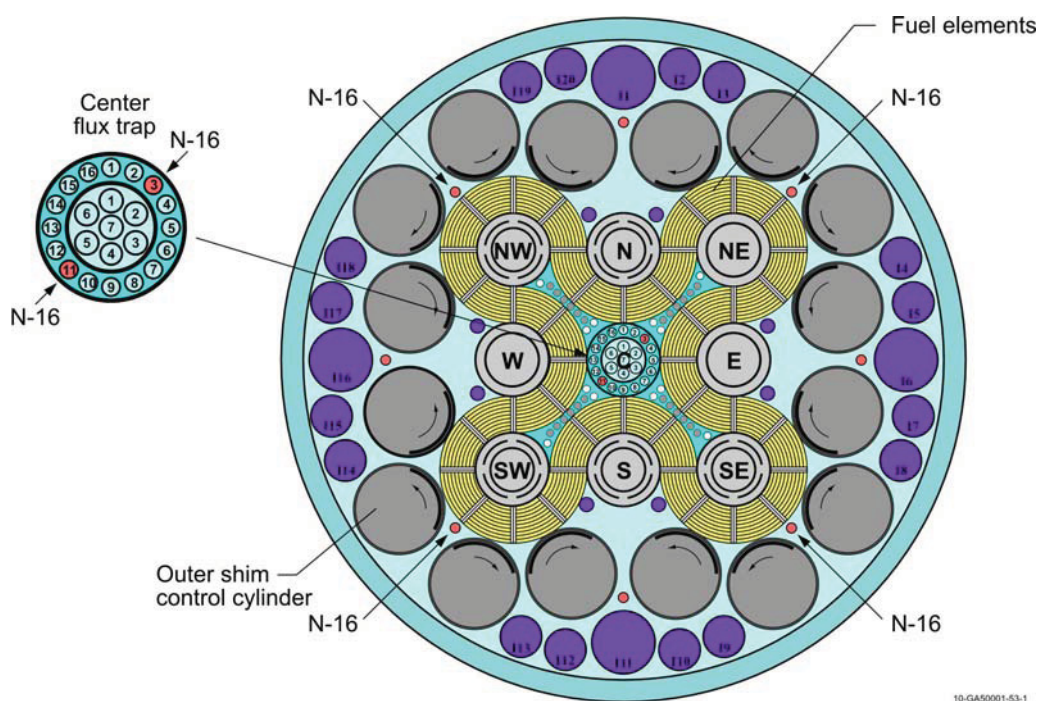


Figure 1-4. ATRC Configuration, showing the NW LIPT Flux Trap and six N-16 positions.

## 1.2 Rationale for the ATR Core Modeling Update Project

Computational reactor physics modeling is used extensively to support ATR experiment design, operations and fuel cycle management, core and experiment safety analysis, and many other applications. Experiment design and analysis for the ATR is generally supported by very detailed and sophisticated three-dimensional Monte Carlo analysis, typically using the internationally-recognized continuous-energy MCNP code (Goorley et al., 2004) coupled to extensive fuel isotope buildup and depletion analysis where appropriate. On the other hand, the legacy computational reactor physics software tools and protocols currently used for ATR core fuel cycle analysis and operational support, largely based on four-group diffusion theory in Cartesian geometry (Pfeifer et al., 1971) with heavy reliance on “tuned” nuclear parameter input data, are obsolete and have been superseded in the general reactor physics community by much higher-order multidimensional transport-theory-based methods in many cases. As a result the historical approach to ATR reactor physics operational support is inconsistent with the state of modern nuclear engineering practice and nearly impossible to properly verify and validate (V&V) according to modern standards. Furthermore, some aspects of the analysis process are highly empirical in nature, with many “correction factors” and approximations that require very specialized experience to apply, and the legacy staff knowledge from the 1960s and 1970s that is essential for the successful application of the various computational processes is rapidly being lost due to staff turnover and retirements. Finally, future clients of the ATR NSUF are anticipated to be experienced in the use of modern computational methods available for nuclear systems modeling and are likely to expect corresponding computational support services within the NSUF infrastructure.

Figure 1-5 illustrates one of the challenges experienced recently with the legacy physics computational methods used for ATR operational support. A fueled experiment associated with the DOE Next Generation Nuclear Plant Advanced Gas Reactor development program was scheduled for irradiation in the south flux trap of the ATR as shown. However, uncertainties in the supporting computations were such that it was not possible to determine the neutronics effects of this experiment on neighboring flux traps to what was considered to be sufficient accuracy, and the operational margins of conservatism that were thereby required caused the experiment to be delayed until a later ATR cycle, at significant expense. In a second example of the impact of uncertainty in the current computational methods, it may also be noted that there were some issues in December 2009 triggered by a larger than acceptable discrepancy between the calculated and measured excess core reactivity. These issues were resolved via standard procedures, but schedules were adversely impacted and the root cause was largely traced to problems with the legacy computational model of an experiment in the central flux trap.

Continued successful operation of the ATR is thus dependent, in part, on the proactive introduction of modern higher-fidelity computational software and protocols, with appropriate V&V, within the next 3-4 years via the ATR Core Modeling and Simulation and V&V Update (or “Core Modeling Update”) Project described in this report. This aggressive computational and experimental campaign will have a broad strategic impact on the operation of the ATR, both in terms of improved computational efficiency and accuracy for support of ongoing DOE programs as well as in terms of national and international recognition of the ATR NSUF. The new computational and V&V protocols will be broadly applicable across all programs that use the ATR and ATRC. The developmental effort is in fact already leveraged with several other INL projects including the ATR Life Extension Program (LEP), the DOE Reduced Enrichment for Research and Test Reactor (RERTR) initiative, and an INL collaboration with Idaho State University (ISU), the Atomic Energy Commission of France (CEA) and the National Atomic Energy Commission of Argentina (CNEA) to evaluate various options for in-core ATR and ATRC instrumentation upgrades under the auspices of the NSUF (Rempe et al., 2010).

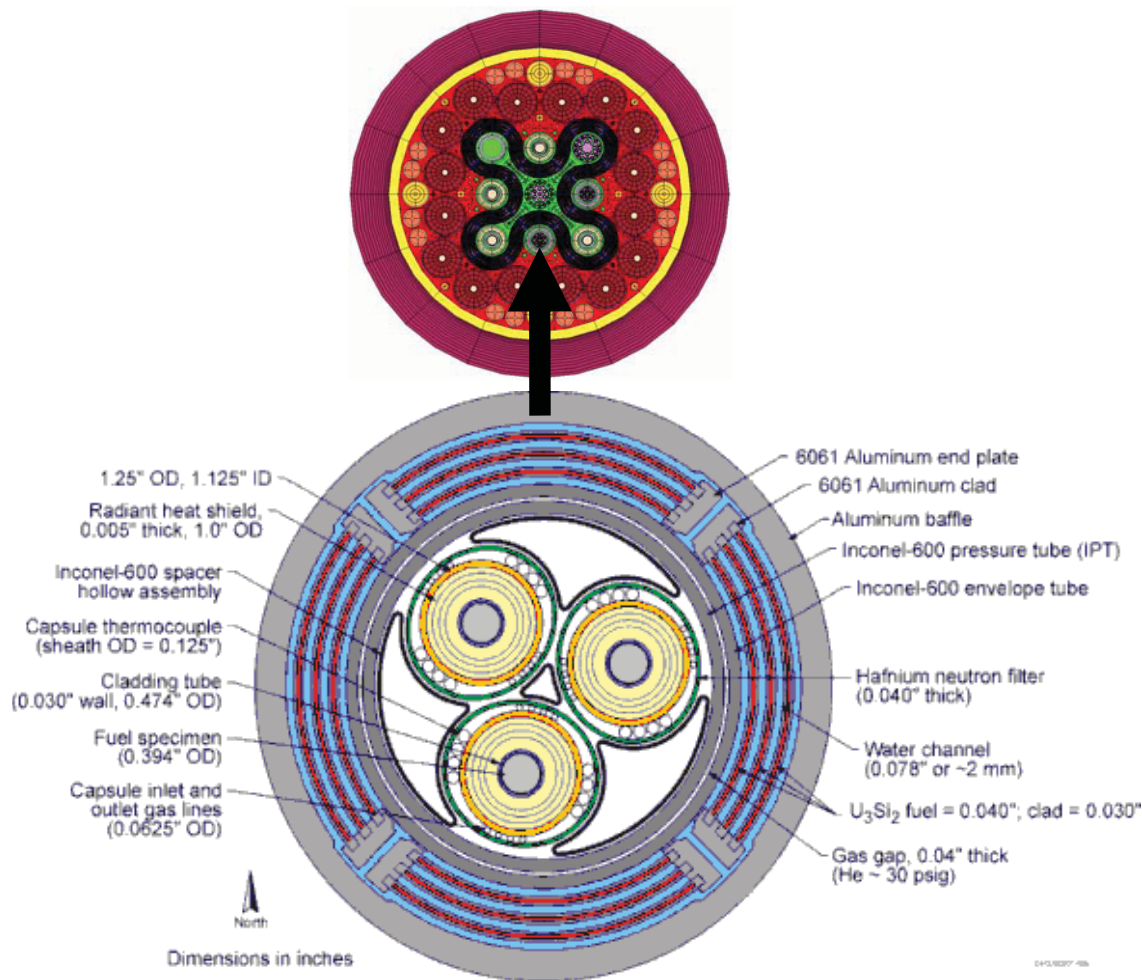


Figure 1-5. Gas Test Loop experiment designed for placement in the ATR south flux trap.

### 1.3 Technical Objectives of the Core Modeling Update Project

Prior to the initiation of the Core Modeling Update Project in late 2009 we were in fact already making significant efforts to modernize ATR reactor physics analysis capabilities using current standard software, and notable progress was made over the past several years in a few areas, especially for experiment design and analysis as noted earlier. However, this has largely been reactive, on an *ad-hoc* basis, not proactive, and several key tasks remain. These tasks include:

- Implementation of complementary, self-consistent multidimensional stochastic and deterministic neutron transport models of the ATR and ATRC cores using well-established and recognized science-based software packages consistent with current practice
- Standardized computational procedures and training, more easily transferred to new staff members

- Additional Verification & Validation, with development of standard apparatus and protocols for detailed neutron flux distribution and spectrum validation measurements in the core and selected flux traps that can be repeated on a regular basis. This also offers an opportunity to make much more effective use of ATRC both within the INL and as a key component of the National Scientific User Facility

Figure 1-6 shows the suite of new tools that will be available. It should be noted that this illustration is not a computational flow chart or procedure in and of itself. Specific computational protocols using the tools shown in Figure 1-6 for routine ATR support applications will be specified in approved procedures. These procedures will prescribe the geometric modeling input files, nuclear data files and other aspects of a specific computational protocol, for example performance of core-follow calculations for a particular ATR operational cycle.

The most recent release of the Evaluated Nuclear Data Files (ENDF/B Version 7) will be used for the most part to provide the basic cross section data and other nuclear parameters required for all of the modeling codes. The basic ENDF physical nuclear data files are processed into computationally-useful formats using the standard publically-available NJOY or AMPX (Radiation Safety Information Computational Center, 2010) codes as applicable to a particular module as shown at the top of the Figure.

As noted earlier, the MCNP three-dimensional stochastic simulation code is already used extensively for ATR experiment design and analysis and, to some limited extent, core analysis. Under the Core Modeling Update Project, we are also introducing the KENO stochastic simulation code (Hollenbach et al., 1996), primarily for detailed core analysis in connection with ongoing ATR and ATRC operations as well as for support of the possible conversion of the ATR (and presumably ATRC) to low-enrichment fuel (LEU) under the DOE RERTR Program. The KENO code is useful both as a stand-alone analysis and verification tool as well as in conjunction with the TSUNAMI (Broadhead et al., 2004, Williams et al., 2008) sensitivity-uncertainty analysis system available with the SCALE nuclear system analysis package (Bowman et al., 2009).

The right-hand side of Figure 1-6 shows the suite of new high-fidelity deterministic transport computational tools that are being integrated into the system. HELIOS (Studsvik Scandpower, 2008) and ATTILA (McGhee et al., 2006) are commercial grade software products now in place at the INL under permanent sitewide licenses. NEWT (DeHart, 2006) and its SCALE-based support infrastructure is a well-established and verified software tool suite developed within the DOE National Laboratory system. All three code packages have various strengths and weaknesses, but taken together they will provide the necessary high-fidelity neutron and gamma transport capability that is required for various aspects of ATR and ATRC core modeling as summarized in Figure 1-6 and described in much more detail in Sections 2 and 3 of this report.



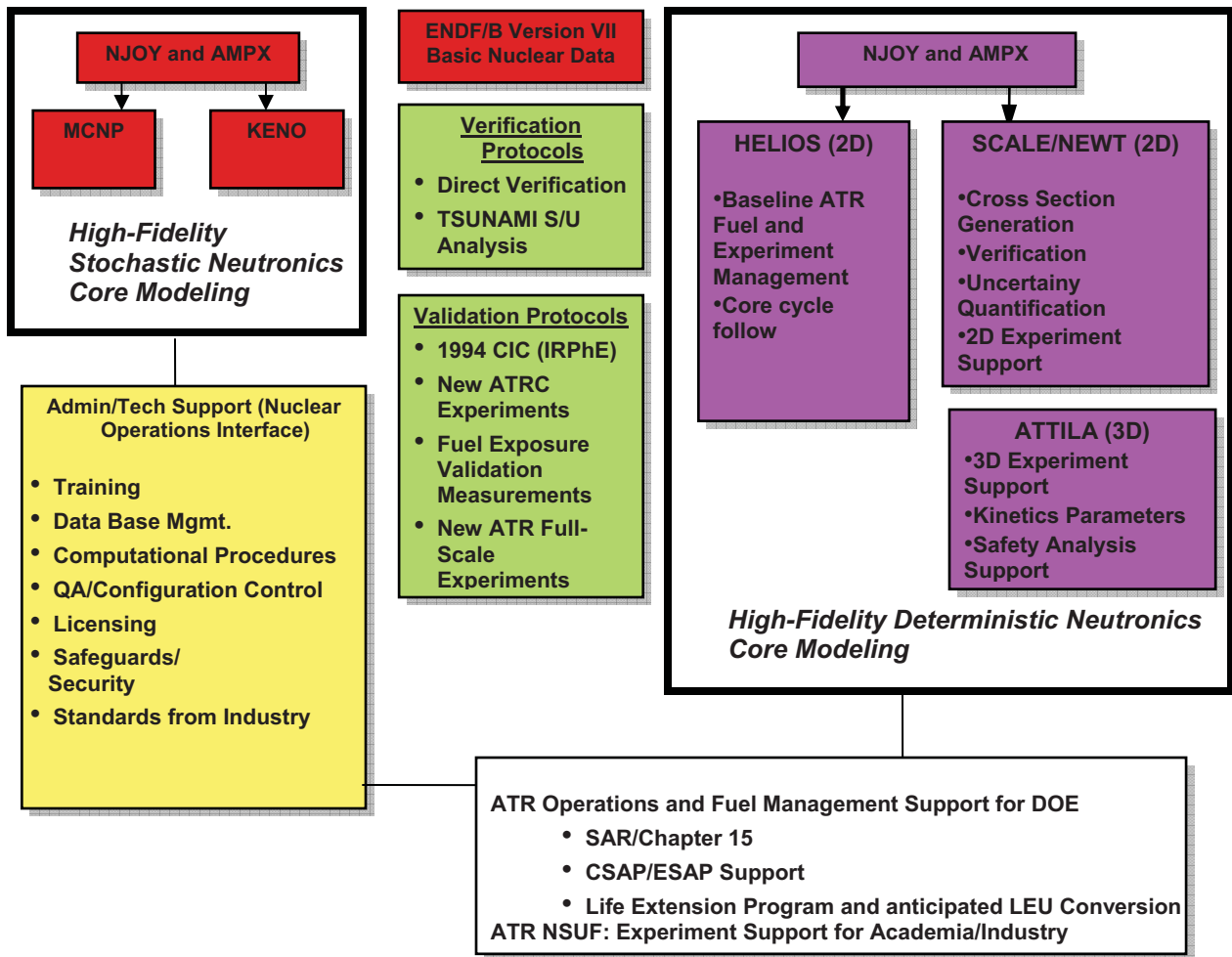


Figure 1-6. Advanced computational tool suite for the ATR and ATRC, with supporting verification, validation and administrative infrastructure.

As always, theory and experiment must be self-consistent in any scientific or engineering enterprise. The Core Modeling Update Project also includes several activities designed to incorporate historical validation data from earlier ATR and ATRC experiments as well as to develop new validation data specific to the new computational models and protocols. In particular, much of the initial model development has been based on a very well documented critical experiment conducted as part of the 1994 ATR Core Internals Changeout (CIC) activity (Kim and Schnitzler, 2008), as will be described in detail later. New core flux measurements in both ATRC and ATR are also planned. Section 4 of this report describes plans and accomplishments in this area during FY-2010. In addition, the Core Modeling Update Project includes a task described in Section 5 to develop non-invasive methods for post-irradiation measurement of exposure (or “burnup”) in ATR fuel elements, both as an aid in characterizing the existing inventory of used elements as well as to provide additional validation data for the new ATR core follow and fuel cycle design models.

## 1.4 Project Structure and Technical Team

The ATR Core Modeling Update project includes 5 technical tasks. It is largely organized and funded as a part of the larger ATR Life Extension Program (LEP), but additional support was provided by the RERTR project, reflecting the early importance of the new computational methods to that DOE program as well. The five tasks, which also provide the framework for the structure of this Annual Report, are as follows:

*Task 1: Project Management:* Includes sponsor/Collaborator interface maintenance, project documentation and planning, software licensing, travel, and university interfaces including student support.

*Task 2: ATR Model Development and V&V:* Includes development, verification, and validation of baseline KENO, HELIOS, NEWT and ATTILA models for current ATR reactor applications and to support the possible conversion of the ATR to LEU under the RERTR program. This includes fuel cycle management and neutronics support to core safety analysis, and limited development of capabilities for experiment analysis to the extent that experiment neutronics impacts the operation of the reactor overall. (Detailed ATR experiment design and analysis is ordinarily handled separately, as part of the workscope for each individual experiment series, and is not considered to be a part of the Core Modeling Update project *per se*). Details of FY-10 activities and accomplishments in connection with this task are reported in Section 2 of this Annual Report.

*Task 3: ATRC Model Development and V&V:* Includes development and application of baseline KENO, HELIOS, NEWT, and ATTILA models for support of ATRC validation experiments pertinent to the Core Modeling Update project as well as for the RERTR Program as it applies to the possible conversion of the ATR to LEU fuel. This task also largely includes the development and application of new capabilities for rigorous sensitivity studies pertinent to uncertainty quantification in the new computational models. Details of FY-10 activities and accomplishments in connection with this task are reported in Section 3 of this Annual Report.

*Task 4: Neutronics Validation Experiments:* This task includes the performance and reporting of new validation experiments in ATRC and ATR (as feasible) that are pertinent to quality assurance of the new computational models. It will support development of apparatus and protocols for a standard set of neutron activation spectrometry measurements that can be used on a more routine basis in the future for code validation as dictated by evolving ATR applications. This task also includes collaboration with various other DOE and NSUF projects where there is mutual benefit in terms of new physics validation data. Currently these include a project funded under the NSUF to investigate the feasibility of various techniques for online neutron flux measurements in the experiment positions as well as a near-term experiment involvement involving the testing of a prototype LEU ATR fuel element in the ATRC. Details of FY-10 activities and accomplishments in connection with this task are reported in Section 4 of this Annual Report.

*Task 5: In-Canal ATR Fuel Exposure Validation Measurements:* This task is focused on development of a non-invasive method and apparatus for measurement of burnup of used ATR fuel elements. The current workscope includes a series of scoping measurements conducted in FY-10, with ongoing data analysis through the first part of FY-11, and specification of a conceptual design for a permanent measurement system that can be installed in the canal. Final design, construction and qualification of a permanent system will then be formally proposed for inclusion in the long-term scope of the Core Modeling Update project. Details of FY-10 activities and accomplishments in connection with this task are reported in Section 5 of this Annual Report.

The leadership team for the ATR Core Modeling Update project consists of a Principal Investigator, a Project Manager, and several co-Investigators who are responsible for various key aspects of each task listed above. It is important to recognize that the ATR Core Modeling Update Project represents not only

an investment in new technology. It also represents a key investment in people – an investment in the new generation of INL scientific and engineering staff who will, by demographic necessity, assume leadership roles in the overall ATR enterprise over the next several years. Accordingly, several students and early-career INL Scientific and Engineering staff members are being proactively integrated into the effort, and this will accelerate in 2011 and beyond. The students supported by the project in 2010 included two from the University of Utah, one from the University of Idaho, and one from the University of Texas.

## **1.5 Overview of FY-2010 Accomplishments**

The Core Modeling Update Project is expected to require 48-50 months to complete, and is targeted for full implementation in phase with the anticipated ATR Core Internals Changeout (CIC) in the 2014 time frame. The project began during the last quarter of Fiscal Year 2009, and has just completed its first full year. Some key accomplishments in the first 14 months are briefly summarized below, along with a description of planned next steps in several areas during FY-2011 and beyond. Additional technical details are provided in the remainder of this Annual Report.

- Baseline HELIOS, NEWT, ATTILA, KENO, and MCNP models of ATR and ATRC are operational, demonstrating the basic feasibility of these code packages for their intended purpose.
- The initial demonstration-level HELIOS model of the ATR includes the capability to simulate fuel depletion and replacement, and informal cycle follow calculations beginning with Cycle 145A (August 2009 startup) have been initiated. These calculations will be continued and refined in 2011 with the objective of bringing the model current to the cycle being run at the end of that year. This will provide the basis for more formal acceptance testing and qualification of the core fuel cycle computational models and protocols in 2012 and beyond, with the goal of full documented and approved conversion to the new fuel cycle model in time to support the CIC that is anticipated in the 2014 time frame as noted.
- A capability for rigorous sensitivity analysis and uncertainty quantification is being implemented and initial computational results have been obtained. This capability will have many applications in 2011 and beyond as a tool for understanding the margins of uncertainty in the new models as well as for validation experiment design and interpretation.
- New experimental hardware was fabricated and measurement protocols were approved for the first planned set of flux validation measurements in the ATRC. The first irradiations of this series were then conducted in late September in collaboration with the NSUF Instrumentation Evaluation project mentioned earlier. These measurements will continue through much of 2011, with additional new experimental hardware being fabricated and introduced into the protocols along the way. Preparation for collaboration with the first RERTR ATR Full-Element experiment in the ATRC will also begin, and additional validation measurements will be done in connection with that experiment, currently scheduled for August 2011. Additional opportunities to collaborate with various planned experimental campaigns in the ATRC and ATR will be identified as the Core Modeling Update Project proceeds. Such opportunities are expected to include additional RERTR-related experiments in the ATRC and possibly a so-called “depressurized” low-power run of the ATR itself.
- In-canal feasibility measurements for construction of a permanent fuel burnup validation system were completed in June 2010. Results indicate that construction of a permanent measurement system is feasible. Data analysis for these measurements will continue through the first part of 2011 and conceptual design of a permanent system will be completed in early 2011. A proposal for construction of a permanent system (not funded under the Core Modeling Update Project as it

currently stands) will be then prepared and transmitted to the Department of Energy for consideration.

- Students and early-career INL Scientific and Engineering staff are being integrated into the effort as noted in the previous section. This will accelerate in 2011 and beyond for the reasons already noted.
- Support of possible ATR LEU fuel conversion under RERTR, using the new methods, has been initiated and a technical leader is in place. The recruitment of Dr. Mark DeHart, formerly of Oak Ridge National Lab, for this new position during 2010 was an unanticipated Strategic Hire, significantly augmenting our senior staff capabilities in computational reactor physics for ATR
- The formation of a collaboration with the ATR National Scientific User Facility and ISU instrumentation has allowed us to maintain momentum around the unanticipated delay (>1 year) of the first RERTR Full-Element (FE) test in ATRC, and still initiate new validation studies on schedule.
- In-Canal ATR experimental fuel element burnup measurement feasibility studies completed in FY-10 have already produced some original scientific results, and have served as a very useful model for how the INL R&D organization and the INL Nuclear Operations Organization can positively and proactively work safely and effectively together to accomplish the larger goals of the INL as a whole
- The adoption of the Studsvik Scandpower HELIOS code for ATR fuel cycle physics and fuel cycle analysis has significantly advanced the goals of the BEA Center for Nuclear Systems Design and Analysis, a formal collaboration between Studsvik and INL that was established in 2005 under the then-new INL Management and Operations Contract between Battelle Energy Alliance and the US Department of Energy.



## **2.0. HIGH-FIDELITY TRANSPORT THEORY MODELS OF THE ADVANCED TEST REACTOR**

This section documents the details of the various high-fidelity transport theory models being developed to support ATR operations and the possible conversion of the ATR to LEU fuel under the RERTR Program.

### **2.1 Baseline Validation Models for the 1994 Core Internals Changeout (CIC) Integral benchmark.**

The initial development of the HELIOS, NEWT and ATTILA models of the ATR has been based on the 1994 CIC integral benchmark (Kim et al., 2008). This benchmark features a core composed of 40 new fuel elements, with a well-documented geometric and material configuration and a variety of reported physics measurements, including the associated experimental uncertainties. Although additional validation measurements are being conducted under the Core Modeling Update Project, the 1994 CIC benchmark will continue to be a primary resource for validation.

#### **2.1.1 HELIOS Model of the ATR**

HELIOS is a 2-D lattice physics code developed by Studsvik Scandpower that has been applied to a number of different reactor types, with an emphasis on light-water moderated systems having essentially any geometry. The solution method uses current coupling collision probabilities (CCCP) or the Method of Characteristics (MOC) to solve the neutron transport equation with minimal geometric approximation. Commercial and research reactors have been modeled. There is a large collection of verified and validated benchmark cases for HELIOS. HELIOS is used to generate cross sections, flux, power generation, fuel exposure and other reactor physics calculations pertinent to core design as well as operational support and safety analysis. HELIOS also can be used to calculate the resonance and geometric self shielded microscopic cross sections needed for additional reactor calculation codes.

An infinite homogeneous flux calculation with resonance absorbers is calculated as part of the base calculation in HELIOS. The cross sections without geometric effects, i.e. based on an infinite homogeneous approximation, are first calculated and then the fluxes in the system as a whole including the effects of heterogeneous shielding are calculated. The critical flux values are then calculated including the up scattering terms. The fluxes are used to define fuel power, isotopic depletion and buildup and safety parameters.

##### ***2.1.1.1 HELIOS ATR Model Overview***

An initial model of the ATR 1994 CIC configuration (Figure 2-1) was developed in previous work by Studsvik Scandpower and INL in collaboration under the auspices of the INL Center for Nuclear Systems Design and Analysis. The base model thus reflects a well-defined critical configuration at the time of the most recent measurements for which reliable and publically-available benchmark data have been published (Kim et al., 2008). The input files for the 1994 CIC model were therefore used as the starting point for the ATR Core Modelling Update activities. Multiple updates have added significantly to the code's useful computations and made the HELIOS capable of providing initial core calculations for the current ATR configuration and fuel cycle protocols.

### 2.1.1.2 HELIOS ATR Model Results

The first results, from running the initial 1994 CIC input files, were evaluated compared to both NEWT and MCNP results. The results successfully demonstrated reasonable eigenvalues ( $k_{\text{eff}} = 1.0306$ , no axial leakage,  $k_{\text{eff}} = 0.9967$  critical axial leakage) and reasonable relative fuel element and plate power distributions (Figures 2-2 and 2-3). The results were also consistent with previous MCNP calculations. The results from the ATR model were also benchmarked against results from startup measurements, NEWT, and ATTILA calculations. The HELIOS execution time for a single exposure time step was approximately 15 minutes on a standard INL desktop computer system running under LINUX. This is a very acceptable execution time for routine fuel management calculations performed for each ATR cycle.

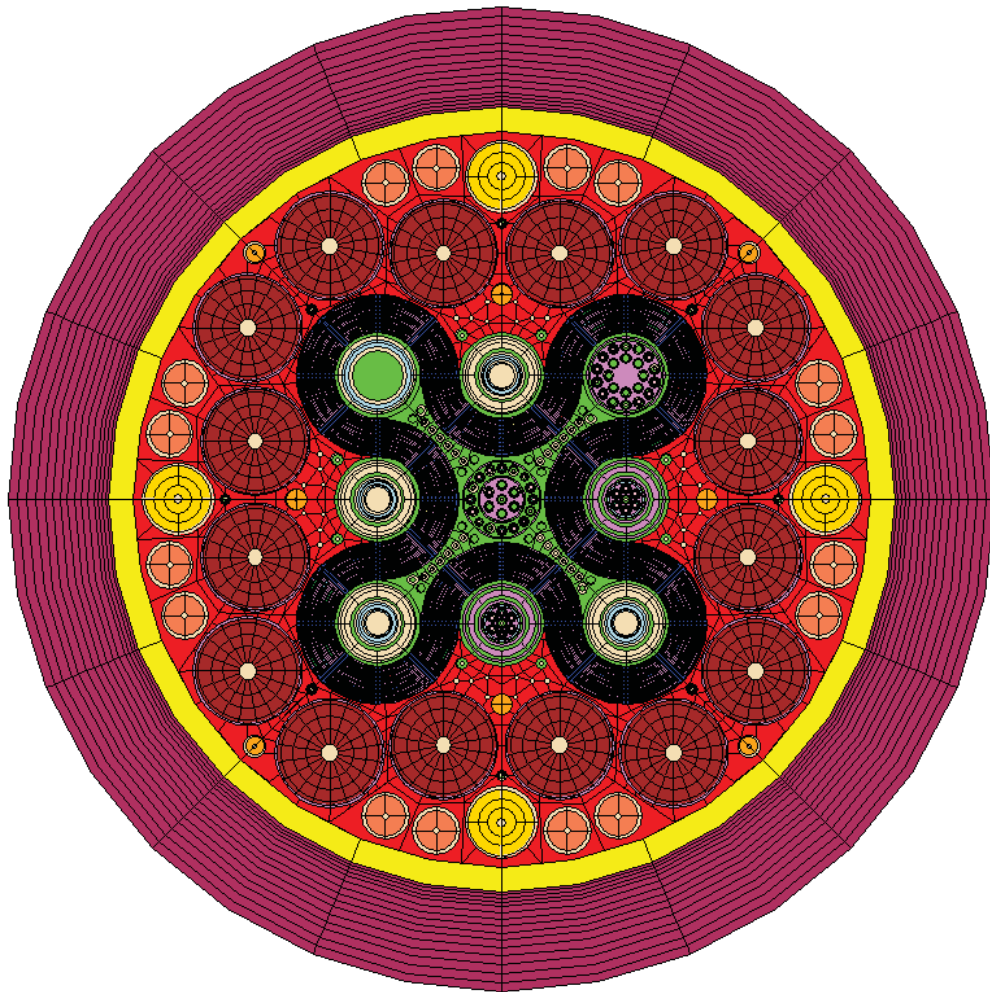


Figure 2-1. HELIOS ATR model geometry - 1994 CIC.

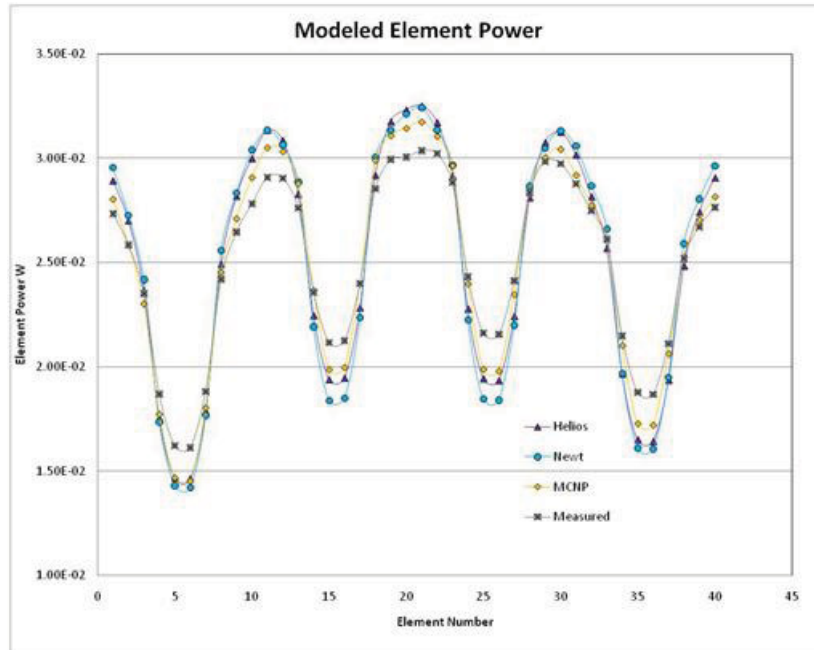


Figure 1-2. Relative Assembly Powers in HELIOS ATR Model.

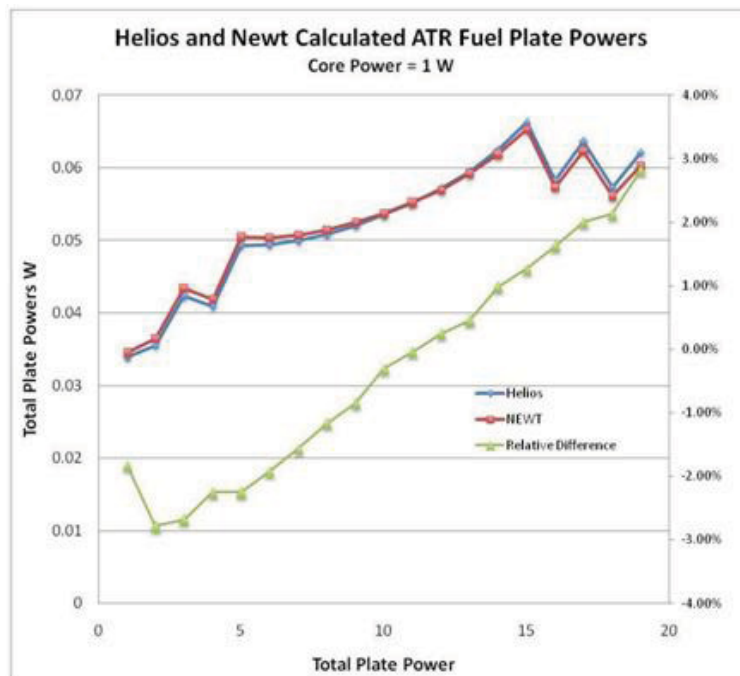


Figure 2-3. Average Relative Plate Powers for the HELIOS ATR Model.

The radial plate-to-plate power profiles computed by HELIOS are in very close agreement with results from other codes. The azimuthal, or element to element, profiles differ more significantly. The differences appear to be tied to small differences in the control shim/drum position models. The ATR model azimuthal power distribution is observed to be very sensitive to shim position in each of the models.

The base 1994 CIC input files were used to add the necessary details to make the HELIOS model useful for core follow (burnup) calculations. The modified input file and the HELIOS code can also produce flux-weighted cross sections in energy group structures suitable for ATTILA. Individual fuel plate and fuel assembly power edits were created adding a new capability to the model required to demonstrate the potential to perform necessary fuel cycle and operational support calculations for the ATR.

### ***2.1.1.3 Addition of Individual Fuel Element and Plate Power Edits***

The initial ATR core model for the 94 CIC had a single fresh 7F fuel element type repeated throughout the core. To support core fuel cycle management, safety analysis and core follow calculations, individual fuel element specifications were assigned to each of the 40 fuel positions in the core. This allows different types of fuel with a continuum of exposures to be tracked as well as allowing multiple assembly types to be used in the same core.

Additional detail in the fuel element calculations includes tracking the fluxes and interaction rates in each of the individual fuel plates in each element (Figure 2-4). The properties of the fuel isotope vectors, separate from the structural plate cladding, are tracked as uranium is burned out while generating fission products. The build up of the modest plutonium and higher actinide content is also tracked. The power production in each plate at each exposure point can be tracked.

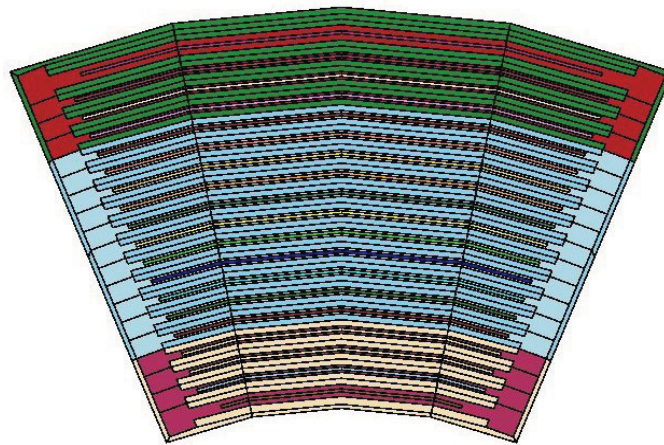


Figure 2-2. HELIOS ATR Fuel Assembly Model

#### 2.1.1.4 Addition of Variable Control Drum and Neck Shim Positioning

Modeling the ATR core over an entire cycle requires an accurate representation of the reactivity control structures that move during the cycle to balance the changing reactor properties. The initial model included changing control drum positions in increments of five degrees through changing materials in control drum structures. These coarse reactivity control changes are shown in Figure 2-5.

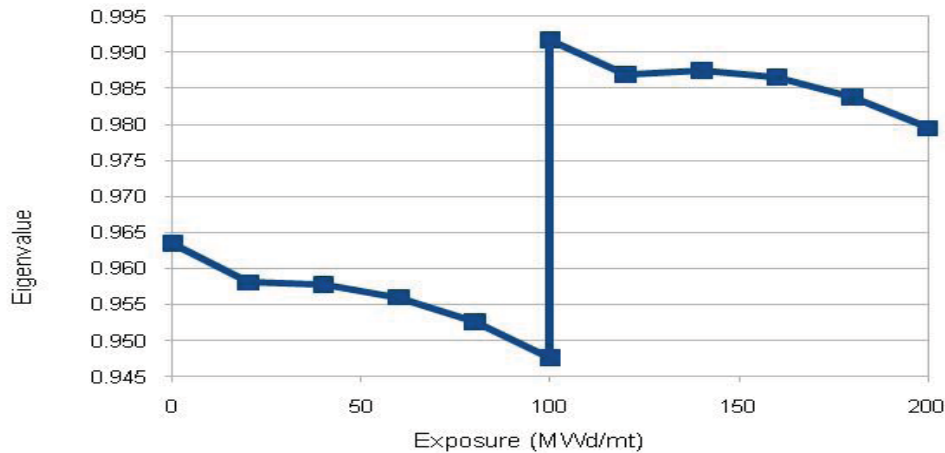


Figure 2-5. ATR cycle eigenvalues for a simple 1994 CIC test case that models increasing exposure and a single control drum rotation at 100 MWd/MTU.

Updating the ATR core model input file allows for the control drum structure to be rotated by exact angular values. The finer resolution of motion allows more accurate drum positioning and reactivity control. This is shown in Figure 2-6. The importance curves are largely symmetric except where asymmetries are expected due to neutronic effects of the flux traps

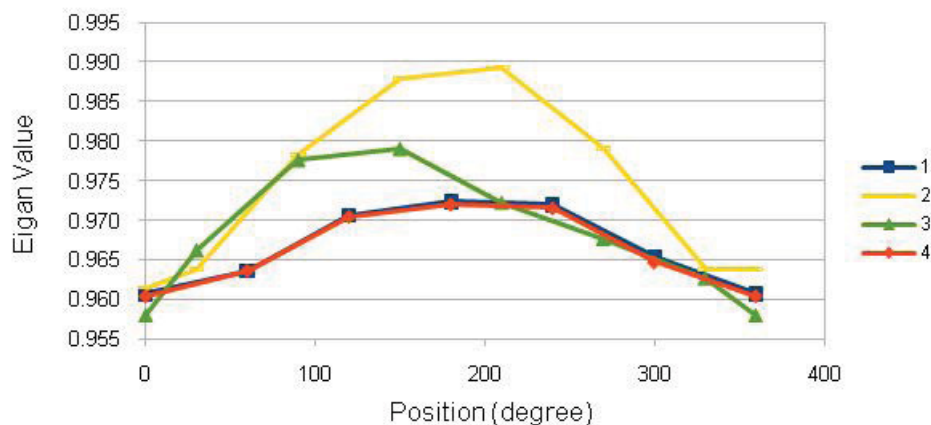


Figure 2-6. Eigenvalue as a function of control drum position.

Neck shim positioning was also added to the model. The shim positions are modeled as either in or out. The importance of the shims is shown in Figure . The regulator rods are currently not modeled and are assumed out in all cases. Their 3-D reactivity worth, created by their variable vertical position, has not yet been modeled. A relative worth generated by vertically variable geometry or absorber density can be added as required to account for their relatively fine reactivity control.

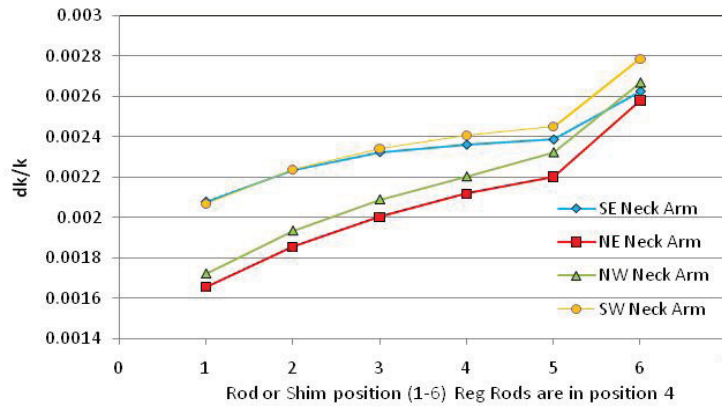


Figure 2-7. ATR neck shim relative reactivity worth curves

#### 2.1.1.5 Demonstration of Core Reloading

The need to simulate reloading of the ATR core from one cycle to another is also a modeling requirement. Currently the core is initially loaded by the analyst and the end-of-cycle information can be written to a file for storage. The stored end-of-cycle information can then be reloaded into the core model creating a model to initiate the following cycle. This is verified with the same fuel elements being discharged and reloaded for a single cycle. The comparison with a single exposure run demonstrates the core is being reloaded correctly. The eigenvalue trends for the reloaded and single run core are shown in Figure 2-8. Realistic individual assembly reloading and shuffle will be discussed in Section 2.2.

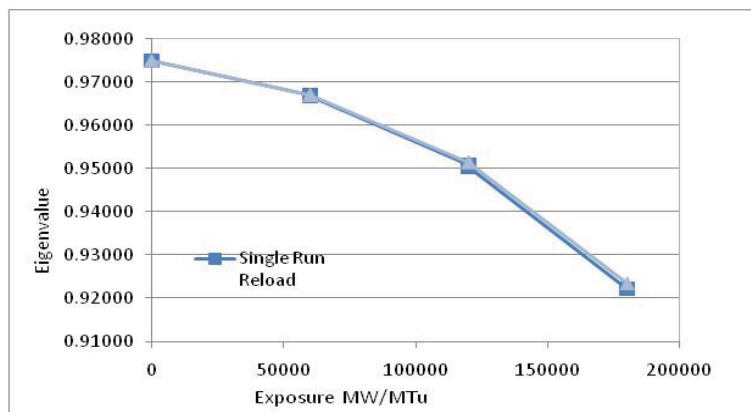


Figure 2-8. Single run and reloaded core eigenvalue trend.



### 2.1.1.6 AFIP Analysis

An early demonstration of the practical engineering utility of the HELIOS ATR model during the year involved an analysis of the ATR Full-Size Plate In Center Flux Trap Position (AFIP) experiment irradiated in cycle 145B, where some issues arose because of an unacceptably large difference between the measured core excess reactivity relative to the calculated value obtained using legacy ATR physics methods. The HELIOS 1994 CIC core model, all fresh fuel, was utilized by HELIOS (and NEWT, as will be described later) to evaluate the core excess reactivity for three cases: 1) the AFIP-6 experiment in the center flux trap,, the aluminum dummy plug with a half inch void at its center in the center flux trap, and a water-filled center flux trap. The results from the analysis showed good agreement with the existing MCNP results available from a variety of prior analyses. The HELIOS model showed the ability to correctly predict the reactivity equivalence of the AFIP experiment and the aluminum dummy, whereas the legacy methods did not. Furthermore, the analysis provided results in a reasonable time that could have supported root cause analysis if required. The analysis results are shown in Figure 2-9.

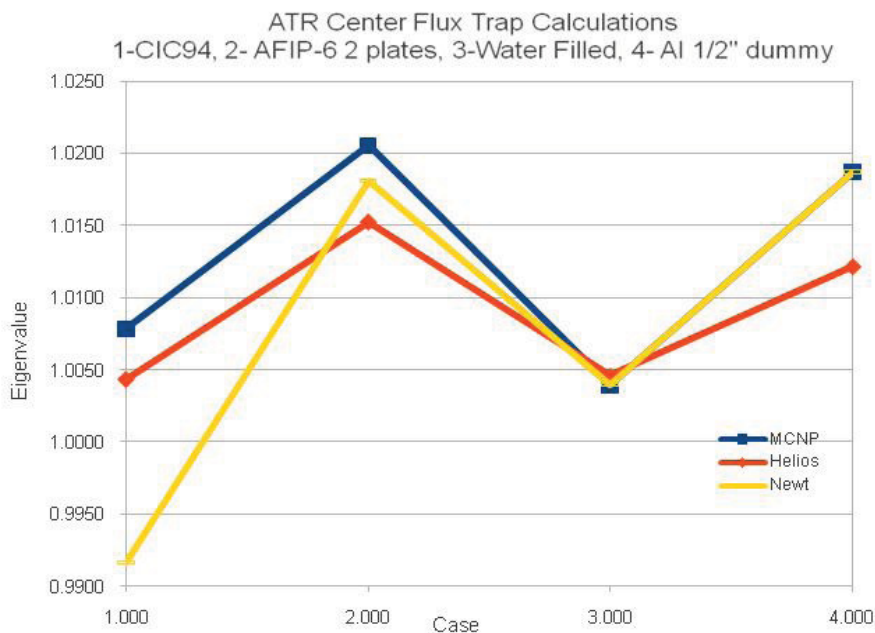


Figure 2-9. ATR Center Flux Trap calculation results.

The geometries modelled in the AFIP exercise are shown in Figures 2-10 through 2-12, which illustrate the power of HELIOS to model very complex configurations. The AFIP model geometry has a fuel density adjustment to account for the AFIP fuel plates not running the full length of the core. (The HELIOS model is two dimensional and assumes the core is vertically unchanging.) The uranium density was reduced to account for the limited vertical coverage of the core. The fuel density was reduced by the integrating the flux over the vertical length of the AFIP plates and normalizing to the flux integrated across the vertical length of core. The resulting correction value matched the value created as part of the NEWT calculation but using independent methods. The developed models are very sensitive to included water content. Small adjustments in the AFIP geometry that change the water content change the calculated eigenvalue significantly.

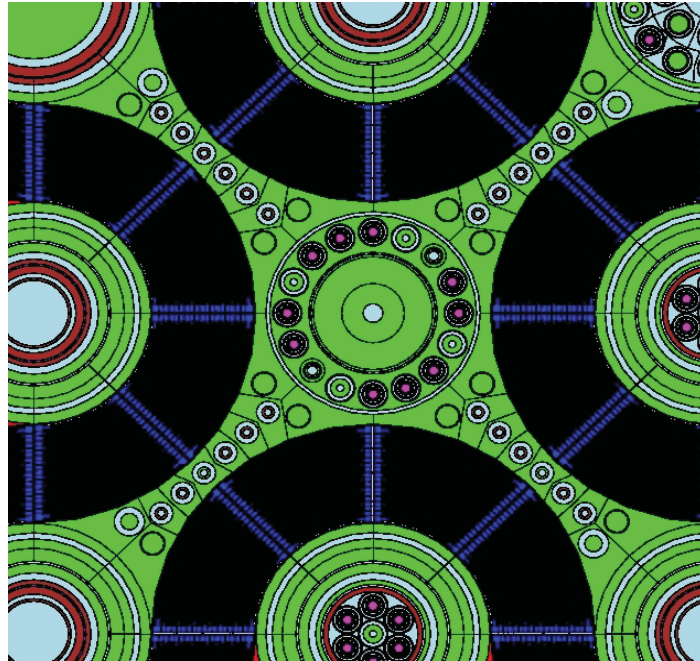


Figure 2-10. 1994 CIC Center Flux Trap Geometry

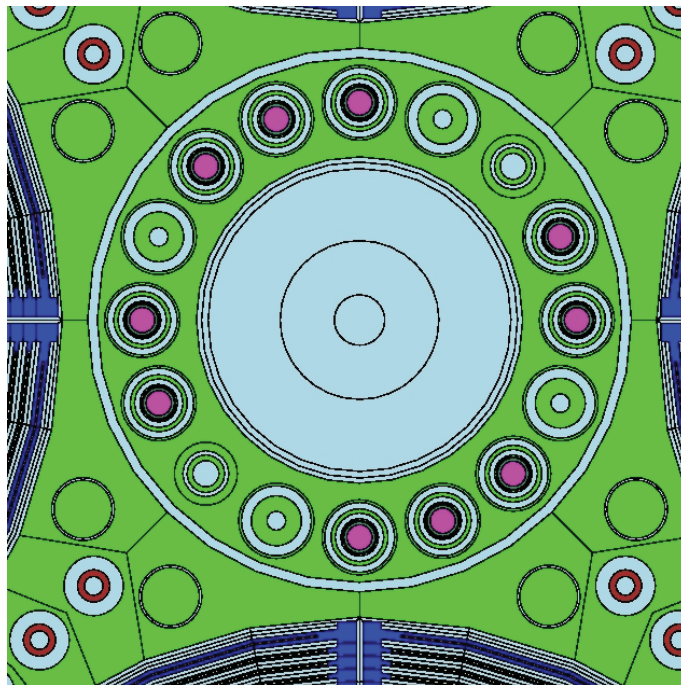


Figure 2-11. Water Filled Center Flux Trap Geometry



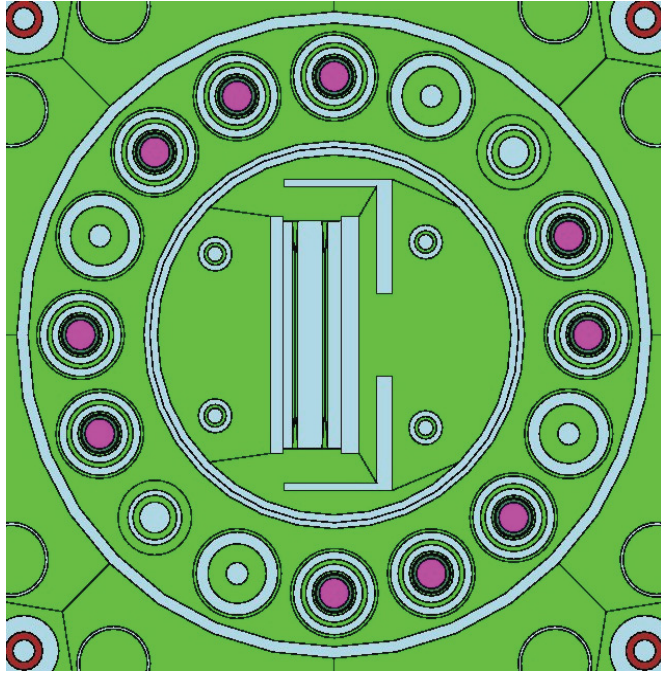


Figure 2-12. AFIP-6 Center Flux Trap Geometry

### 2.1.2 The NEWT Module of the SCALE Computer Code Package

The NEWT (New ESC-Based Weighting Transport Code) computer code is a multigroup radiation transport code with flexible meshing capabilities that allow two-dimensional neutron transport calculations using complex geometric models. NEWT is based on the Extended Step Characteristic (ESC) approach for spatial discretization on an arbitrary mesh structure. NEWT collapses cross section libraries into specified group structures for each nuclide in each material mixture in the model. Cross sections are flux weighted by using the average flux in the mixture (material) for each energy group in the library. As part of the SCALE code package, NEWT is also capable of performing fuel burnup calculations using the ORIGEN-S module of SCALE.

#### 2.1.2.1 NEWT 2D Model of the ATR

A full core two-dimensional (2D) model of the ATR was generated for the NEWT computer code. The model is based on the information provided in the ATR 1994 CIC criticality benchmark documentation (Kim et al. 2008). The model uses MARK VII fuel element properties modeled explicitly as 19-plate fuel elements (see Figure 2-13). The experiment locations in the reactor contain the materials as designated in the ATR 1994 CIC benchmark.

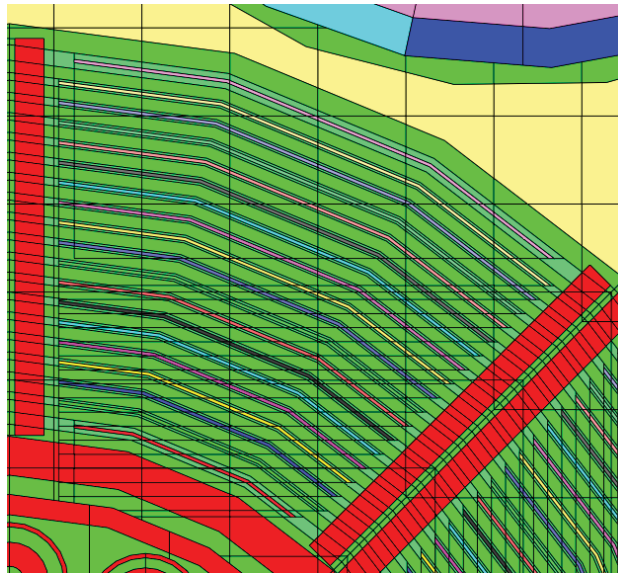


Figure 2-13. NEWT 19 plate fuel element detail.

### 2.1.2.2 NEWT ATR Model Results for the 1994 CIC

The NEWT 2D model of the ATR was used to demonstrate the system at initial critical (Figure 2-14 and 2-15). The model calculated individual plate powers in all 40 fuel elements and generated transport corrected cross sections capable of being used in ATTILA. The displayed results show the model run time, the calculated eigenvalue, core average plate powers (Figure 2-16) , and the fuel element powers (Figure 2-17). Also displayed is the outer shim control cylinder (OSCC) worth curve overlaid with the measured OSCC worth curve (Figure 2-18). The model demonstrated a reasonable eigenvalue, relative bundle powers and plate powers. The OSCC worth curve demonstrates the expected shape but is lacking about 2\$ in total reactivity worth at this point in the development.

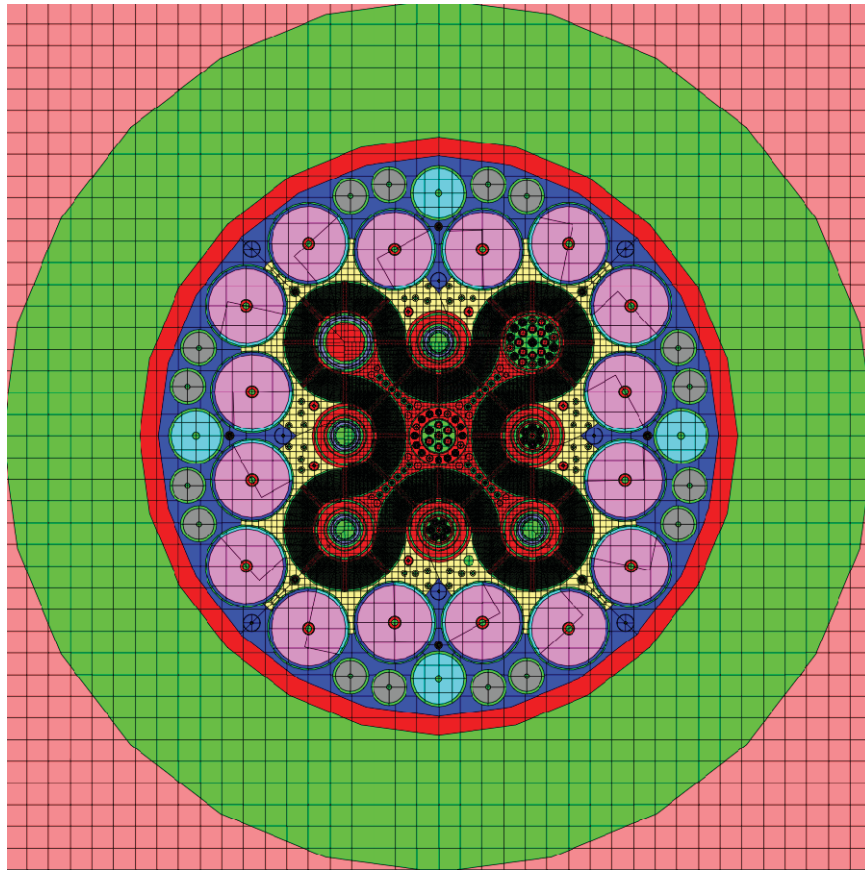


Figure 2-14. 1994 ATR CIC core configuration (Core Number: 103A-2, Reference: Kim et al., 2008,  $K_{eff}=0.9968$ , Run Time:  $\approx 36$  hours).

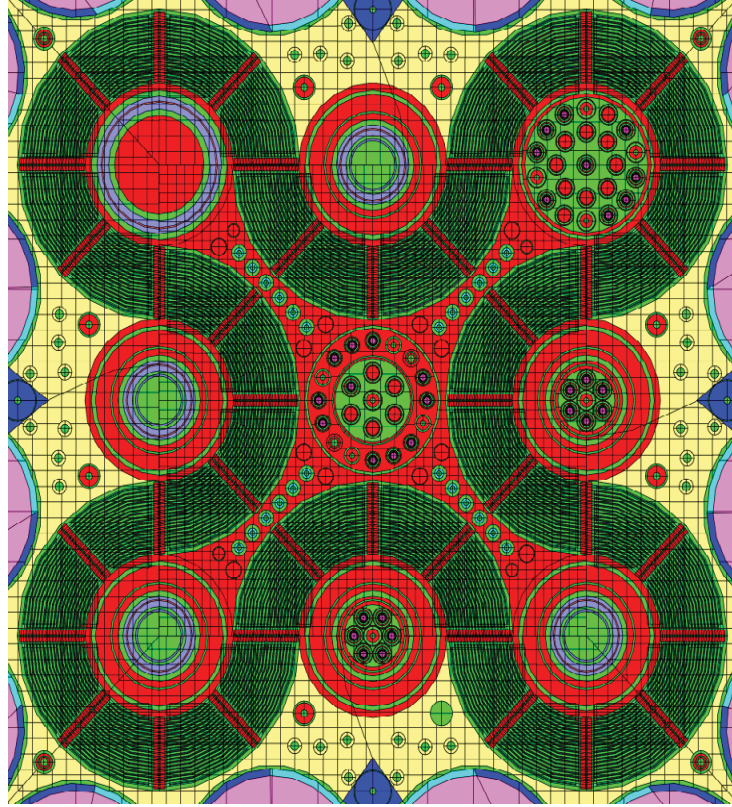


Figure 2-15. Additional Detail of ATR 94 CIC core configuration.

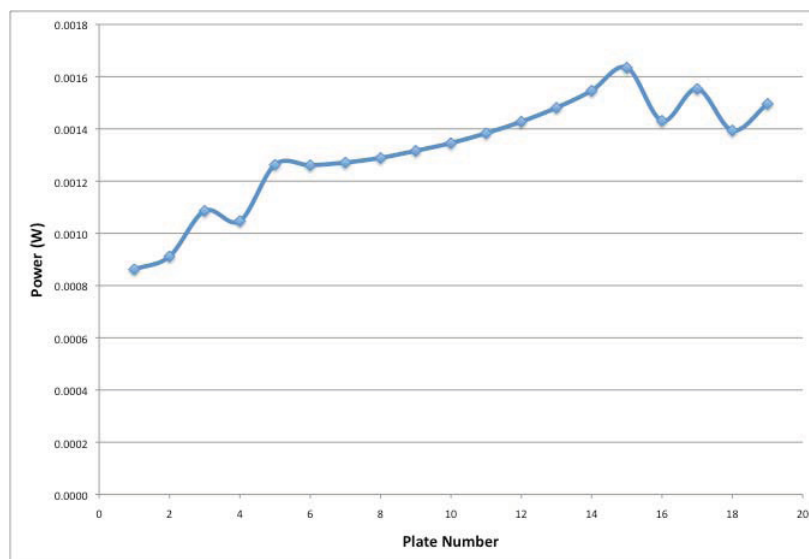


Figure 2-16. ATR 94 CIC average plate powers.

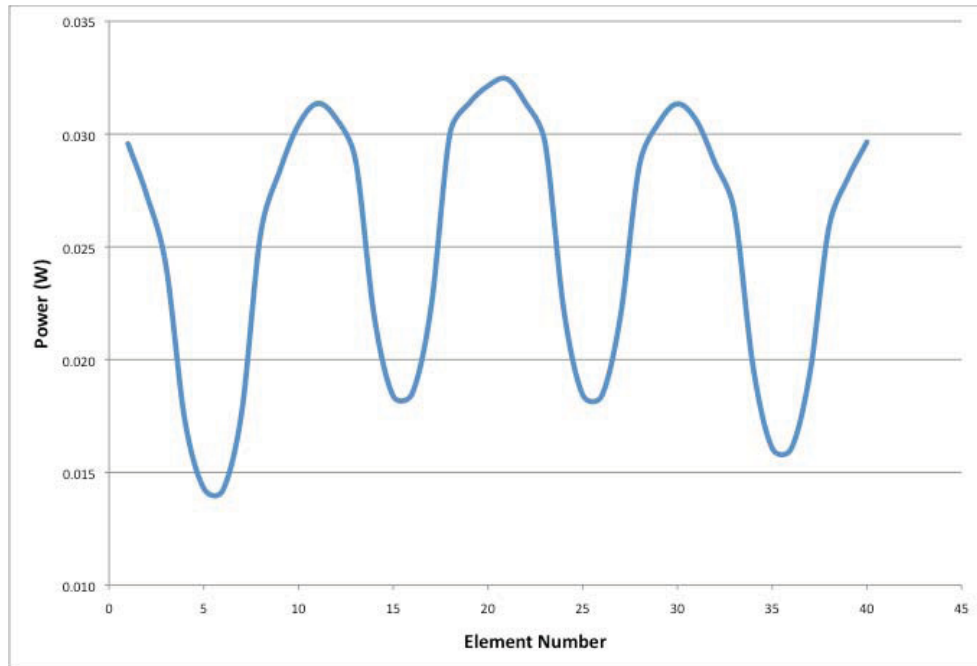


Figure 2-17. ATR 94 CIC fuel element powers.

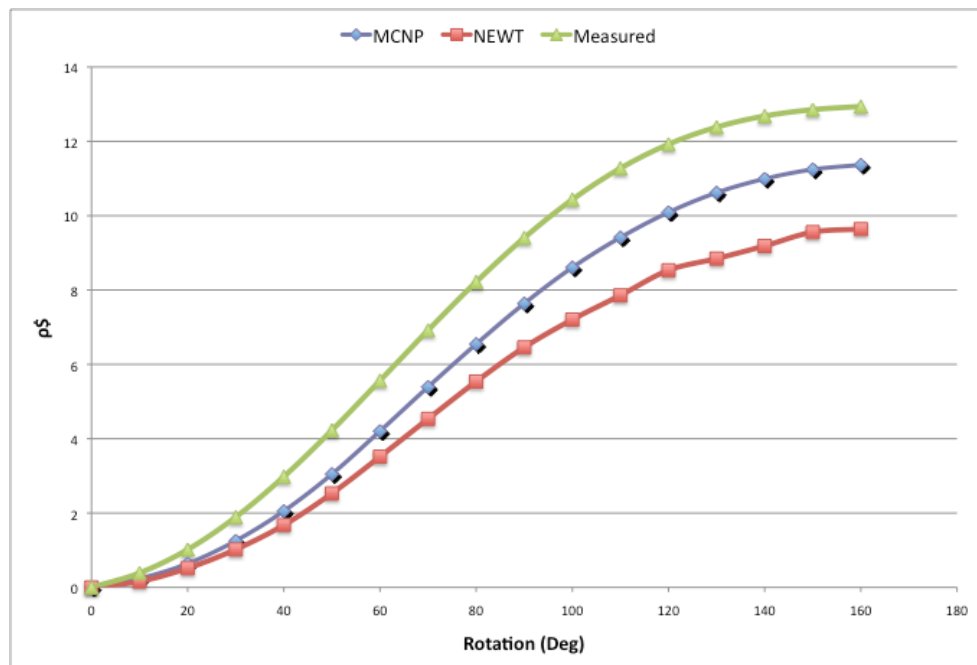


Figure 2-18. ATR 94 CIC OSCC worth curves.



### 2.1.2.3 AFIP Reactivity Comparison

During ATR Cycle 145B some issues arose as a result of differences between actual core excess reactivity and predicted core excess reactivity (Roth 2010) in the cycle Core Safety Assurance Package (CSAP). The differences were evident in the startup critical shim position and the excess reactivity estimate that is derived from this measured position. Investigation indicated that the cross-sections used in the physics analysis for the AFIP backup test in the center lobe of the ATR were inaccurate.

When a new test is proposed for inclusion in ATR, cross sections specific to the test in the specific ATR location must be developed to represent the test in the 2-dimensional PDQ physics model. An internal INL discrete-ordinates code SCAMP ( $S_n$  Code for the Analysis of Multigroup Problems), is often used for ATR cross-section development. The legacy process for this is complicated and potentially error-prone. Cross-section sets were developed in 2007 using SCAMP to represent two AFIP test configurations and two AFIP backup test configurations. Several AFIP tests were successfully irradiated in the center flux trap of the ATR from February 2008 through October 2009. ATR Cycle 145B in November 2009 was the first time a backup test for AFIP was inserted into the ATR.

The temporary delay in Cycle 145B resulting from this situation was traced to a cross section inaccuracy in the PDQ physics analysis for that cycle as noted above. This offered an opportunity to determine whether the new ATR core modelling update codes could have accurately modelled the ATR CYCLE 145B reactivity. None of the codes being considered for the new ATR methods require experiment specific cross section generation. They are all capable of directly modelling the geometry and materials of the experiments and provide a capability to visualize the geometry modelled. A significant geometry error in the model would be readily apparent with any of the new codes.

The NEWT model of the ATR was used to simulate the AFIP test, the AFIP backup test, and a water filled center flux trap. The reactivity difference between these three configurations was determined and the reactivity worth ( $\rho$ \$) was determined. It is customary to scale the reactivity worth of ATR experiments to a flat power weighted reactivity often called Tappendorf weighting. The Tappendorf weighting equation (McClure 1991) is applied to flat power weight reactivity worths. The Tappendorf equation is given below.

$$\rho_A \$ = \rho_B \$ \times P_A \times \left( \frac{P_A + P_B}{2 \times P_B^2} \right) \quad (1)$$

The values for  $\rho_A$  and  $\rho_B$  are the reactivity worths for the corresponding lobe powers  $P_A$  and  $P_B$ , respectively.  $P_A$  is assumed to be equal to 50 MW (flat core power) while  $P_B$  is the modeled or measured lobe power scaled to 250 MW total core power. The flat power weighted MCNP calculated results for each configuration are also provided. The flat power weighted reactivity difference between the AFIP-6 experiment and the AFIP backup was calculated by NEWT to be 0.135\$ (1.535\$ - 1.400\$ = 0.135\$). This compares very well with the MCNP calculated difference of 0.146\$ (1.418\$ - 1.272\$ = 0.146\$) as well as with a measurement conducted in the ATRC that demonstrated the nearly equivalent core reactivities associated with the two experiments. Some details of the three models and the computed results from them are illustrated in Figure 2-19.

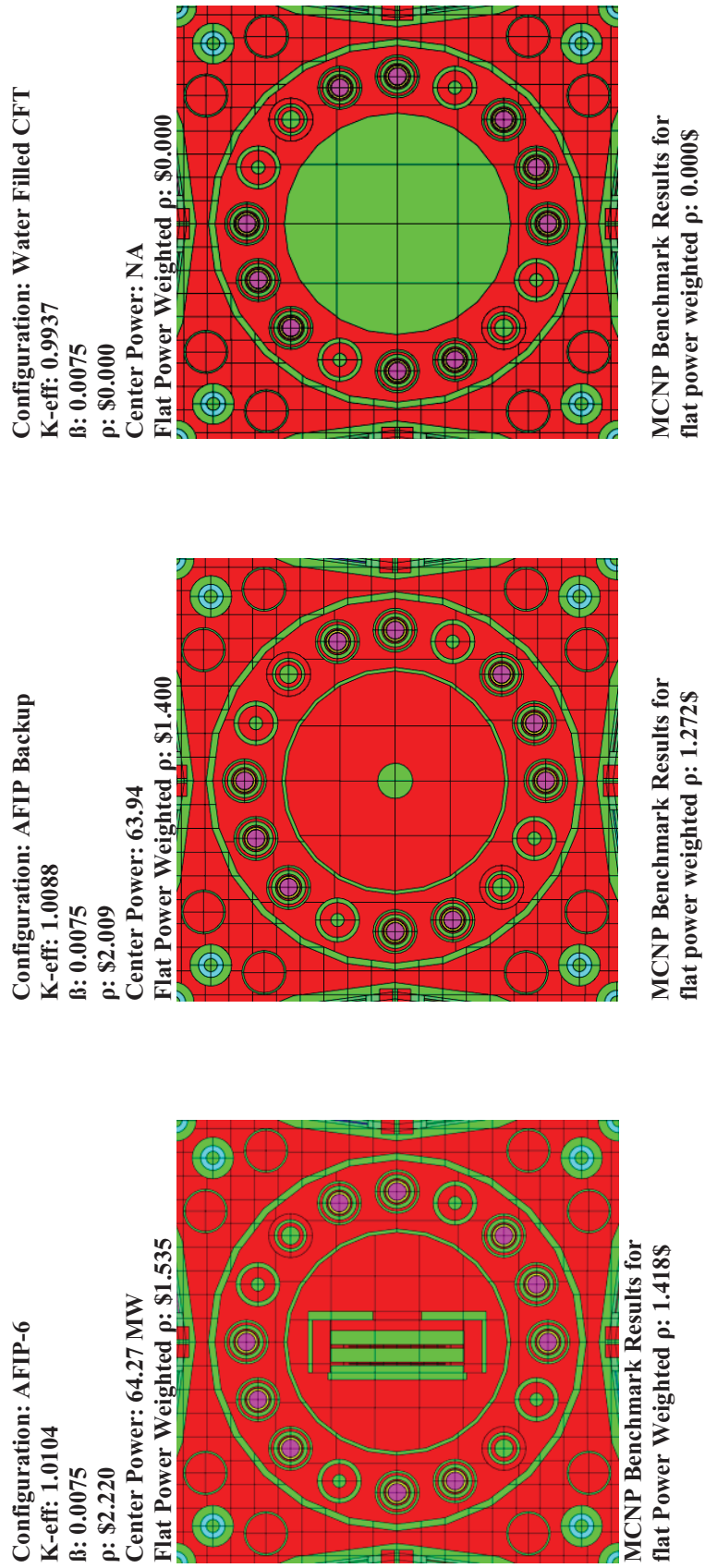


Figure 2-19. NEWT Results for AFIP.

### 2.1.3 ATTILA Model of the ATR

The ATTILA neutron transport code package uses a third order spatially accurate three dimensional, Discrete Ordinates ( $S_n$ ) Linear Discontinuous Galerkin Finite Element Method (FEM) steady state solver with tetrahedral elements. The code also uses multi-group cross sections with a variety of formats including DTF, NJOY and AMPX from the ORNL Scale code package. ATTILA allows the user to coalesce the cross section sets with constant flux weighting or a spectrum. The group structure can be used and collapsed for both neutrons and gammas. ATTILA can perform depletion in serial and parallel mode and has been benchmarked against MCNP, however; the documentation for parallel depletion has not been finished as of this date (Fallia, 2010)

#### 2.1.3.1 General Description of the ATTILA Code

ATTILA allows full three (3D) and two-dimensional (2D) models of the Advanced Test Reactor (ATR) to be constructed. The models can be thin to approximate 2D applications or used as thicker models to actually incorporate 3D effects at the thin two-dimensional level such as the boron sphere simulations described below. The models are constructed by using SolidWorks<sup>TM</sup> (SW). This is CAD based software which can export a large number of file types to be meshed and used in a variety of applications. Since ATTILA is Finite Element based, it uses a mesher supplied by Simmetrix on a tetrahedral mesh for highly accurate isoparametric (curve fitting) boundaries and geometries. ATTILA can perform both structured and unstructured meshing. Currently, the SolidWorks<sup>TM</sup> models used in ATTILA support the construction of MCNP models using DAG-MCNP (Wilson et al., 2008). The same models used in ATTILA built from SolidWorks<sup>TM</sup> can now be used in Cubit<sup>TM</sup> for supplying the input to MCNP. This allows ATTILA to be used for reducing the variance in MCNP calculations and decreasing the runtime enormously (Transpire, 2010)

ATTILA can be executed in parallel or serial mode. Currently, it is installed in the INL High Performance Computing (HPC) enclave on ICESTORM, a parallel system with up to 2000 cpus. This allows ATTILA to calculate problems on the order of several hundred million degrees of freedom. Execution times that range from minutes to a few hours, depending on the ordinate degree of integration and error tolerance. ATTILA can model problems as quarter core in so-called “thin 3D” (a simplifying approximation that produces a transverse 2-dimensional solution) as well as full three-dimensional problems with reflectors. This can be performed since ATR is a thermal reactor with a very short path length for interaction. This allows confidence in applying ATTILA to short term problems that run in a few minutes on a personal computer to large full 3D problems on ICESTORM, producing the same results.

Since ATTILA is a discrete ordinates code it can produce a core-wide flux map, modeling any level of detail required. This allows ATTILA to be used for designing and analyzing experiments down to very fine detail. ATTILA has access to TecPlot, VisIt and GMV for graphics viewing. This allows ATTILA the capability to examine any model for comparison to data. Also, the viewer within the ATTILA GUI provides a second to third tier level for checking materials and regions, since the same material shows up in the model as the same color throughout the field of view.

Verification of ATTILA has been performed with the Method of Manufactured Solutions (MMS) as discussed by Pautz and Roache (Roache, 2002; Pautz, 2002). The MMS consists of using explicit or linearized source terms on the right hand side of the equations to be solved that allows the numerical method and its programming to be verified. ATTILA has been placed through this process for a large number of problems. Deterministic methods such as  $S_n$  or  $P_n$  can be debugged in this manner. Monte Carlo and Method of Characteristics solvers cannot use MMS. This necessitates the use of experimental



data for validation. ATTILA has also undergone a large number of validation studies with experimental data.

### **2.1.3.2 ATTILA 3D and 2D Computational Models of the ATR**

Full core three (3D) and two-dimensional (2D) models of the Advanced Test Reactor (ATR) have been created using ATTILA and applied to several practical ATR situations. The models used in all of these calculations relied upon information from the ATR 1994 CIC criticality benchmark (Kim et al., 2008). The ATTILA model has ATR fuel elements modeled as 19 plate fuel elements and as three-region fuel shown in Figure 2-20 for the CIC criticality benchmark. The CIC configuration was used for the calculation and comparison of radial and azimuthal power distributions with data from MCNP, NEWT and HELIOS. This configuration was also used for the calculation of the shim cylinders reactivity worth as a function of position and compared to ATR measurements. A similar configuration was also used for the ATR Full-Size Plate In-Center Flux Trap Position (AFIP) test to demonstrate the calculation for the production of Mo-99 using the 19 plate and three region models. Finally, the reactivity worth comparisons of the boron sphere insert (see Section 4.0) for the Northwest Large IN-Pile tube flux trap were calculated.

**Nineteen Fuel Plate Model Comparison to CIC-94 Data and MCNP.** The results from ATTILA using the nineteen plate fuel model for the ATR in 3D have been compared to CIC-94 along with MCNP, NEWT and HELIOS as shown in Figures 2-21 and 2-22. The azimuthal power profiles between ATTILA and the data are in close agreement. ATTILA is quite close to the MCNP results for the radial power profile. This is most likely due to being able to rotate the shims to any continuous angular degree desirable in SolidWorks™ since the ATR model radial power is very sensitive to shim position in each of the models.

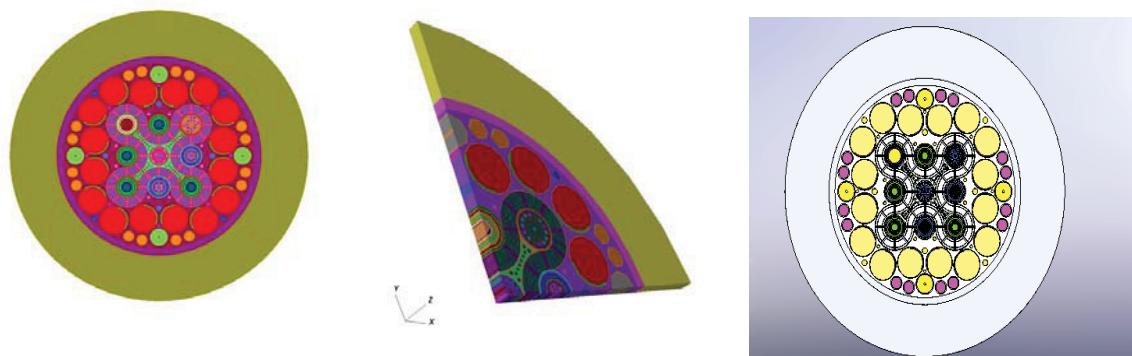


Figure 2-20. ATR 3D 19 Plate & Thin 3D Qtr Core Cross-Section Models.

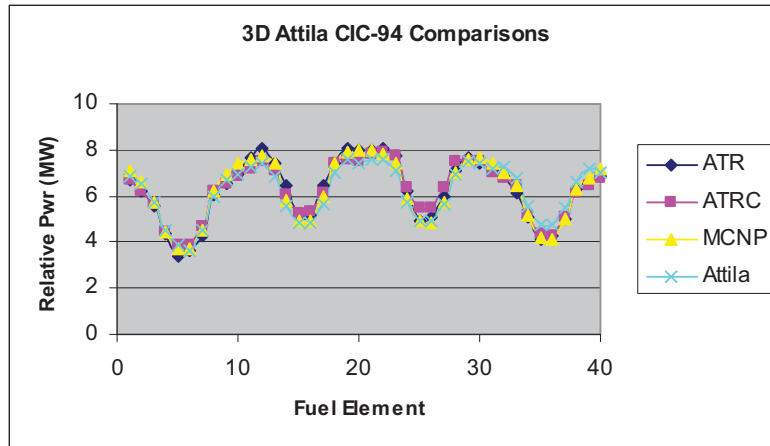


Figure 2-21. Three Dimensional Azimuthal Power Comparisons

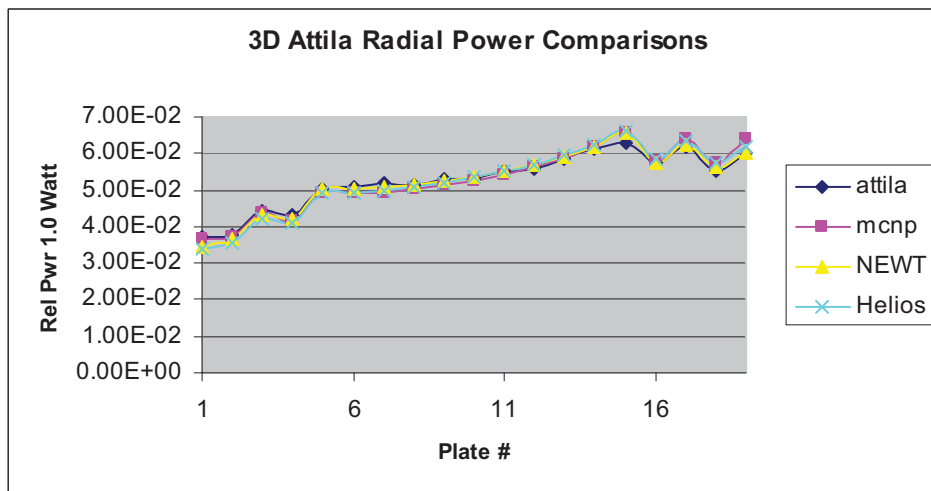


Figure 2-22. Three Dimensional Radial Power Distribution.

Typical run times for the nineteen plate model are three hours using 128 cpus, with an eigenvalue or  $K_{eff}$  of 0.9988.

The rotational shims in the ATR and ATRC are extremely important for testing and prediction. As part of this effort, the shim worth predictions for ATR were computed. The ATTILA computation for shim worth is shown in Figure 2-23. Note that the ATTILA results are close to the experimental data.

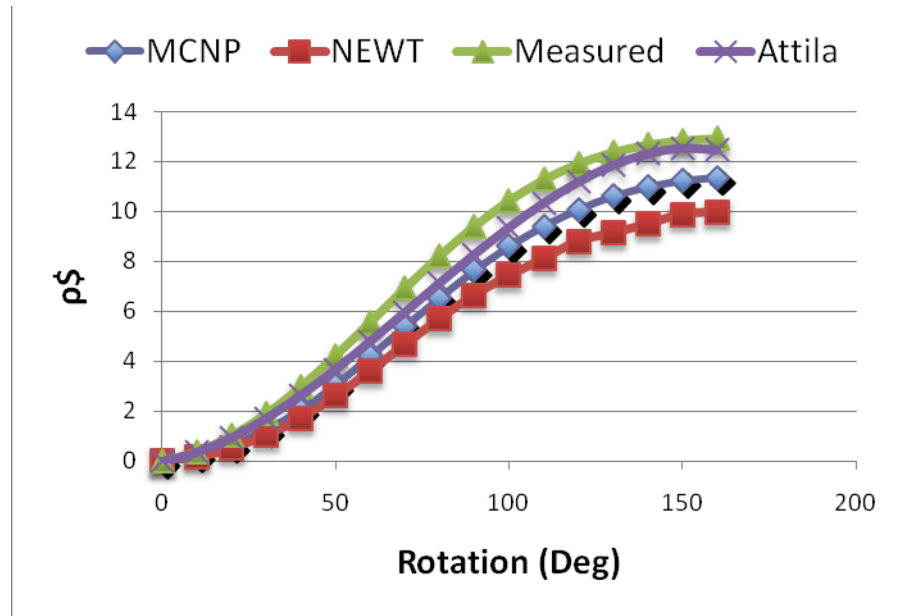


Figure 2-23. Rotational Shim Worth for CIC-94 Configuration.

Figures 2-24 and 2-25 show quarter core results using the thin 3D model for the CIC-94 configuration compared to test data and MCNP results, with ATTILA executed on a Windows based PC in less than one-half hour.

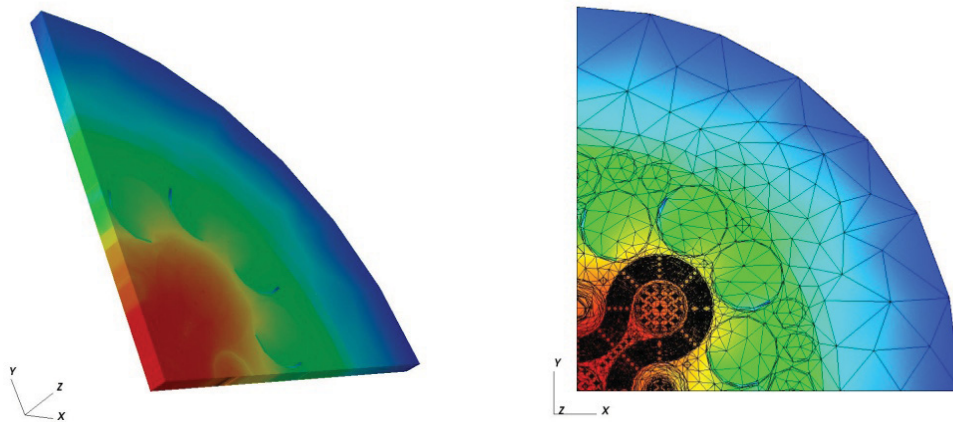


Figure 2-24. Quarter Core Geometry and Mesh for CIC-94

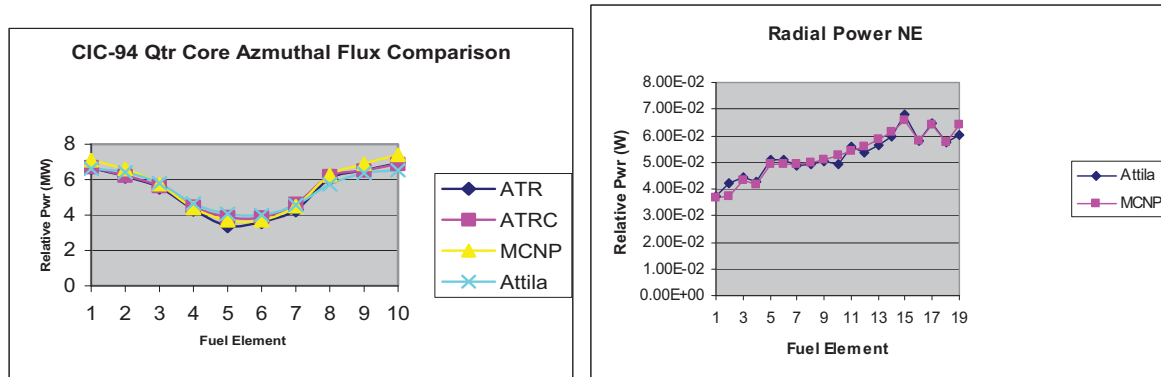


Figure 2-25. Thin 3D Quarter Core Results for CIC-94.

**AFIP Reactivity Insertion.** ATTILA was also used to perform an examination of the relative worth of the AFIP backup test of the ATR. Some issues with this experiment were largely traced to problems with the effective diffusion theory parameters used to represent the AFIP hardware, as noted earlier. PDQ does not have a general set of cross-section sets as ATTILA does, nor does it have the continuous energy cross section representation of MCNP. Moreover, the Cartesian mesh used for PDQ is cumbersome to adapt to irregular shapes and it presents a number of debilitating homogenization issues for any experiment hardware with inhomogeneous geometry and materials.

The AFIP experiment of interest here was irradiated in the center flux trap of the ATR. The November 2009 irradiation was the first time a backup test (Aluminum) for AFIP was inserted into the ATR. This situation provided a basis to determine whether the new ATR codes could accurately model the reactivity insertion associated with the AFIP test. The codes used to implement the new ATR methods have general sets of cross sections available and are capable of modelling the experiment with visualization. With the new codes any geometry error would be readily visible, which is not the case for PDQ.

The ATTILA model for ATR was used to simulate: 1) the AFIP test, 2) the backup test with aluminium and, 3) a water-filled center flux trap. The Radion NJOY 55 group cross section was used for the ATTILA calculation with all groups for neutrons and gammas. The difference in reactivities of the AFIP experiment and the aluminium backup relative to a water-filled flux trap were determined. The results (Table 2-1) show reasonably consistent worths of the AFIP and Backup hardware, as expected. The absolute reactivity worths are somewhat higher in the case of ATTILA relative to the reference MCNP case, however.

Figure 2-26 shows some visualizations of the ATTILA model and the calculated results. The mesh consisted of approximately one-million elements and the calculations took two hours each on 128 cpus with a 0.0001 relative convergence criteria for the flux. Based on this preliminary modelling effort, it appears that ATTILA can be useful for 3D reactivity difference calculations for the ATR, although it is highly likely that additional attention to detail and to careful cross section generation will be crucial.

Table 2-1. Comparisons of ATTILA with MCNP for AFIP Reactivity.

ATTILA Case	$K_{eff}$	$Beta_{eff}$	Reactivity ( $\beta$ )
AFIP	1.008516	0.0075	3.71516603
AL	1.005796	0.0075	3.357686516
Water	0.98095	0.0075	0.0
MCNP Case	$K_{eff}$	Beta	
AFIP	1.02053	0.0075	2.16
AL	1.01869	0.0075	1.92
Water	1.00397	0.0075	0.0

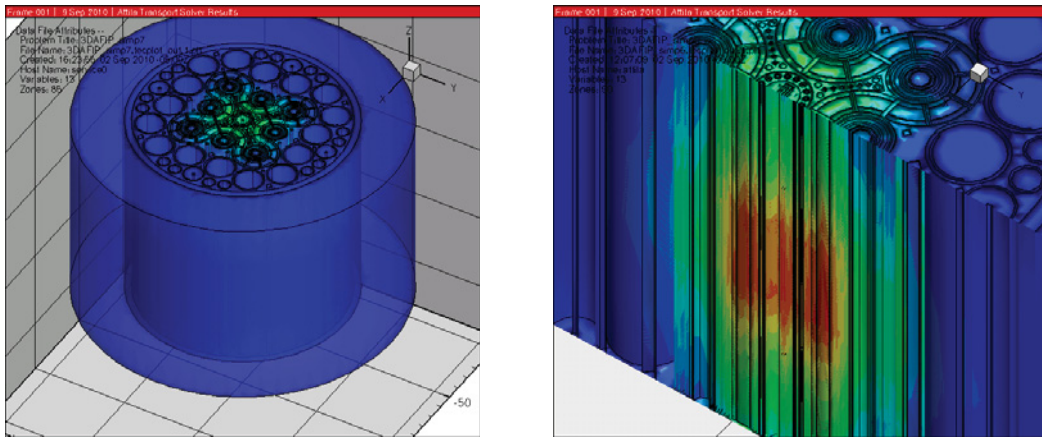


Figure 2-26. Cross-section Views of the ATTILA AFIP Models showing the full ATR core (L) and detail around the central flux trap (R).

**Reactivity of the boron sphere insert fitting for the ATR NW LIPT.** The ATR and the ATRC lack real-time methods for detecting thermal neutron flux and fission reaction rates for irradiation capsules. The ATRC has no instrumentation to measure real-time fast neutron flux. A test series is currently being conducted in the ATRC to cross-compare the accuracy, response time, and long duration performance of French Atomic Energy Commission (CEA)-developed miniature fission chambers, specialized self-powered neutron detectors (SPNDs) by the Argentinean National Energy Commission (CNEA), commercially-available SPNDs, and back-to-back fission (BTB) chambers (Rempe et al., 2010). Ultimately, the goal is to select a detector that can provide online regional power measurement in the ATRC.

As described in Section 4 of this report, extensive measurements using neutron activation spectrometry will be conducted in connection with this experimental campaign, and to provide additional transport code validation data for the ATR Core Modeling Update project. One of the neutron spectral shifters that will be used for these measurements is a boron sphere that will be placed in a special insert fitting located in the North-West Large In-Pile Tube (NW LIPT) flux trap. The purpose of this analysis described here was to assess the feasibility of using ATTILA to determine the reactivity effect of the boron sphere insert. The model was built in SolidWorks<sup>TM</sup> and imported into ATTILA as a parasolid file. The structured option for meshing was used in the code. Figure 2-27 shows the 19 Plate and three fuel region models used for the analysis. Figure 2-28 displays the boron sphere insert in the NW LIPT along with the mesh used for the sphere itself. It is imperative to use a fine mesh for the sphere or a “re-entrant” condition will

exist. The Radion 55 energy group library was used with all neutron and gamma groups. The analysis used 1.5 million tetrahedral mesh elements and required two hours on IceStorm with 256 processors.

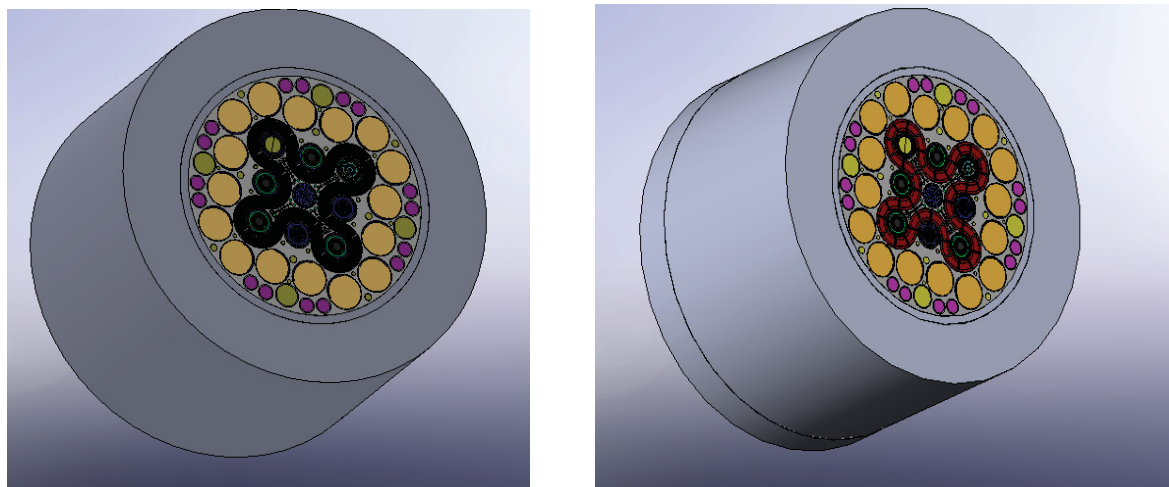


Figure 2-27. Boron Sphere ATILA Models

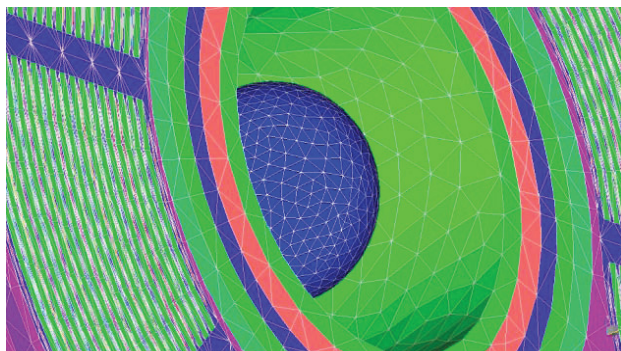


Figure 2-28. Boron Sphere Insert Mesh with 19 Plate Fuel

Table 2-2 displays the calculated eigenvalues, reactivity and a comparison to MCNP. The effect of the boron sphere is small and negative, as expected. ATILA produces a larger absolute value of the reactivity change than in the MCNP calculation. This may be due to ATILA using a coarser mesh than needed, and will be addressed by a convergence study as the verification process continues in FY-11. Figure 2-29 shows a typical visualization of the neutron flux distribution that can be produced by ATILA.

Table 2-2 Boron Sphere reactivity comparisons with MCNP

<b>ATILA Case</b>	<b>Keff</b>	<b>Beta</b>	<b><math>\rho</math> (\$)</b>
Boron Sphere	1.0755306	0.0075	-0.14479
Aluminum	1.0767882	0.0075	
<b>MCNP Case</b>	<b>Keff</b>	<b>Beta</b>	<b><math>\rho</math> (\$)</b>
Boron Sphere	0.99058	0.0075	-0.013
Aluminum	0.99068	0.0075	



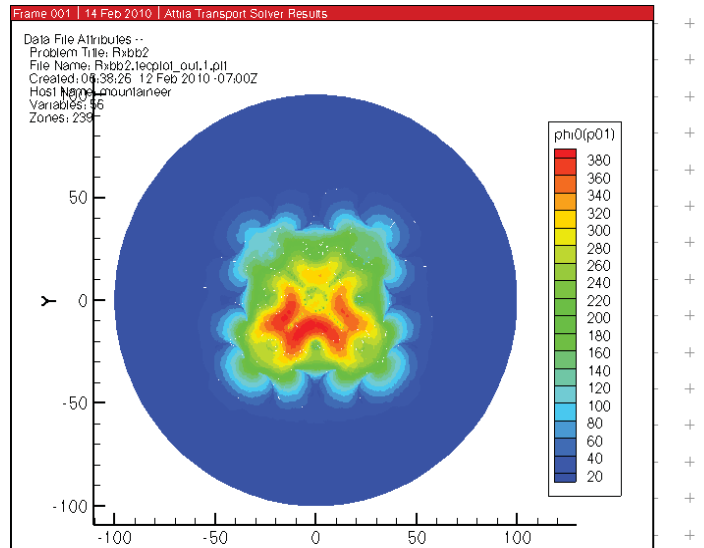


Figure 2-29. Two-Dimensional ATTILA visualization of the neutron flux distribution in the ATRC.

#### 2.1.4 Investigation of Accelerated Methods for ATR Shim Rotation Analysis

At present, multiple calculations are required for repositioning the rotating control drums to simultaneously produce critically and desired power splits for each new ATR reactor cycle. The positions of the shims have been calculated in the past by an iterative method involving estimation of the initial shim position, running the model, evaluating the results, and refining the shim estimation, and so forth. This method has been acceptable with the legacy PDQ-based methodologies because of the minimal computational time that was required to solve a four energy group coarse grid diffusion model. However, with the newer models being developed for ATR cycle analysis it may be desirable to minimize the number of transport calculations via application of a simplified method that can still retain the improved accuracy of the updated computational methodologies. In this context, two different approaches, spectral corrected perturbation theory and linear regression analysis, are of potential interest.

##### 2.1.4.1 Spectral Corrected Perturbation Theory.

The NEWT and ATTILA codes have the ability to calculate both forward and adjoint flux solutions. With these two codes, perturbation theory can thus be used to approximate small changes to the reactor system such as predicting the needed location of the shims. The initial investigation of perturbation theory outlined here was performed using NEWT. The same perturbation theory method could also be applied using the three dimensional code ATTILA

First order eigenvalue perturbation theory has been known to work well for small changes in the system, but shim rotations cause large spectral changes and first order theory alone was found to produce inaccurate results. A new perturbation method, called spectral corrected perturbation theory, was developed specifically for predicting changes in reactivity as a function of shim rotation and control rod removal.



The SCALE suite, which includes NEWT, contains programs that use perturbation theory for sensitivity and uncertainty calculations but not for predictive purposes. Therefore, a specialized wrapper that used perturbation theory in a predictive capacity was developed. This stand-alone wrapper, PertN, was written in Fortran 90. It inputs forward and adjoint angular flux moment files, multigroup cross section sets, and other information provided by NEWT. The wrapper can then use either first order perturbation theory, spectral corrected perturbation theory, or “exact” high-order perturbation theory to predict the changes in reactivity associated with different material densities or compositions.

The PertN code is currently undergoing verification to ensure that the computational model accurately represents the underlying mathematical model and its solution accurately. The verification process includes software quality engineering, code verification, and calculation verification. A flow chart showing the process for verification can be seen in Figure 2-30 below.

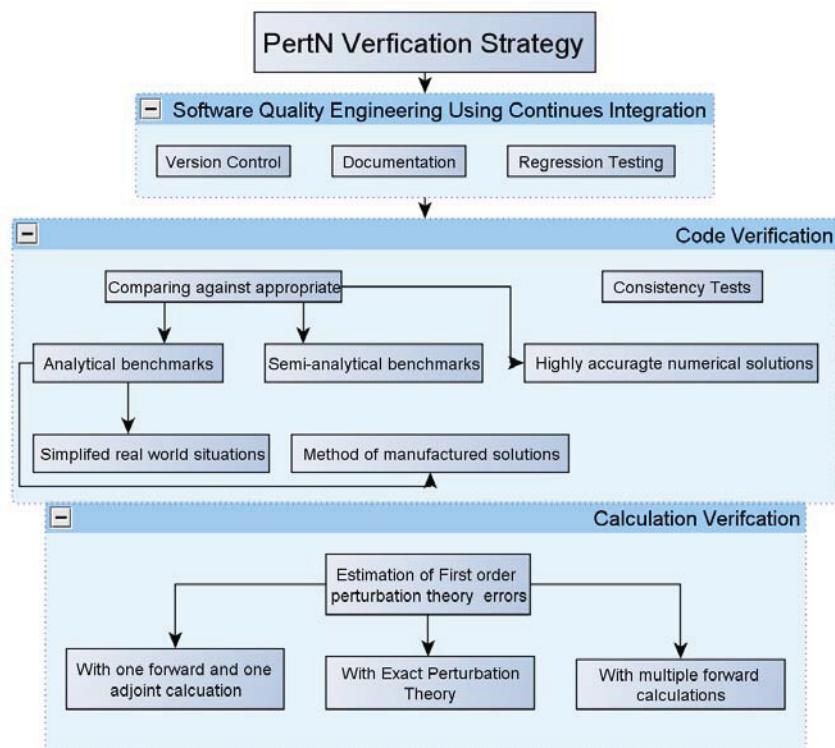


Figure 2-30. Verification plan for the perturbation theory code PertN.

Spectral corrected perturbation theory uses the same algorithm as first order perturbation theory, but with a different adjoint function, defined for an appropriate bounding scenario that represents a selected perturbed reactor condition. As seen in Figure 2-31 spectral corrected perturbation theory appears to produce sufficiently accurate results to enable shim rotation prediction under large perturbations. The initial results from spectral corrected perturbation theory are thus promising and will be further verified and refined during the first part of FY-11.

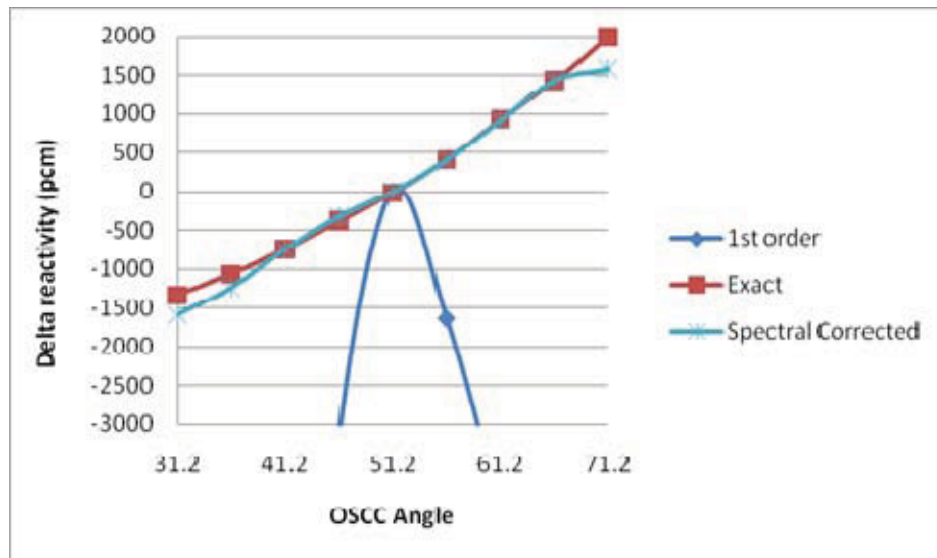


Figure 2-31. Integral shim reactivity worth curves computed using various approximations.

#### 2.1.4.2 Linear Regression Method

The linear regression method offers a potential alternate approach for automating shim rotation for any neutronic code, including those that do not provide the adjoint solution. The method uses a linear regression learning algorithm to predict the appropriate shim rotation for simultaneously for obtaining criticality and the desired lobe power split. In addition, through statistical analysis the linear regression method also provides a 95% confidence interval for the solution.

The linear regression method can be optimized for two different parameters depending on the users' needs and computational capability. If the number of processors is not a concern then the linear regression method can be optimized for time by running multiple jobs in parallel. However, if the number of processors is a concern then the linear regression method can be optimized to decrease the total number of forward solutions needed, but this method will require a larger amount of total time needed to obtain the solution.

Initial results from the linear regression method also appear promising and the development will continue in FY-11.

With either spectral perturbation theory method or the linear regression method the total amount of computational time and engineering time needed to accurately calculate the shim position should be significantly reduced. This should help ease the complexity of transitioning from a very fast legacy code to the more modern transport methods.

## 2.2 Baseline HELIOS ATR Fuel Management Model Development

After development of representative fuel and reactivity controls the basics for a full cycle simulation were available. The ATR 145A core was used as the first cycle in the demonstration of a near fully detailed simulation.

### 2.2.1 Description of Model and Initial Verification Studies

Simulating the operation of a reactor core to produce operating, design and safety information throughout the cycle is referred to as core follow modeling. The core follow calculations use short discrete exposure steps to approximate the continuous reactivity changes seen in an operating core. Commercial reactors update their core follow simulations every hour in an automated process utilizing a dedicated computer system that assimilates data directly from the core flux monitoring system. The ideal simulation time step will depend on how dynamic the operation of the reactor is. The optimum time steps will need to be evaluated and optimized for best results.

The ATR simulation will make steps that are relatively large, in exposure units, because of the high power density. The steps were selected based on power changes tied to control drum position and shim rod position changes. Not every reactivity control change was included in the simulation. There are several hundred reactivity control changes through a cycle. All may need to be simulated to maximize the accuracy of the results. The power history for cycle 145A is shown in Figure 2-32. The large number of small power changes can be seen and a temporary reactor shutdown is apparent near the end of the cycle. The required level of power detail for an accurate safety analysis needs to be established.

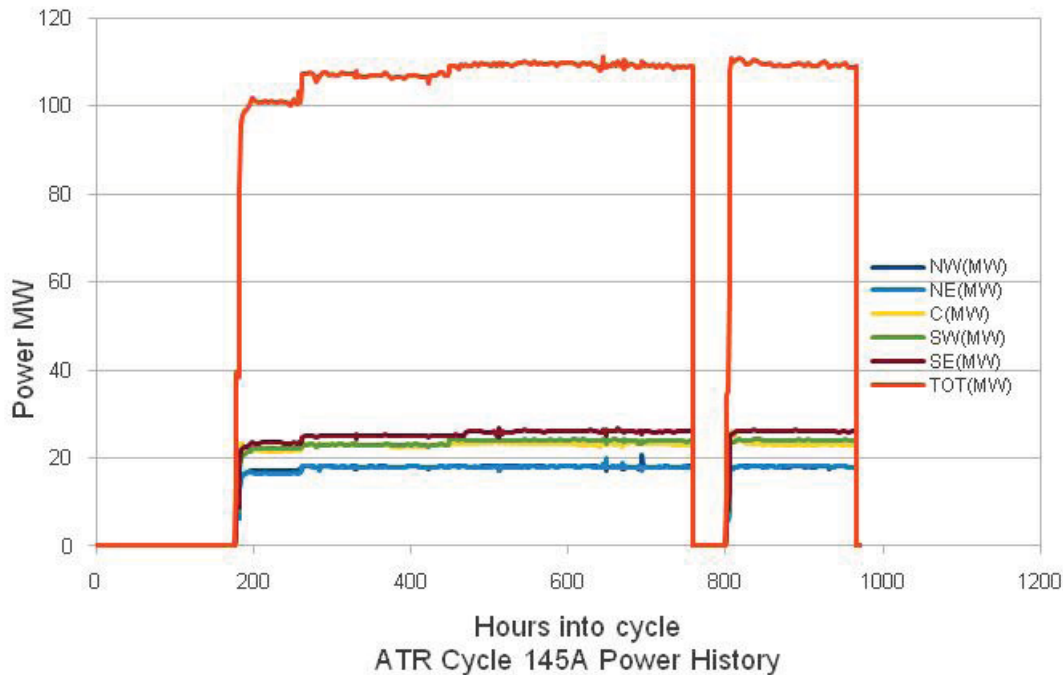


Figure 2-32. ATR Cycle 145A Power History.

Modelling cycle power and power shape through a core follow simulation will allow downstream reloads to be modelled from start-up to end-of-cycle and include the changing fuel element isotopics. These

exposure-based isotopic values will allow exposure based reactivity and safety case calculations. This calculation is supported by the individual assembly and plate detail.

### 2.2.2 August 2009 Initial ATR configuration and Depletion Studies

The 145A reactor core was the base starting point to simulate ATR operation. The initial 145A fuel isotopics were taken from the best available data contained in the core simulation database generated by PDQ. The content of the 760 plates in the 40 bundles, fresh and exposed, was created. The 145A core was started with isotopic data from the current data base derived from PDQ with the approximate bundle isotopics, including 3 isotopes of uranium and 3 isotopes of plutonium and 10 fission products. These isotopes will be supplemented with the more inclusive HELIOS isotopes, using a data base and calculations for more than 300 isotopes, derived as the core is exposed through the cycle. This will create more accurate results as additional cores are run in succession and each core is computed with a more complete data set. In the same way the exposure steps must be optimized the number of cores run may need to be increased to achieve the best results.

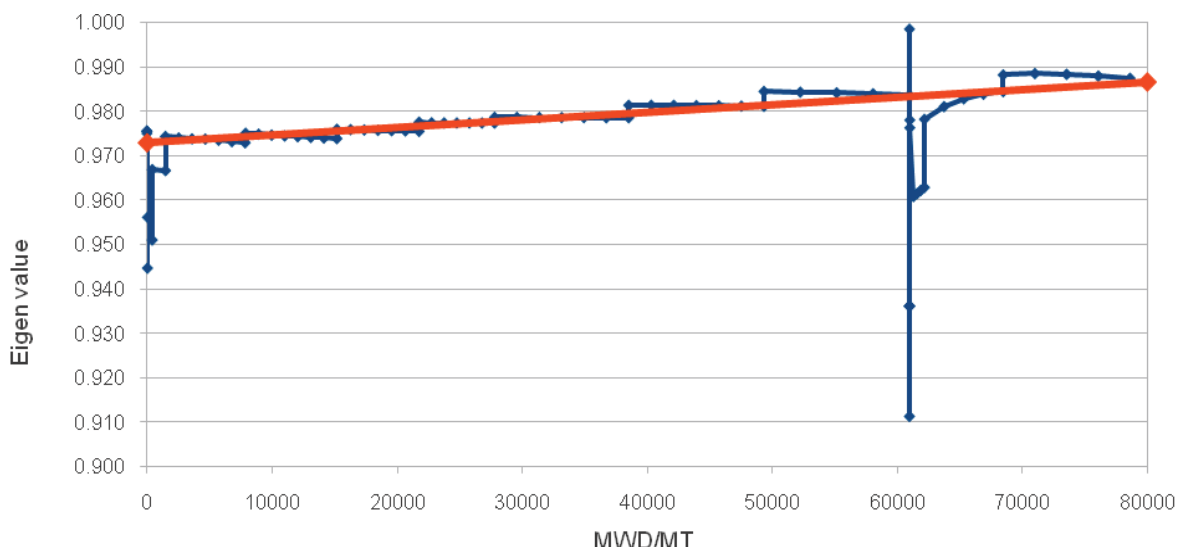


Figure 2-33. Eigenvalue Trend for ATR cycle 145A

The relatively smooth and predictable Eigenvalue trend (Figure 2-33) would allow a core design to be established as part of the design cycle. Deviations in the curve are at the beginning of the cycle when isotopics and fission products change most rapidly and are least accurate. The second significant deviation at 60,000 MWD/MT is from a temporary shutdown that creates inaccuracies similar to the start of cycle. The core is also greatly subcritical where the calculation may not be accurate. Running additional cycles will improve the understanding of the core and model similarities. Additional reactivity controls, temperature for example, that are not currently simulated by the HELIOS model may also be influencing the results early in cycle and during any mid-cycle shutdowns that may occur.

The next cycle, 145B, was simulated after the 145A core was simulated. Fuel assembly isotopic values were again started from the current PDQ data base since none of the assemblies are common between cores. (Fuel is held out a cycle after discharge and reuse.) The power history is largely similar to the 145A cycle. The Eigenvalue trend in exposure and time are given in Figure 2-34. Learning from the 145A simulation, smaller time/exposure steps were selected for 145B. The number of reactivity control adjustments was also increased and includes most rod shim changes. These improvements may account

for the reversal of the in the trend line from a positive trend to a negative trend. The difference could also be dependent on core loading or the result of errors in either simulation. Further simulations and a consistent modeling approach will allow improvements to be made.

The intent of the cycle simulations is to develop a fuel data base for accurate performance predictions and to allow prediction of the eigenvalue trend throughout a given cycle for design purposes. Ideally the simulated core would have an eigenvalue of 1.0 at all times since it is always critical at power, by definition. However, differences inevitably exist at all levels of the simulation activities, physics, geometry, cross sections and measurement error, that drive the results away from 1.0. But having a predictable eigenvalue trend allows for a useful design tool for performance predictions. Initial results show good promise to provide useful core management and safety analysis.

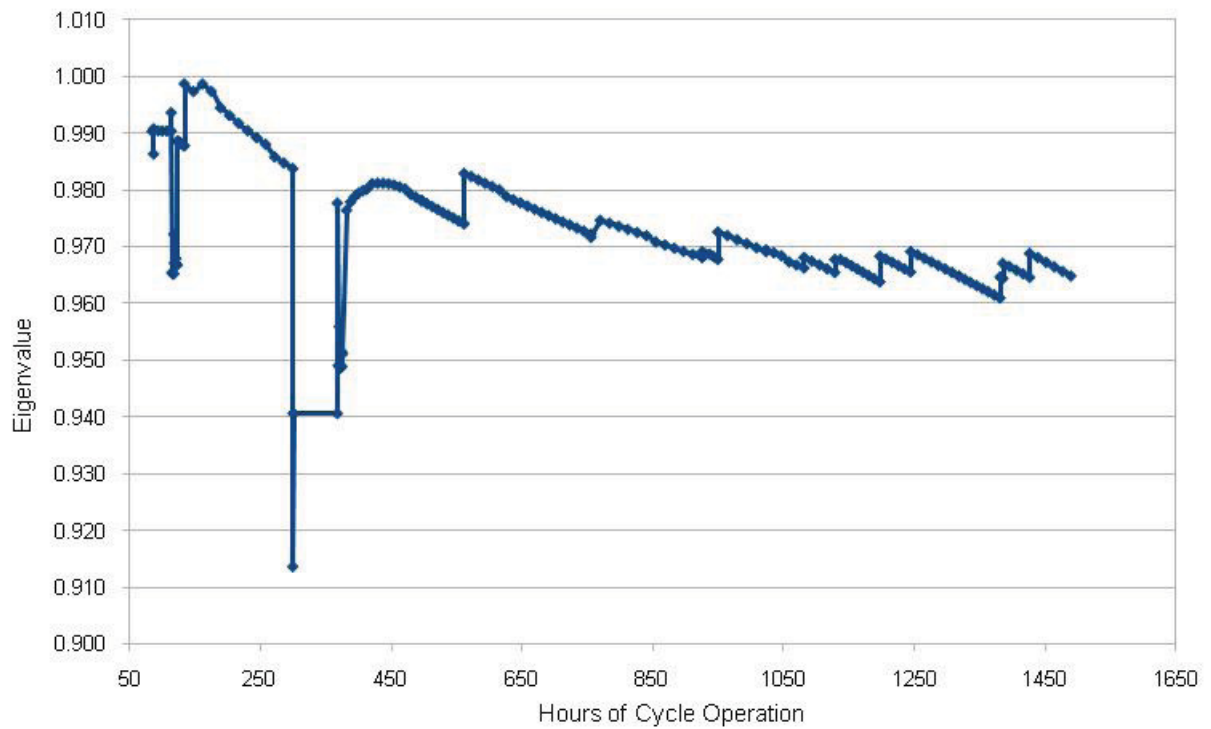
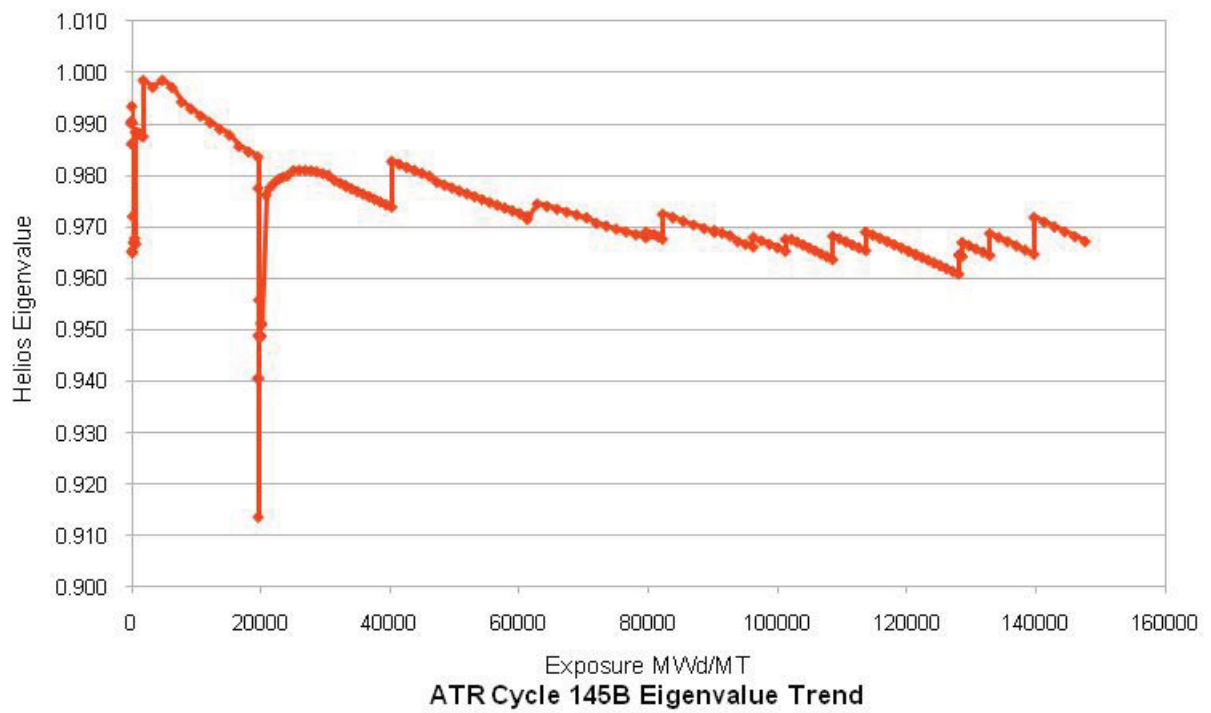


Figure 2-34. ATR Cycle 145B Eigenvalue Trend based on Exposure (top) and Time in Cycle (bottom)



### 2.2.3 Further Work

The results from the ATR model have been benchmarked and agree reasonably with results at this point with measured data and other codes. Progressively improving simulations of full ATR fuel cycles is ongoing. The computed radial (plate-to-plate) power profiles are very self consistent. The azimuthal (element-to-element) profiles differ more significantly and need to be calculated with exact control drum rotational positions and other improvements. The ATR model power shape is very sensitive to shim position in each of the models.

The addition of exposure steps and realistic fuel isotopic vectors during each cycle has allowed full fuel cycles to be simulated. The addition of realistic fuel that can be reloaded will start to further improve the model accuracy. A systematic and defined process to select exposure steps will also improve the accuracy of the core model.

The addition of more accurate experiment hardware models in the various flux traps and irradiation positions for each cycle continues. This will provide a realistic distribution of the azimuthal power distribution which is important to calculating accurate assembly exposures. The MICE flux trap is being updated to available data currently. Further improvements in other stations will occur going forward.

Changes to the input files will be made when possible to simplify changing the core model to reflect cycle-to-cycle configuration changes more easily. These changes will also facilitate configuration control of the model as it is migrated into routine production use. As a consistent set of models is developed the past cores will be rerun to create a self-consistent set of cycle models starting with the baseline Cycle 145A. This activity will establish the code performance and allow standardized computational procedures, configuration control, and quality assurance procedures to be defined.

## 2.3 ATR Model Development for RERTR Support

KENO-VI was introduced as an analysis tool for ATR primarily because the TSUNAMI-3D sensitivity analysis sequences support KENO-VI and its predecessor, KENO Va. While the value of information provided by TSUNAMI analyses is still being evaluated (preliminary work is reported in Section 2.6), the sensitivity data derived from that model is only as good as the KENO-VI representation itself. If the KENO-VI model has errors that alter the spectrum in the ATR core and ATR-C, sensitivity calculations may provide misleading results. Hence, before trying to extend this model to RERTR analysis, it is important to demonstrate the validity of the model for the existing fuel design.

A full model of the IRPhE benchmark specification for the ATR 94-CIC core configuration [Kim et al, 2008] has been developed using KENO-VI within SCALE 6.0. A CSAS6 criticality calculation was performed using the ENDF/B-VII-based 238-group library, yielding a  $k_{\text{eff}}$  value of  $1.00433 \pm 0.00064$ . This is within less than 0.5% of the measured critical state for the core, and provides a good integral assessment of the validity of the model. However, additional more localized validation is desirable. Other data available includes measured reactivity of outer shim control cylinders as a function of rotation angle, with MCNP- and NEWT-calculated worths. Additional fuel assembly data include relative assembly powers and plate-to-plate power distributions. Although the latter represents solely a code-to-code comparison, measurements in progress and reported herein will provide actual plate power distributions that will be used in direct validation in the future.

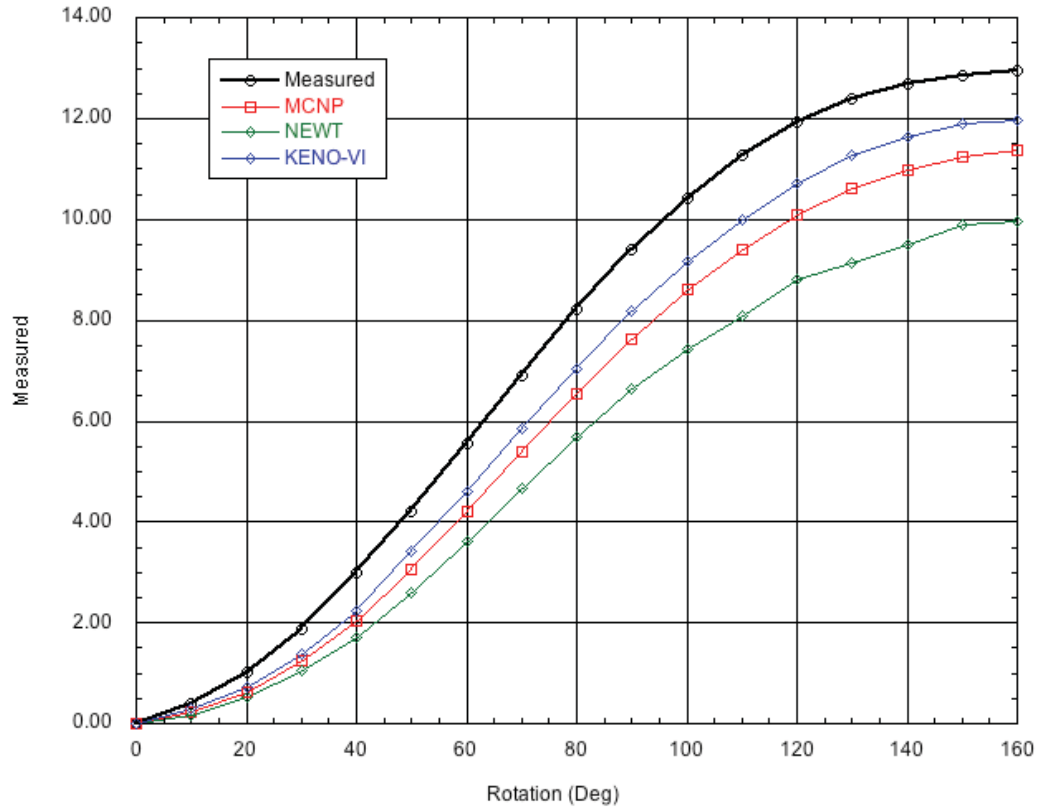


Figure 2-35. Measured and Computed Reactivity Worth as a Function of OSCC Rotation -  $\beta=0.0075$ .

The 94-CIC KENO-VI model was used to calculate the reactivity worth of ATR OSCCs as a function of rotation (all cylinders rotated to the same angle for each state point). Fig. 2-35 shows the results for the various codes. KENO-VI results are in very good agreement with measured data. Note that the discrepancy may result from the value of  $\beta_{\text{eff}}$  (0.00075) assumed for the reactivity calculations. A lower value of 0.00069 (which has also been used in ATR design calculations) brings the curves much closer together (see Fig. 2-36). Note however that the exact value of  $\beta_{\text{eff}}$  is not known and that the use of the value that shows the best match to calculations is not a valid basis for selection of this value. Instead, the lower value was shown to illustrate the uncertainty associated with the measurement process. In addition, one should note that the calculations do not exactly represent the precise core conditions. In the calculations, all drums were rotated to a given angle and an eigenvalue was calculated. In the core, the exact procedure is not known, although it is likely that some drums were counter-rotated to offset the reactivity increase, or regulating rods were repositioned, in order to maintain criticality. Total reactivity worth was inferred from the positioning required to maintain the critical state.

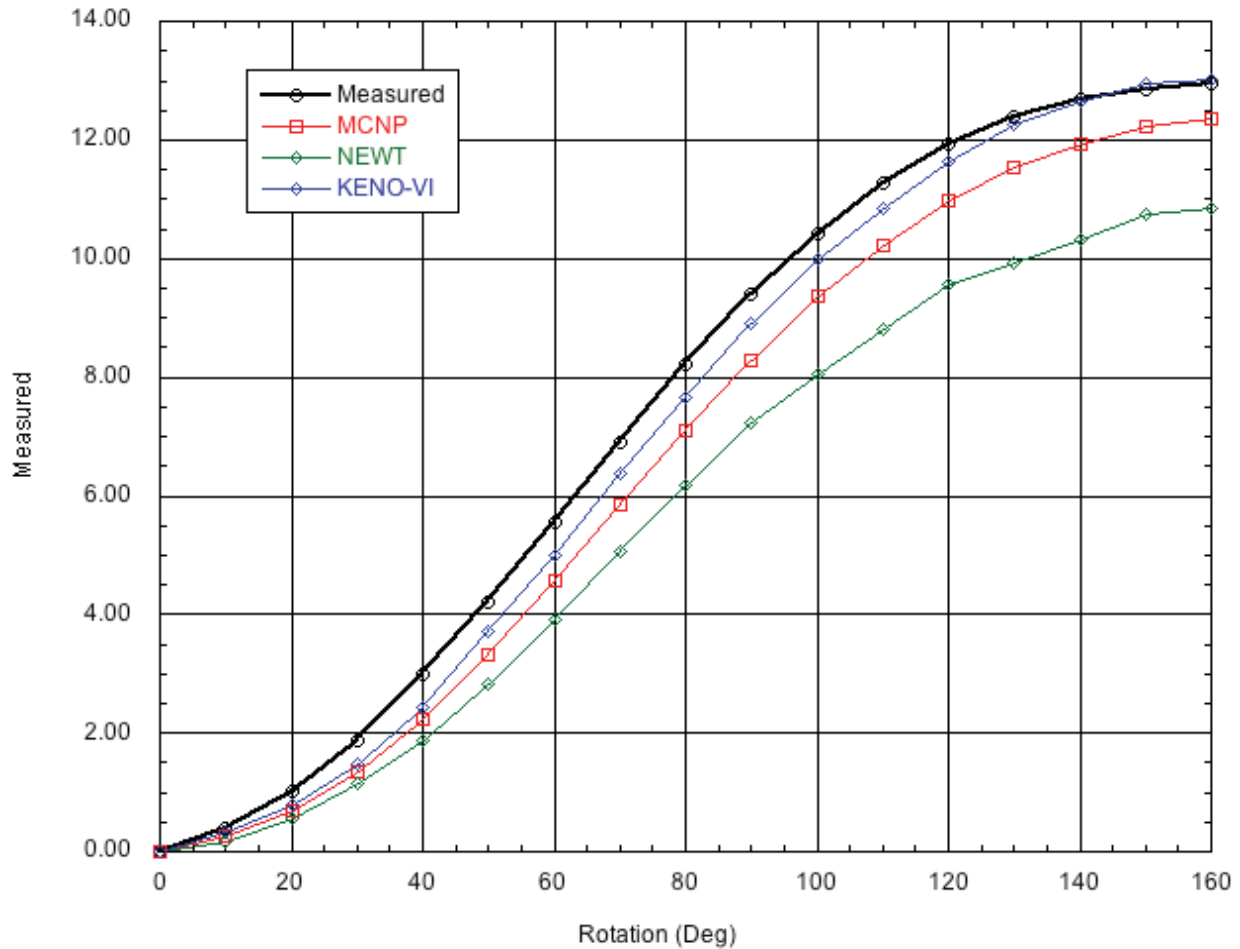


Figure 2-36. Measured and Computed Reactivity Worth as a Function of OSCC Rotation -  $\beta=0.0069$ .

Measurements of the power on a per-assembly basis for the 94-CIC configuration are also available, and calculations have been performed to estimate the power distribution around the core. Figure 2-37 provides a comparison of MCNP, NEWT, and KENO-VI results to measured data. The codes appear to be more self-consistent with clear departure from the high and low points in measured data.

Unfortunately, because these data are normalized, it is not possible to determine whether the differences occur at the four (NW, NE, SE, SW) fuel lobes nearest the control drums (lower dips in the plot) or the four inner flux traps (N, E, S, W), which are the four peaks, or both.

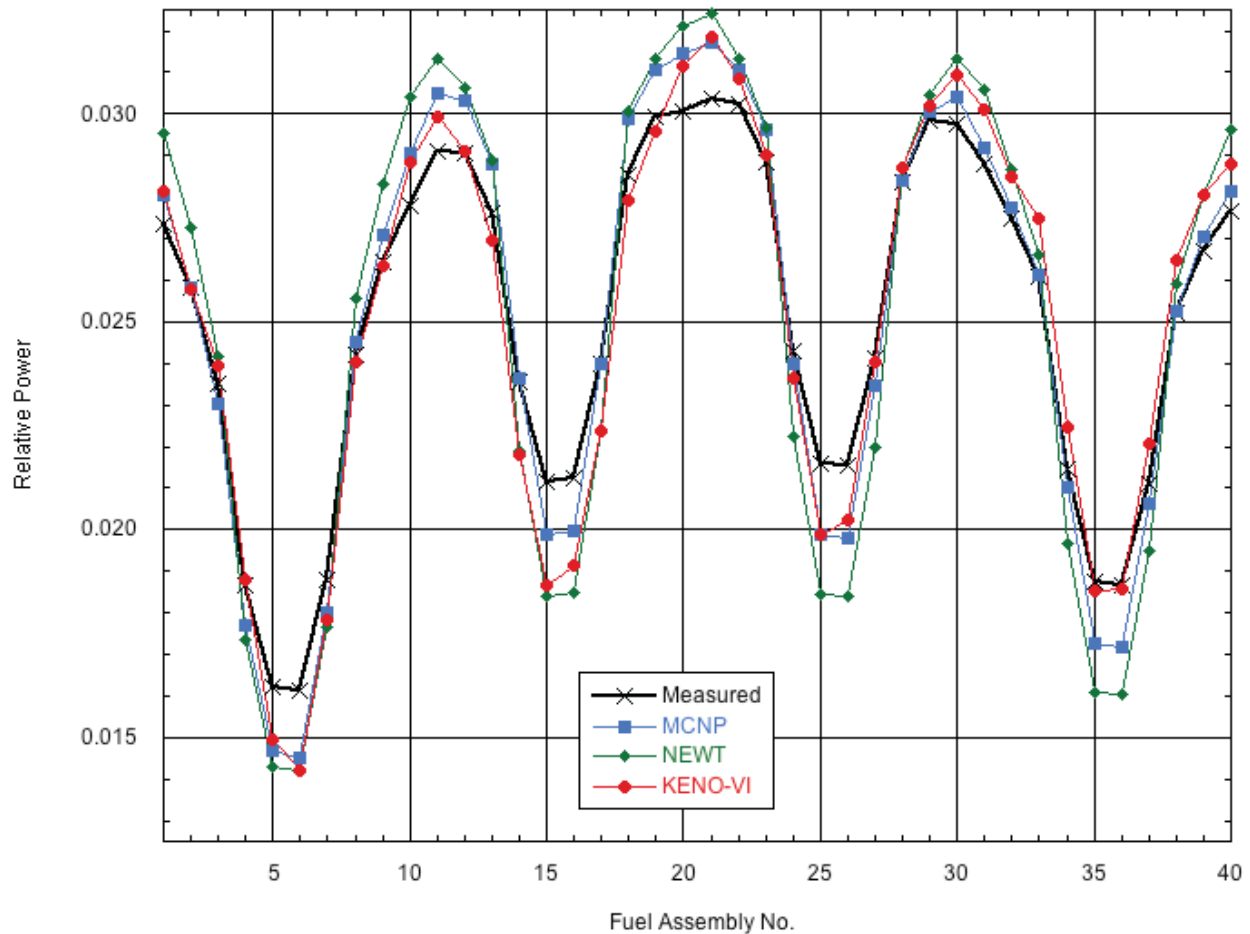


Figure 2-37. Measured and Computed Assembly Power Distribution in the 94-CIC ATR Core.

KENO-VI calculations appear to be consistent with other codes and in relatively good agreement measured data. However, an additional code-to-code comparison is possible, as calculations have been performed to study power distributions plate-by-plate within each assembly. Rather than provide 40 plots showing the power distribution per assembly, the results for each plate are averaged for all assemblies to provide the average assembly profile, as shown in Fig. 2-38. MCNP and KENO-VI are in good agreement over most of the assembly profile, with some difference seen at the inner (plate 1) and outer (plates 18 and 19) regions of the fuel assembly. The reason for the differences is not clear at present and is being studied, but overall the results are in reasonable agreement at this point in the overall model upgrade effort.

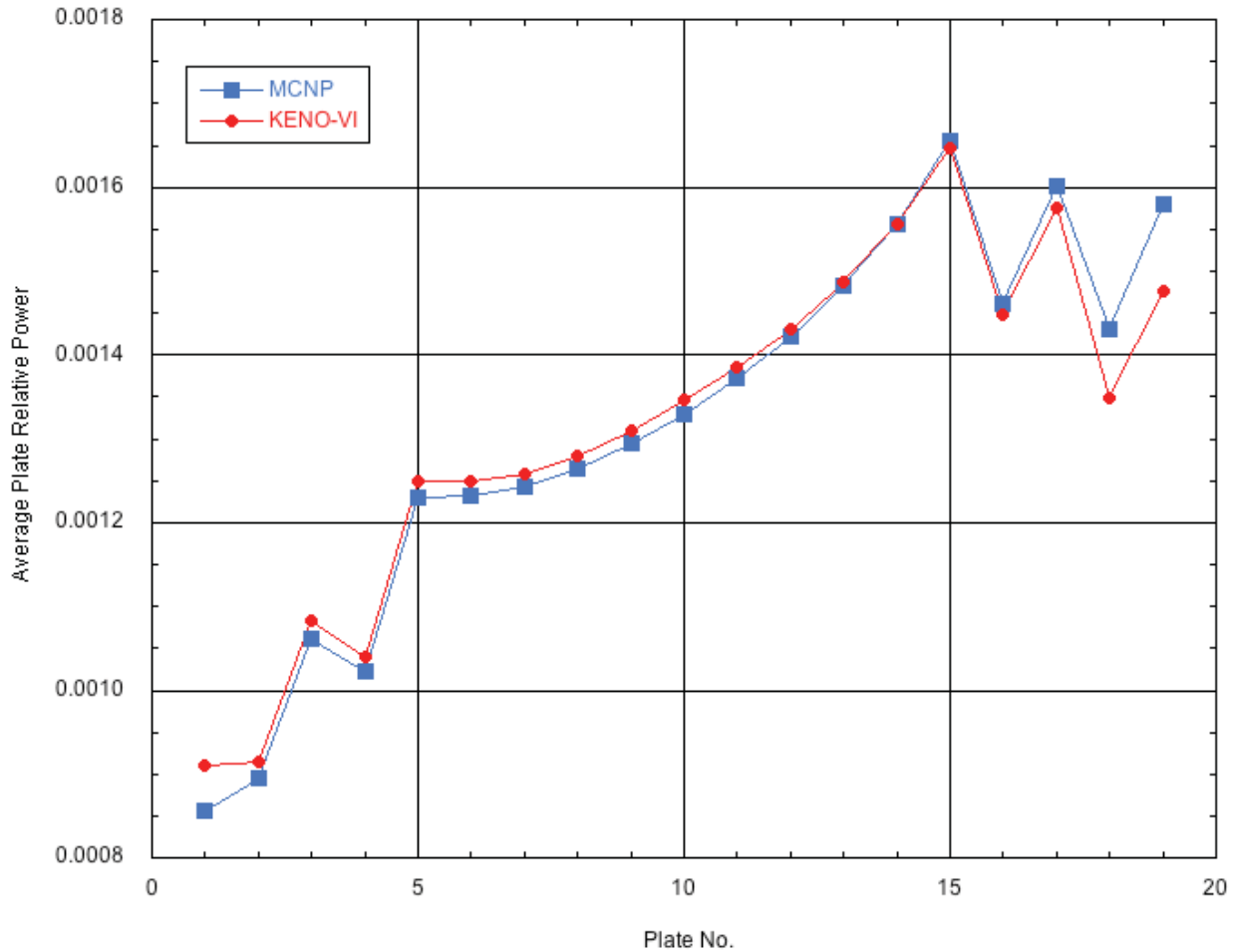


Figure 2-38. Average Plate Powers for 94-CIC ATR Core.

Based on the validation calculations, it has been assumed that the KENO-VI model is appropriate for use in further calculations. Thus, to proceed to RERTR support, a modified model has been developed to represent the expected fuel design for ATR testing.

The first full fuel element experiment for RERTR fuel is anticipated for in-core testing in late 2011/2012, first in ATRC and later in ATR.. This assembly, known as the RERTR Full-size Element (FE) test, is described in [Wachs, 2010]. In this model, plates 5-15 of a current ATR fuel element design are replaced with plates containing a 0.013cm thickness U-10Mo foil centered within a 0.05cm thick Al 6061 plate. The U-10Mo material is expected to be a monolithic mixture of 90 wt % uranium (enriched to 19.75%  $^{235}\text{U}$ ) and 10 wt % natural molybdenum. The current plan for the FE experiment is to place the test element in position 38 of the ATR-C. Once the assembly has been shown to behave as predicted from a neutron physics perspective, the assembly will be loaded into the same position in the ATR for at-power testing.

At this point, our focus is on the behavior of the FE element within the ATR-C. Hence, efforts have shifted to ATR-C modeling. Work in this area is described in Section 3.3.

## 2.4 Initial Sensitivity/Uncertainty Studies

In the comparison of computational methods to measured results, there are a number of sources of bias and uncertainty that result in differences between analysis and experimental measurement. Any measurement itself has an inherent uncertainty associated with it, and there are well-recognized methodologies for quantification of both the random and systematic components of this uncertainty. Computational methods also have a number of potential sources of bias and uncertainty, including approximations or limitations in the solution algorithm(s), convergence criteria or stochastic uncertainty, modeling approximations, and uncertainty associated with input data, especially nuclear cross section data.

Methods exist to address and quantify the magnitude of error associated with each of the above sources of uncertainty. In this section, methods used to quantify uncertainty associated with cross section data are evaluated. The TSUNAMI analysis sequence of the SCALE system has been used to evaluate computational biases that are caused by fundamental measurement uncertainties in the cross-section data, which are quantified in cross-section-covariance data files included with the basic international cross section data bases [Broadhead, 2004]. In the current work, version 6.0 of the SCALE was used with SCALE's ENDF/B-VII data library and 44-group covariance file. [Bowman, 2009].

As discussed in the previous section, a CSAS6 criticality calculation for the 1994 ATR CIC configuration yielded a value of  $k_{\text{eff}}$  of  $1.00433 \pm 0.00064$ . This model was used as the basis for a TSUNAMI-3D-K6 calculation to evaluate the effect of uncertainty in cross section data on the computed  $k_{\text{eff}}$  value.

Using the SCALE *44groupcov* covariance library, TSUNAMI calculates that the relative standard deviation of  $k_{\text{eff}}$  due to cross-section covariance data is  $0.4789 \pm 0.0001 \% \Delta k/k$ . This translates to a one standard deviation ( $1-\sigma$ ) uncertainty in  $k_{\text{eff}}$  due to cross section uncertainties for this core of  $\pm 0.004810$  with ENDF/B-VII data. This would indicate that the KENO-VI calculation is in very good agreement with the measured critical state of the ATR, within the expected  $1-\sigma$  distribution that is due to cross section uncertainty. Furthermore, TSUNAMI indicates that uncertainty is primarily due to uncertainties in  $^{235}\text{U}$ ,  $^1\text{H}$ , and  $^9\text{Be}$  nuclear data, with by far the largest effect due to uncertainty in the evaluation of the average number of neutrons per fission ( $\nu$ -bar) in  $^{235}\text{U}$ . Sensitivity contributions as a function of energy are shown in Fig. 2-39.

This TSUNAMI-3D analysis is the first step of a process to determine the neutronic similarities and differences between the ATR and the ATRC. In a TSUNAMI-3D calculation, the sequence produces a sensitivity data file containing the sensitivity of  $k_{\text{eff}}$  to each reaction of each nuclide on a group-wise basis. Additionally, the sensitivity of  $k_{\text{eff}}$  for each nuclide and each reaction of each mixture and material zone are available on a group-wise basis. This data file is formatted for further analysis with TSUNAMI-IP. TSUNAMI-IP uses the sensitivity data computed by TSUNAMI-3D to produce relational indices and other parameters that are used to assess the similarity of systems. These similarity measures are intended to determine the applicability of a benchmark experiment for the code validation of a design system. Similarity can be assessed on a "global" basis where all nuclides and reactions are considered, on a reaction-specific basis, where only a single reaction (i.e. all fission in the systems) is considered, and on a nuclide-reaction specific basis, where only a single reaction a single nuclide (i.e. n,alpha reaction for  $^{10}\text{B}$ ) is considered. [Williams, 2008]



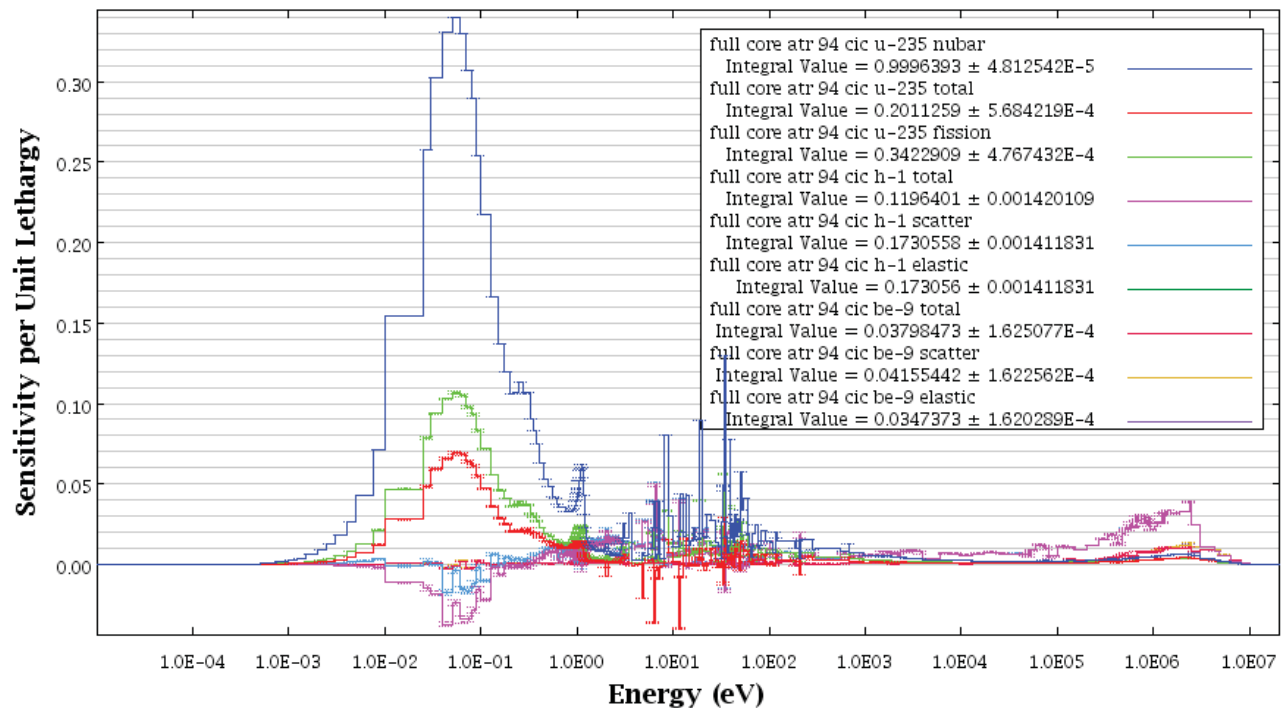


Figure 2-39. Energy-dependent sensitivity coefficients for the largest contributors to uncertainty in the ATR 94-CIC configuration.

Section 3.4 of this report describes generation of sensitivity coefficients for the ATR-C, and the use of the TSUNAMI-IP sequence to compare the sensitivity behaviors of ATR and ATR-C. However, an opportunity was presented to take advantage of these sensitivity analysis capabilities in the form of a proposed molybdenum measurement under the auspices of the International Criticality Safety Benchmark Evaluation Project (ICSBEP). A new experiment has been proposed based on earlier cross section evaluation work performed in Russia for tungsten. The experiment, published as HEU-MET-MIXED-017 [Briggs, 2010], consisted of alternating disks of tungsten foils and highly enriched uranium fuel separated by polyethylene disks. It has been proposed to replace the tungsten foils with molybdenum foils to determine the critical height of a similar stack. The question that arose was how relevant would such an experiment be in term of characterizing the behavior of the U-10Mo fuel being designed under the RERTR program.

To validate a KENO-VI model, the configuration described in [Briggs, 2010] was created and a KENO-VI criticality calculation performed. This model resulted in a predicted eigenvalue of  $1.00071 \pm 0.00082$ . Satisfied that KENO-VI could adequately model the system, the model was altered by replacing the tungsten with natural molybdenum and recalculating. As expected, based on reported Russian calculations, this core was significantly more reactive. Thus, the stack was revised by removing sets of fuel/polyethylene/molybdenum/polyethylene disks from the top and bottom halves to get closer to critical (slightly supercritical). The gap separating the top and bottom halves of this hypothetical core was then increased in order to bring the system closer to a critical state. Figure 2-40 shows the new configuration - the two blue shades represent the two slightly different compositions of polyethylene used in the actual experiment, the red disks represent the fuel, and the thinner yellow/brown disks are molybdenum. Note that due to the scoping nature of this work, no effort was made to center the core or line up with the

spacing diaphragm as would be done in the actual experiment – it was felt that the sensitivity response would not be affected by this approximation. The pictured configuration resulted in a  $k_{\text{eff}}$  value of  $1.00089 \pm 0.00093$ .

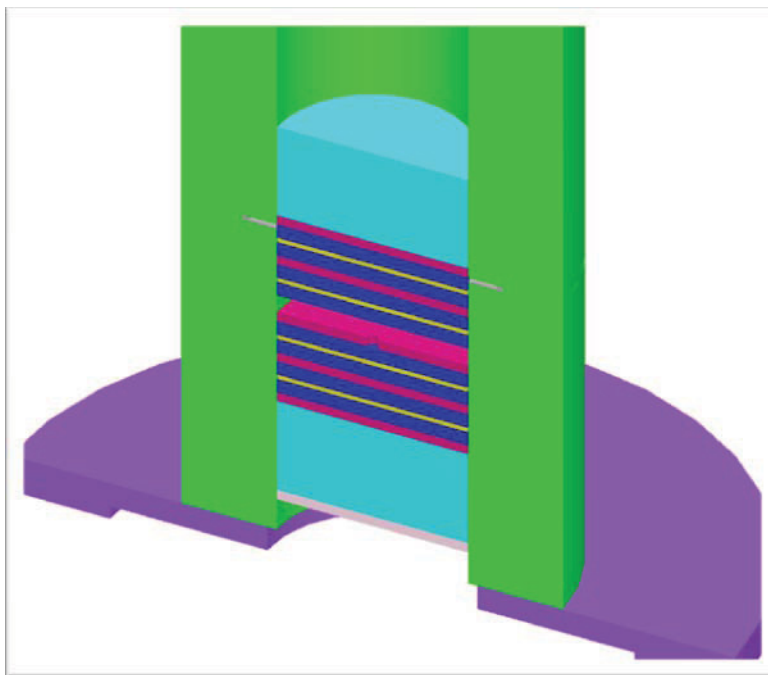


Figure 2-40. Possible critical experiment for Mo validation.

As with the ATR calculation described earlier, the KENO-VI model above was used as the basis of a new TSUNAMI-3D-K6 calculation to generate a sensitivity data file for this core.

The next step in the process was to use the TSUNAMI-IP sequence to analyze and compare the two sensitivity data files in order to assess similarities within the systems. TSUNAMI-IP uses the files to produce relational indices and other parameters that are used to assess the similarity of systems. These similarity measures are intended to determine the applicability of a benchmark experiment for the code validation of a design system. Note that similarity can be assessed on a "global" basis where all nuclides and reactions are considered, as well as on a reaction-specific basis, where only a single reaction is considered, or on a nuclide-reaction specific basis, where only a single reaction a single nuclide is evaluated. In this case, the indices will be used to assess the applicability of the proposed molybdenum experiment as described above relative to a U-10Mo fuelled version of the ATR.

The results of the TSUNAMI-IP calculation were not encouraging. Three correlation indices, referred to as  $c_k$ ,  $E$ , and  $G$ , are produced by a TSUNAMI-IP calculation, all with different physical interpretations, but all characterizing some form of similarity between systems. Identical systems will return index values of 1.0; systems that have similar sensitivities and thus respond to cross section modeling in a similar fashion should have indices of greater than 80-90%. There is no precise cutoff for applicability – at this point, engineering judgment must be applied.

The three calculated indices for the ATR vs the proposed Mo experiment are provided below, with a brief description of the meaning of each index. The TSUNAMI User's Manual [Bowman, 2009] provides more detail in the derivation and meaning of each term.

$c_k=0.4860$ ,  
 $E=0.6808$ ,  
 $G=0.4439$ ,

where  $c_k$ , or correlation coefficient index, is a measure of the similarity of the systems in terms of related uncertainty;  $E$  is the cosine of the angle between the two sensitivity vectors for the analyzed systems, and does not use covariance data; and  $G$  is the ratio of the sum of the sensitivity coefficients of the application that are covered by the experiment to the sum of the sensitivity coefficients for the application based on normalized differences in the energy-dependent sensitivity data for fission, capture, and scatter.

Note that these are global indices representing the similarity of the two complete systems as a whole. For ATR methods/data validation, only similarity of molybdenum within the systems is of interest. The two systems are comprised of different materials (chiefly the polyethylene in the experiment vs. the beryllium in the ATR). But it was felt that perhaps the spectrum within the Mo regions is similar enough that the Mo would respond in a similar manner in the two systems. To assist in such an evaluation, TSUNAMI provides  $c_k$  and  $G$  indices per reaction type in each nuclide in each system. Due to ambiguity in the interpretation of  $c_k$  reaction indices this index was not studied further for Mo. Additional training in the use of calculated tables may be necessary for proper interpretation of the results.

The  $G$  index calculated by TSUNAMI-IP on a nuclide-reaction basis is listed in Table 2-3.

Table 2-3. Nuclide/Reaction Specific  $G$  Indices for ATR vs a Potential Mo Experiment

Reaction → Nuclide ↓	$n,\gamma$	Elastic scatter	$n,n'$
<sup>92</sup> Mo	1.0000	0.4000	0.9999
<sup>94</sup> Mo	0.9999	0.4329	1.0000
<sup>95</sup> Mo	0.7636	0.4327	0.9942
<sup>96</sup> Mo	0.9998	0.7731	1.0000
<sup>97</sup> Mo	0.9999	0.6061	1.0000
<sup>98</sup> Mo	1.0000	0.6120	1.0000
<sup>100</sup> Mo	1.0000	0.5271	1.0000

These results indicate that the experiment provides an acceptable level of “coverage” of almost all ( $n,\gamma$ ) and ( $n,n'$ ) reactions (except  $n,\gamma$  in <sup>95</sup>Mo). However, the  $G$  values for elastic scattering for the various Mo nuclides are all well below 0.8. This would be a good sign overall if scattering was a small component of all reactions, but that is unlikely. To assess the relative importance of each reaction type in the ATR core, the KENO-VI model was again used to calculate activities for these reactions, summed over all fuel elements. Table 2-4 shows the reaction rate for each reaction type per source neutron. Not surprisingly, elastic scattering in Mo is the dominant reaction, by two orders of magnitude; hence the  $G$  values reported in Table 2-4 indicate poor coverage of Mo cross sections in ATR by the conceptual Mo experiment.

Table 2-4. Relative Molybdenum Reaction Rates in ATR

<b>Reaction → Nuclide ↓</b>	<b>n,γ</b>	<b>Elastic scatter</b>	<b>n,n'</b>
<sup>92</sup> Mo	1.02E-04	1.53E-02	5.58E-04
<sup>94</sup> Mo	1.18E-04	9.41E-03	5.89E-04
<sup>95</sup> Mo	5.82E-03	1.98E-02	1.66E-03
<sup>96</sup> Mo	4.42E-04	1.72E-02	1.23E-03
<sup>97</sup> Mo	8.80E-04	9.88E-03	9.92E-04
<sup>98</sup> Mo	6.01E-04	2.45E-02	1.82E-03
<sup>100</sup> Mo	1.51E-04	9.79E-03	8.36E-04
<b>Total</b>	<b>8.11E-03</b>	<b>1.06E-01</b>	<b>7.69E-03</b>

These results do not necessarily mean that the experiment cannot be used in ATR methods validation – it simply means that this particular configuration is not especially valuable for ATR validation. Inspection of the experiment shows that the fuel and molybdenum plates are separated by polyethylene in the experiment, while the U and Mo are integrally mixed to form the fuel in the ATR. Hence, an experiment where the U and Mo fuel plates are adjacent would perhaps be more representative of the ATR design. A second configuration was developed where fuel and molybdenum plates are in direct contact, and the interstitial poly regions between the two removed, as shown in Fig. 2-41. Again, this system was sized to be close to critical ( $k_{\text{eff}} = 0.9969 \pm 0.0029$ ).

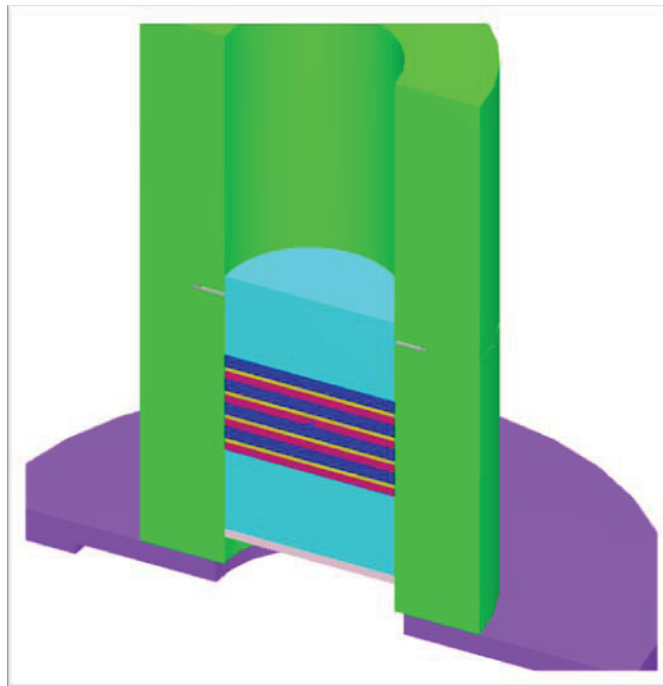


Figure 2-41. Potential alternate configuration for Mo experiment.

Unfortunately, this configuration showed no significant improvement. Neither did other configurations tested (less Mo, more poly, etc.) show any real improvement.

These computational experiments were developed by limiting the components of the experiments to those used in previous real experiment, maintaining the fuel enrichment and disk thicknesses reported in the benchmark. A departure was taken that created a fuel that contained 10% Mo homogenized within the fuel. This, unfortunately, resulted in even lower global and isotopic indices.

It is suspected that the behavior is due not to the Mo placement, but to the fuel itself. The actual experiment used fuel enriched to 96% in  $^{235}\text{U}$ , whereas the ATR model is based on 19.75% enriched fuel. To test this hypothesis, the original KENO-VI model was modified to use 19.75% fuel in place of the original highly enriched uranium. Holding everything else constant, the code predicts a substantially subcritical system ( $k_{\text{eff}} = 0.7707$ ). However, if one assumes that the subcritical sensitivity would be similar to the critical sensitivity, then a sensitivity comparison might be telling. Thus, SDFs were generated for this model and TSUNAMI-IP again used to generate integral indices. This case showed marked improvement in all global indices:

$$\begin{aligned}c_k &= 0.6511 \\ E &= 0.8996 \\ G &= 0.6088\end{aligned}$$

Intrigued by these results, we then endeavored to determine whether the global indices would be improved by taking the system to a critical state. The radii of all components of the experiment were increased by 11 cm (Fig. 2-42) to take the system to a critical configuration. Not necessarily optimized, but critical. With the same 19.75 wt % fuel, the global indices do improve slightly:

$$\begin{aligned}c_k &= 0.7212 \\ E &= 0.8962 \\ G &= 0.6266\end{aligned}$$

The nuclide-specific indices show similar improvement. This is still not the optimum experiment for ATR validation, but perhaps this indicates that such an experiment is possible and can be designed in this manner. These results also indicate that the sensitivity coefficients themselves do not necessarily require a critical spectrum to do a first order comparison

It was concluded that the proposed molybdenum experiment based on HEU-MET-MIXED-017, modified to achieve criticality with Mo plates, would have little value in the validation of ATR calculational methods and data, due to the HEU fuel used in the experiments. However, it does appear possible to use this process to study other candidate critical experiments to determine their relevance for ATR methods validation.

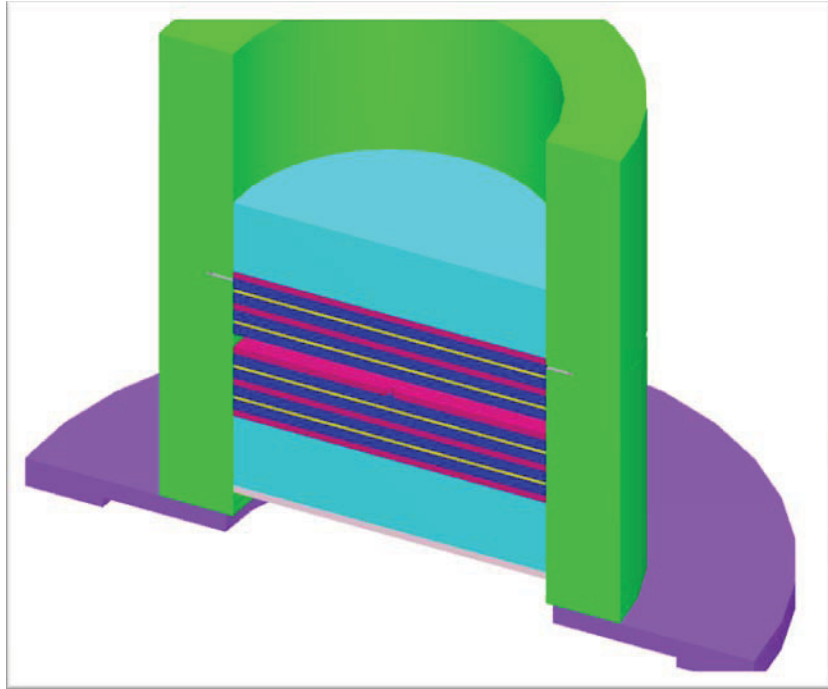


Figure 2-42. Low enrichment experiment with increased radial dimensions.



### **3.0 HIGH FIDELITY TRANSPORT THEORY MODELS OF THE ATR CRITICAL FACILITY**

The ATRC will serve as an essential validation tool during the ATR Core Modeling Update project. It is nearly identical to the ATR in terms of neutronic similarity, and code validations performed using ATRC measurements can be reliably extrapolated to the ATR in most cases. The ATRC is also expected to become a valuable tool for reactor physics experiments as the ATR NSUF continues to evolve into an internationally-recognized resource, and it will be used to support the conversion of the ATR to LEU fuel under the RERTR program. Accordingly, models of the ATRC have also been developed using the suite of transport codes described earlier.

#### **3.1 NEWT 2D Model of the ATRC**

A full core two-dimensional (2D) model of the Advanced Test Reactor Critical Facility (ATRC) was generated for the NEWT computer code. The model is based on the information provided in the ATR Critical Facility Core Reconfiguration (McCracken et al. 1994). Four different ATRC core configurations were modeled in NEWT. The four configurations were designated as 94-1, 94-2, 94-2', and 94-3. Configurations 94-1 and 94-2 use what is designated as standard ATRC fuel elements which nominally contain 975 g of U-235. Each plate contains boron as a burnable poison. Configurations 94-2' and 94-3 both use what is designated as zone loaded fuel elements which are the standard ATR Mark VII fuel elements. There are 3 different experiment loadings for the four core configurations. The experiment loading for configurations 94-2 and 94-2' are identical. The experiment loading for 94-2 and 94-2' is different than the experiment loadings for configurations 94-1 and 94-3.

##### **3.1.1 ATRC Model Results for the Initial Critical State**

A NEWT 2D model of the ATR Critical facility (ATRC) was generated. This model was run for four different ATRC core configurations. Graphical representations for all three core configurations (94 CIC, 94-2, 94-3) are shown below with the results from the analysis. The displayed results show the model run time, the calculated eigenvalue for each configuration, core average plate powers, and the fuel element powers. Also displayed are the outer shim control cylinder (OSCC) worth curves for each core configuration overlaid with the measured OSCC worth curves. The ATRC core configurations not displayed in the side by side comparison with the ATR 94 CIC below are the 94-1 and 94-2' configurations. Results for the 94-1 and 94-2' analyses are shown after the three configuration side by side comparison.

### NEWT Model of the ATRC

**Core Number:** 94-1

**Reference:** R. T. McCracken, L. S. Loret,  
“Results of ATR Critical Facility Core  
Reconfiguration and Requalification Testing for  
Post-Core Internals Changeout Operation,”  
Report No. PG-T-94-006, EG&G Idaho, Inc.,  
June 1994.

**K** = 0.9942

**Run Time:** ≈40 hours

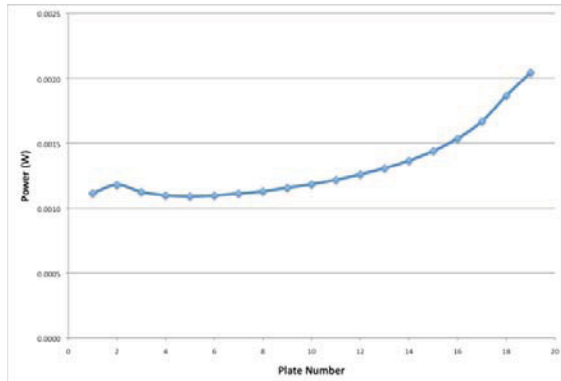


Figure 3-1. ATRC 94-1 average plate powers.

### NEWT Model of the ATRC

**Core Number:** 94-2'

**Reference:** R. T. McCracken, L. S. Loret,  
“Results of ATR Critical Facility Core  
Reconfiguration and Requalification Testing for  
Post-Core Internals Changeout Operation,”  
Report No. PG-T-94-006, EG&G Idaho, Inc.,  
June 1994.

**K** = 0.9921

**Run Time:** ≈38 hours

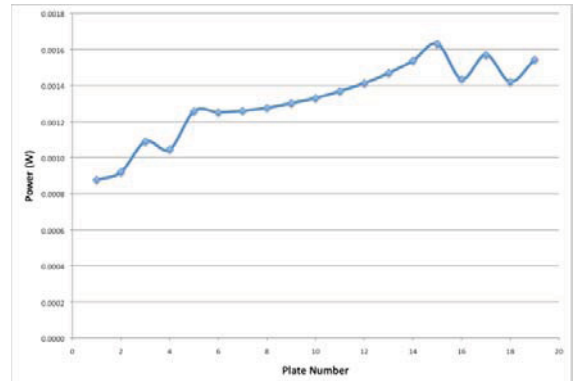


Figure 3-2. ATRC 94-2' average plate powers.

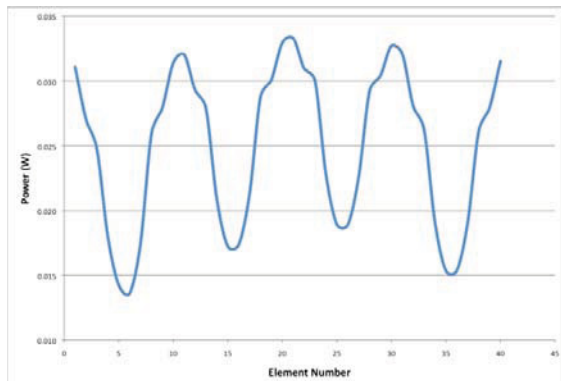


Figure 3-3. ATRC 94-1 fuel element powers.

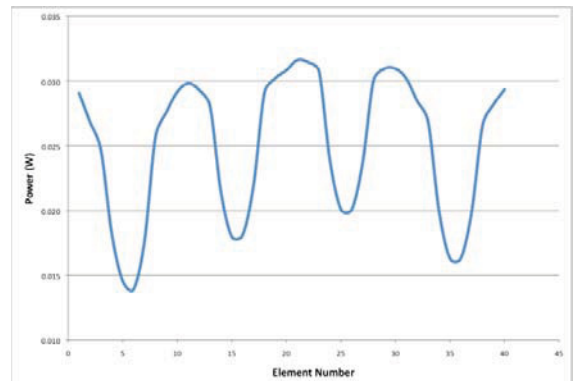


Figure 3-4. ATRC 94-2' fuel element powers.

### NEWT Model of the ATRC

**Core Number:** 94-2

**Reference:** R. T. McCracken, L. S. Loret,  
“Results of ATR Critical Facility Core  
Reconfiguration and Requalification Testing for  
Post-Core Internals Changeout Operation,”  
Report No. PG-T-94-006, EG&G Idaho, Inc.,  
June 1994.

**K** = 0.9895

**Run Time:** ≈38 hours

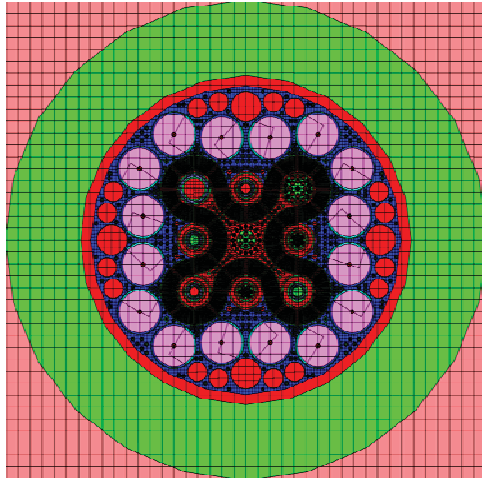


Figure 3-5: ATRC 94-2 core configuration.

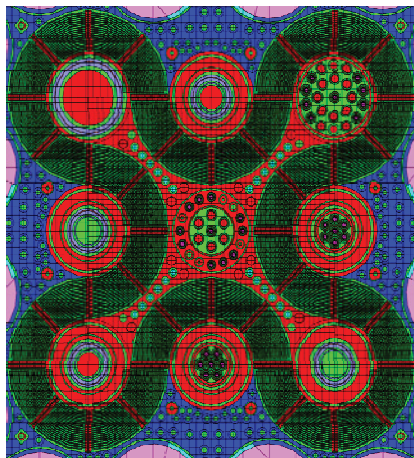


Figure 3-6: ATRC 94-2 core configuration.

### NEWT Model of the ATRC

**Core Number:** 94-3

**Reference:** R. T. McCracken, L. S. Loret,  
“Results of ATR Critical Facility Core  
Reconfiguration and Requalification Testing for  
Post-Core Internals Changeout Operation,”  
Report No. PG-T-94-006, EG&G Idaho, Inc.,  
June 1994.

**K** = 0.9908

**Run Time:** ≈40 hours

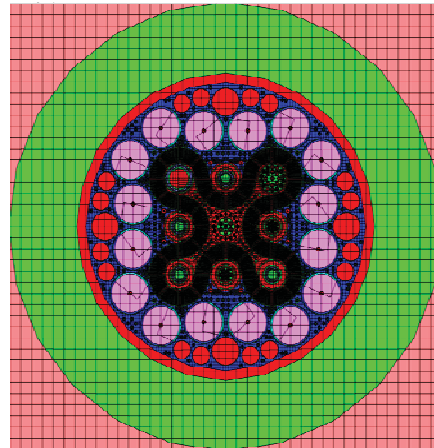


Figure 3-7: ATRC 94-3 core configuration.

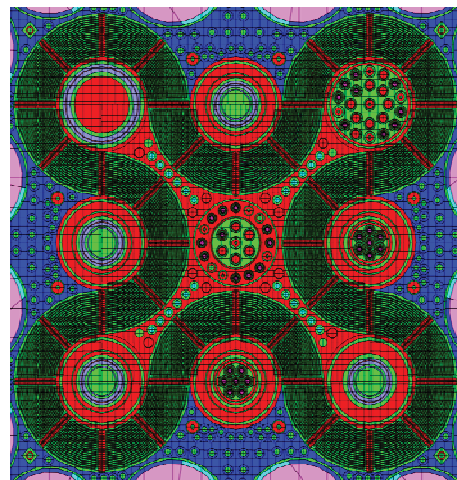


Figure 3-8: ATRC 94-3 core configuration.

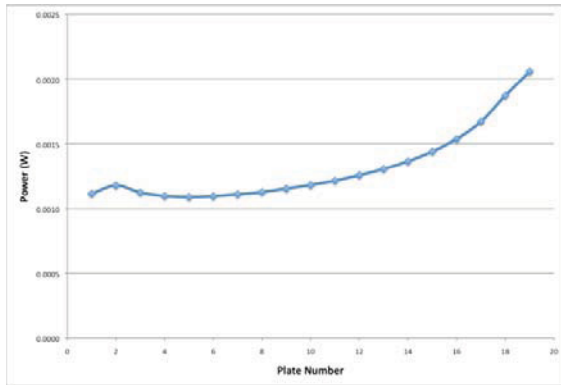


Figure 3-9: ATRC 94-2 average plate powers.

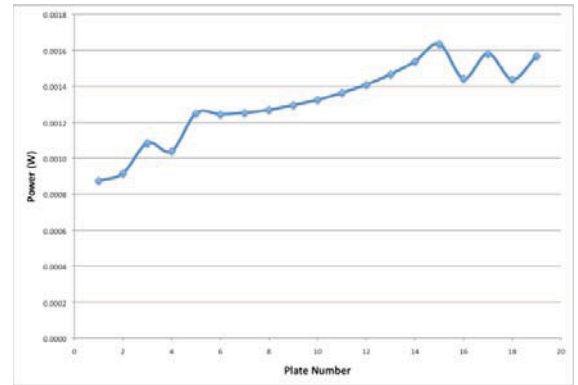


Figure 3-12: ATRC 94-3 average plate powers.

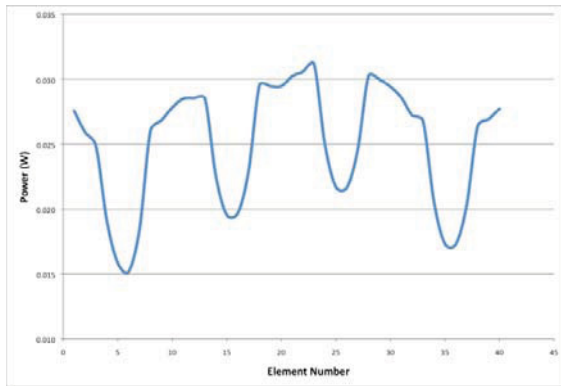


Figure 3-10: ATRC 94-2 fuel element powers.

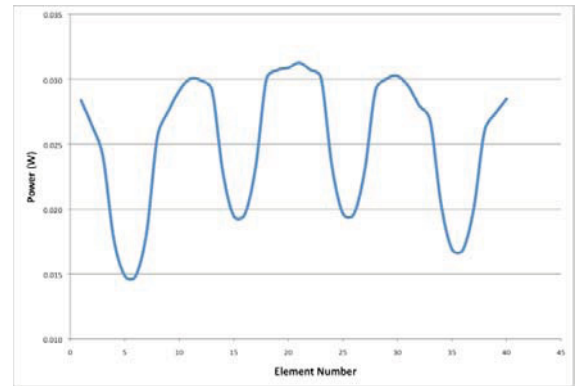


Figure 3-13: ATRC 94-3 fuel element powers.

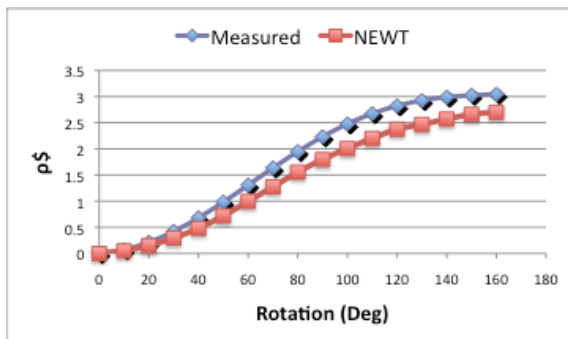


Figure 3-11: ATRC 94-2 OSCC worth curves.

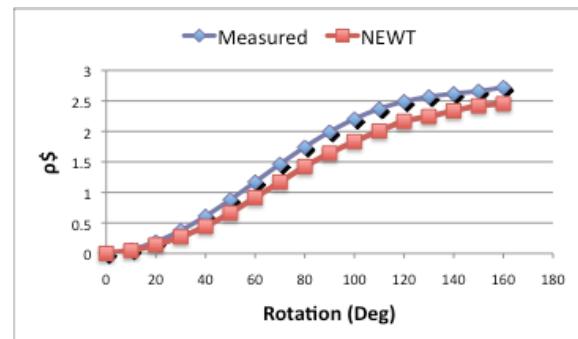


Figure 3-14: ATRC 94-3 OSCC worth curves.



### 3.1.2 NEWT Model for Validation Experiment Support

NEWT will be used to support the ISU/INL NEUP instrumentation experiments in the ATRC. NEWT is able to calculate neutron flux and neutron reaction rates for materials in the ATRC. The NEWT model of the ATRC will be modified to represent the different experiment configurations and provide the neutron flux spectrum and neutron reaction rates needed to perform the spectral unfolding for the neutron activation experiments.

The NEWT model of the ATRC has been modified to include flux wire positions in the ATRC fuel elements (see Figure 3-15). A neutron spectrum and neutron reaction rates for each of the modeled flux wires will be calculated in NEWT for spectral unfolding calculations. The experiment apparatus for the NW IPT will also be modeled to provide the same needed information for the activation experiments irradiated in the NW IPT of the ATRC.

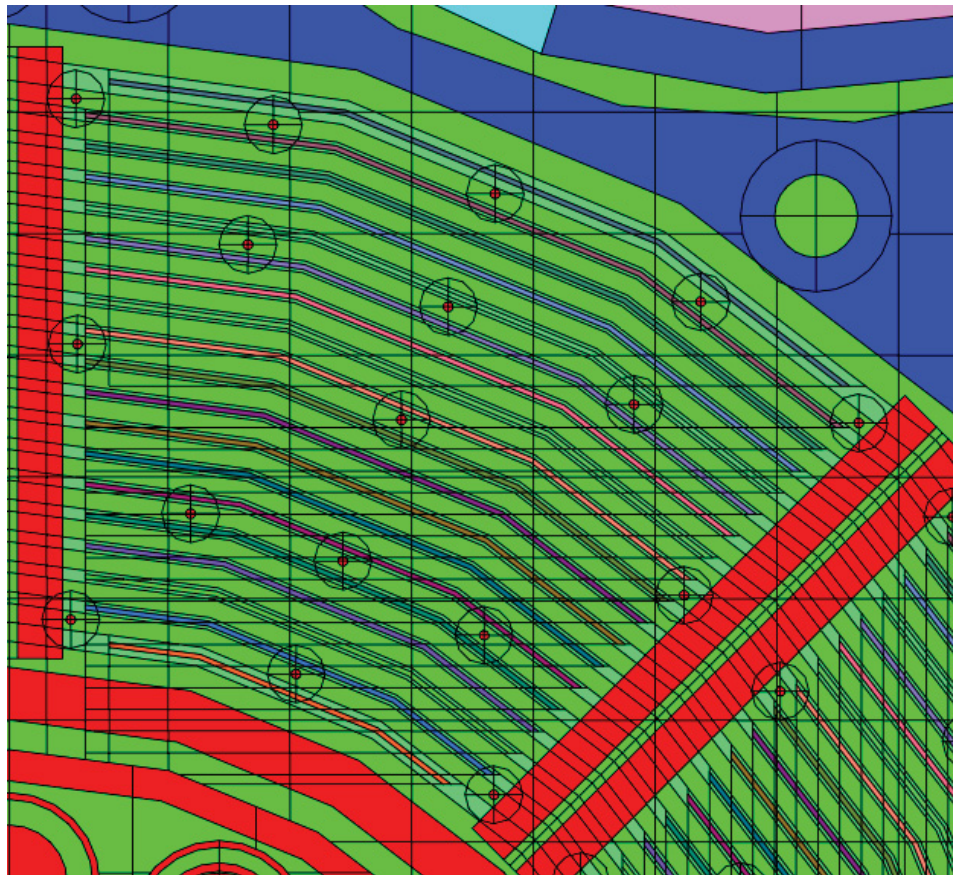


Figure 3-15: NEWT model of the ATRC showing flux wire modeling in the fuel element coolant channels.

### 3.2 MCNP Model for Validation Experiment Support

The MCNP code has been used routinely for ATR experiment design and performance modeling for many years. As noted previously it also serves as a verification tool for new reactor core models developed under the ATR Core Modeling Update Project.

#### 3.2.1 Description of MCNP Code and Model

MCNP5 is a general-purpose Monte Carlo N-Particle code (Breisemeister 1999) that can be used for neutron, photon, electron, or coupled neutron-photon-electron transport, including the capability to calculate eigenvalues for critical systems. It treats an arbitrary three-dimensional configuration of materials in geometric cells bounded by first, second, and in some cases forth-degree polynomial surfaces. Continuous or discrete cross-section data are used. For neutrons, all reactions in particular cross-section evaluations are considered. For photons, the code takes into account incoherent and coherent scattering, the possibility of fluorescent emission following photoelectric absorption, and absorption in pair production with local emission of annihilation radiation. A continuous slowing down model is used for electron transport that includes positron, k-shell x-rays, and bremsstrahlung, but does not include the effects of external or self-induced electromagnetic fields. Photonuclear physics is available for a limited number of isotopes. Important standard features that make MCNP very versatile and easy to use include a powerful general source, criticality source, and surface source; both geometry and output tally plotters; a rich collection of variance reduction techniques; a flexible tally structure; and an extensive collection of cross-section data. Energy ranges are from 10<sup>-11</sup> to 20 MeV for neutrons with data up to 150 MeV for some nuclides, 1 keV to 1 GeV for electrons, and 1 keV to 100 GeV for photons.

The MCNP model used to support the validation experiments described in this Annual Report was based on the full core ATR model documented in Reference (Kim et al., 2008). Although ATRC is not totally identical in design to ATR, the differences are minor and the model for ATR is applicable in estimating the reactivity worth of experiments. The calculated reference eigenvalue for the ATR full core model was 0.99854 which is based on a known and documented critical configuration. A full core 3-dimensional model of the ATRC is currently under development.

#### 3.2.2 MCNP Experiment Support Computations

Details of specific ATRC experiment support computations performed during FY-10 are provided in the following sections.

##### 3.2.2.1 Northwest Large In-Pile Tube Reactivity Insertion

Figure 3-16 shows the test train that will be inserted in the ATRC Northwest Large In-Pile Tube (NW-LIPT) for the activation measurements (Nigg 2010). There are two insert fittings that will go into the standard midplane section of the test train. On the left (Case 1) is a fitting to hold either bare or cadmium-covered activation foils that are primarily sensitive to the thermal and epithermal neutron energy range. On the right (Case 2) is a device that will hold a hollow boron-10 sphere containing several types of threshold activation foils at the same axial position. Both insert fittings (Cases 1 and 2) are made of aluminum and have the same mass, with the remaining space in the cylindrical test train section filled with water.



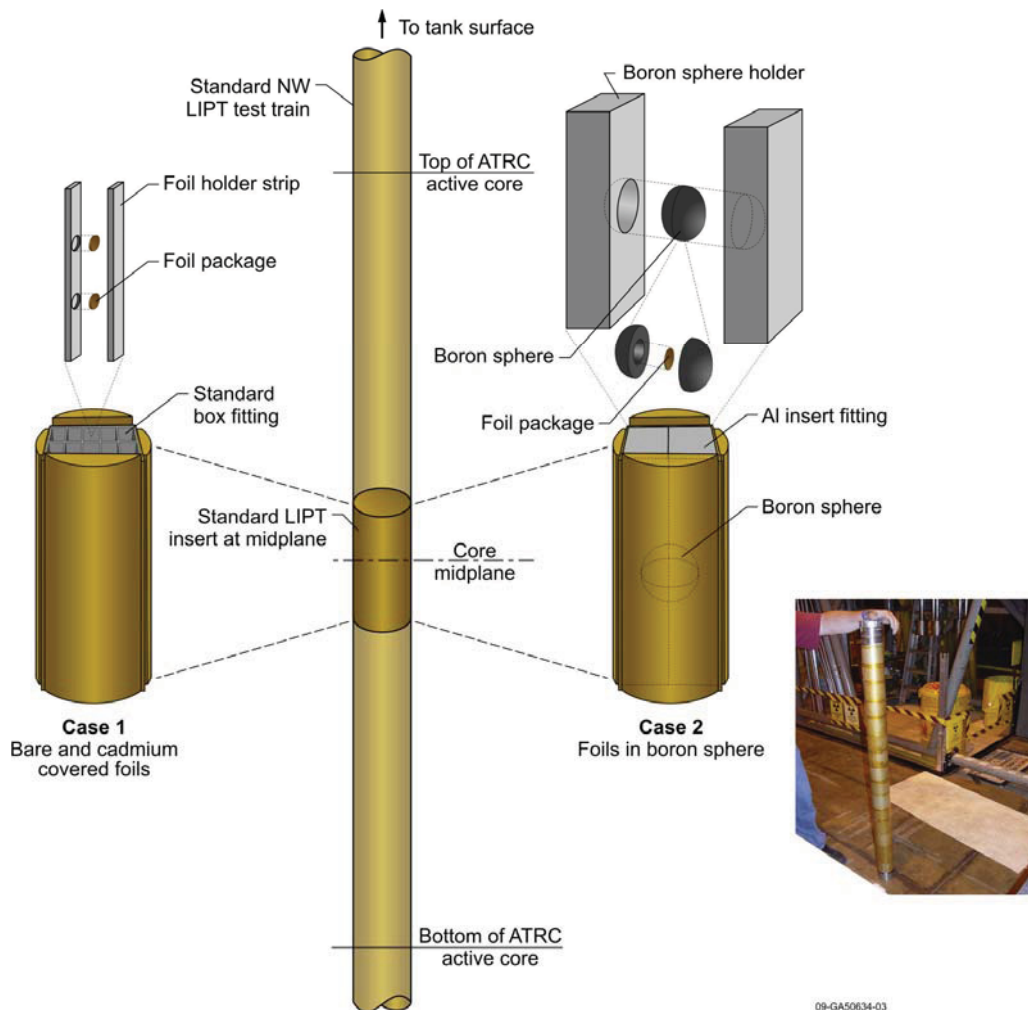


Figure 3-16. Positioning of the activation detector apparatus in the ATRC NW IPT Test Train (the inset photo shows the entire test train assembly).

The test assembly calculations included several cases. The first case is the ATR 1994 CIC reference to critical (Kim et al., 2008). The second case models a water-filled NW flux trap, which makes the system about a dollar less reactive. The third case includes the test train insert with the Case 2 midplane insert and its internal fitting (right side of Figure 3-16) in the NW flux trap modeled as a solid volume of aluminum with height of 17.78 cm (7", see Drawing 602321) and a radius of 5.07 cm, and with a spherical cavity with a radius of 2.413 cm located in the center of the insert fitting at core mid-plane. This cavity is intended to hold the boron sphere noted earlier. The test train above and below the midplane insert is estimated to contain 64% water. The fourth case includes the boron sphere in the NW LIPT insert fitting with everything else the same as in Case 3. The sphere has a mass of 114.75 g with a B-10 enrichment of 95 wt%. The outer radius of the boron sphere was 2.413 cm, and the inner radius was 1.3335 cm. The calculated reactivity parameters for the various cases are shown in Table 3-1.

Table 3-1. Calculated reactivity worth of the NW LIPT configurations.

Case	Description	K-eff	Uncertainty in K-eff (2 sigma)	Reactivity Relative to Reference Case	Uncertainty in Reactivity Worth
1	1994 CIC Model Base Case	0.99854	0.00016	\$0.0	0.0
2	Water filled NW IPT	0.99055	0.00016	-\$1.08	\$0.02
3	Midplane insert without boron sphere and 64% water above and below	0.99505	0.00016	-0.47	\$0.02
4	Midplane insert with boron sphere and 64% water above and below	0.99433	0.00016	-0.57	\$0.02

As can be seen, the maximum reactivity worth of the modeled NW LIPT insert relative to a water-filled NW LIPT is \$0.61 (\$-0.47-(-\$1.08)) if it is assumed that the midplane insert is solid aluminum and the water volume fraction above and below the midplane insert is 64%. The aluminum filler that is currently installed in the ATRC NW LIPT has a reactivity worth relative to a water-filled IPT of +\$1.67. Thus the new test train is estimated to have a maximum reactivity worth relative to the current filler of -\$1.06 and, as noted earlier, a maximum reactivity worth relative to a water-filled NW IPT of 0.61. Both of these bounding reactivities are within the limits specified in TSR 3.192.4.1 (+\$1.20).

Introducing the boron sphere into the NW LIPT center section insert fitting reduces the reactivity relative to that of the configuration with the insert fitting alone by a small amount as expected, with a reactivity worth of -\$0.10 assuming a water volume fraction above and below the midplane insert of 0.64.

### 3.2.2.2 SPNDs in the N-16 Positions

Various types of self-powered neutron detectors (SPNDs) and miniature fission chambers will be inserted into the six N-16 positions shown in Figure 3-17 in connection with the NSUF experiments noted earlier. The calculated eigenvalues for various cases are compared to a water filled N-16 position to show the approximate worth of removing and inserting the SPNDs.

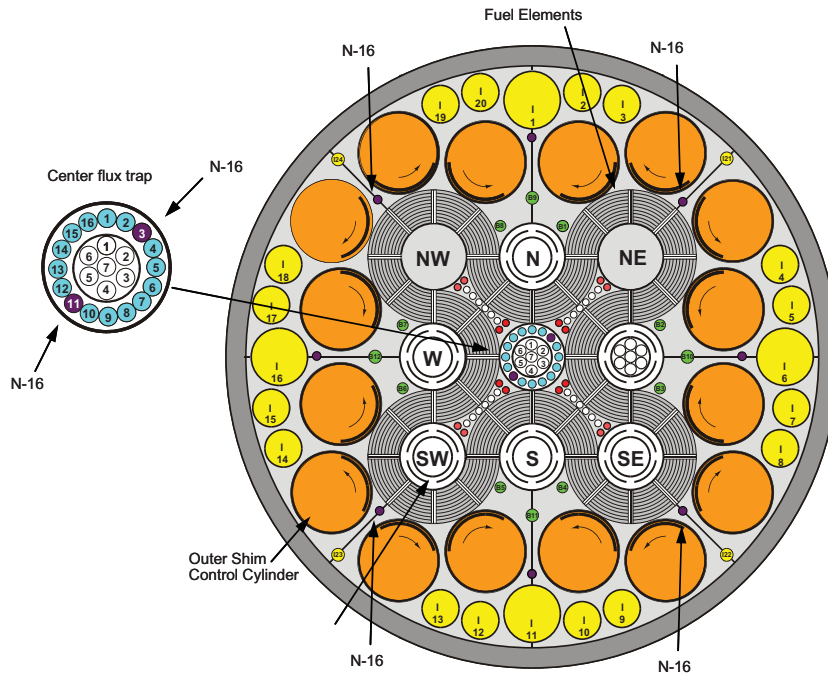


Figure 3-17. N-16 Positions in the ATRC.

The calculated reactivity worths of the SPNDs are presented in Table 3-2. All of the cases modeled with the SPNDs included the boron sphere positioning fixture in the NW LIPT test train. Removing the N-16 dry tubes and filling the N-16 positions with water reduces the reactivity relative to the reference 1994 CIC case by about 0.10\$. Placing one of each SPND type in all six N-16 position reduces the reactivity by another 0.03\$, for a total of 0.13\$ of reactivity reduction relative to the reference case.

In anticipation of a future experiment where miniature fission chambers will be inserted in the N-16 positions, two thermal fission chambers were conservatively modeled to be simultaneously present in each of the N-16 positions, for a total of 12 thermal fission chambers in the reactor. Each chamber was assumed to contain 30  $\mu\text{g}$  of U-235, 12 g of stainless steel, and 150  $\mu\text{g}$  of Argon fill gas. This case was modeled as “fistch” and has a reactivity worth of approximately 0.01\$ relative to water filled N-16 position.

Table 3-2: Reactivity worth of the SPNDs and thermal fission chambers.

Model Name	Description	K-eff	Uncertainty in K-eff (2 sigma)	Reactivity Relative to Base Case	Uncertainty in Reactivity Worth
ATR08	1994 CIC Model Base Case	0.99854	0.00016		
nwfil	Empty B-10 holder in NW Flux Trap	1.00217	0.00016	0.48	0.02
wsnb	Empty B-10 holder in NW Flux Trap and Water Filled N-16 Position	1.00141	0.00016	0.38	0.02
spnd	Empty B-10 holder in NW Flux Trap and SPNDs in all 6 N-16 Positions	1.0012	0.00016	0.35	0.02
spndc	Same as spnd except only center N-16 water density is changed	1.0012	0.00016	0.35	0.02
fistch	Thermal Fission chambers modeled with an empty B-10 holder in NW Flux Trap	1.00147	0.00024	0.39	0.03

### 3.3 ATRC Model Development for RERTR Support

The ATR and the ATRC have essentially the same physical layout, but with somewhat different uranium and boron content in the fuel plates (ATRC has less uranium and more boron). For current preliminary studies, the ATR 94-CIC configuration was assumed for the ATRC. Specifications for fresh ATRC fuel were obtained and edited into the ATR model to create an ATRC model; temperatures were also reduced to 293.2K. A KENO-VI based CSAS6 calculation resulted in a value for  $k_{eff}$  of 0.98716 +/- 0.00093. The ATR 94-CIC model described in Section 2.3 calculated a value of 1.00433 (which is selected as the goal for the critical state in the ATRC as well, assuming a 0.433% bias). Clearly, the fuel in the ATRC is less reactive than in the current ATR fuel, and adjustments are necessary to increase the net reactivity of the core. Again, the current configuration of the ATRC is not readily available; however, personal communication with ATRC Reactor Supervisor Kirk Stueve indicates that neck shims are not used in the ATRC and all rods are inserted. With all shims inserted the core multiplication will be further decreased, hence OSCC rotation will be necessary to calculate a  $k_{eff}$  value near 1.00433. Using CSAS6 for a eigenvalue search, it was determined that an OSCC rotation of 70.5° yielded an eigenvalue of 1.00317 +/- 0.00061, which was judged acceptably close to that of the ATR for sensitivity studies.

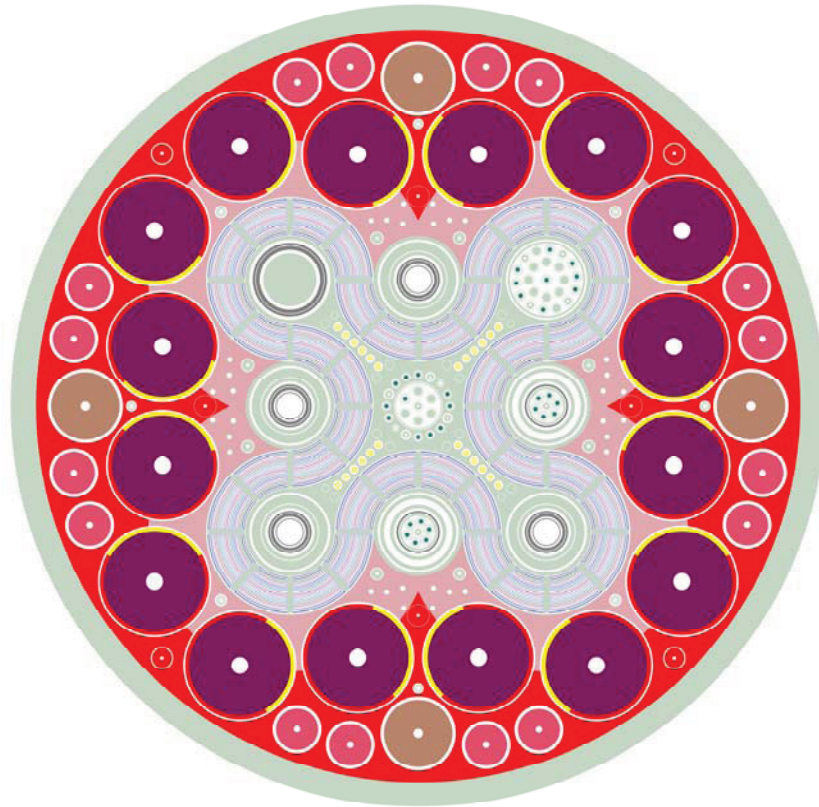


Figure 3-18. KENO-VI generated core facemap for critical ATRC configuration.

Figure 3-18 illustrates the model used for the ATRC (outer water region not shown). The biggest difference between the cores is of course the fuel composition, which cannot be seen in the figure. The ATR uses a slightly different uranium fuel loading, but has a significantly different boron distribution. While the ATRC fuel uses boron in all fuel blades with a very small ( $\sim 3\%$ ) gradient moving from outer to inner interior plates, ATR uses considerably less boron, loaded in the four inner and four outer fuel plates. The  $^{10}\text{B}$  concentrations in each fuel plate, moving from inner (1) to outer (19), are plotted in Fig 3-19, in units of atoms/barn-cm. The different boron loadings result in a significantly different flux distribution for two reactors that are otherwise similarly configured. Figure 3-20 illustrates the relative power distributions computed for a reactor-averaged fuel element in both reactors. The difference in profiles is significant, which could potentially cause misinterpretation of results of experiments performed in the ATRC when applied to the ATR. Hence, this model was used for a study of the similarity of the ATR and ATRC cores in terms of data sensitivity to begin to develop a process to relate ATRC calculations to those of the ATR by a systematic and rigorous means. Section 3.4 will discuss the results of that study.

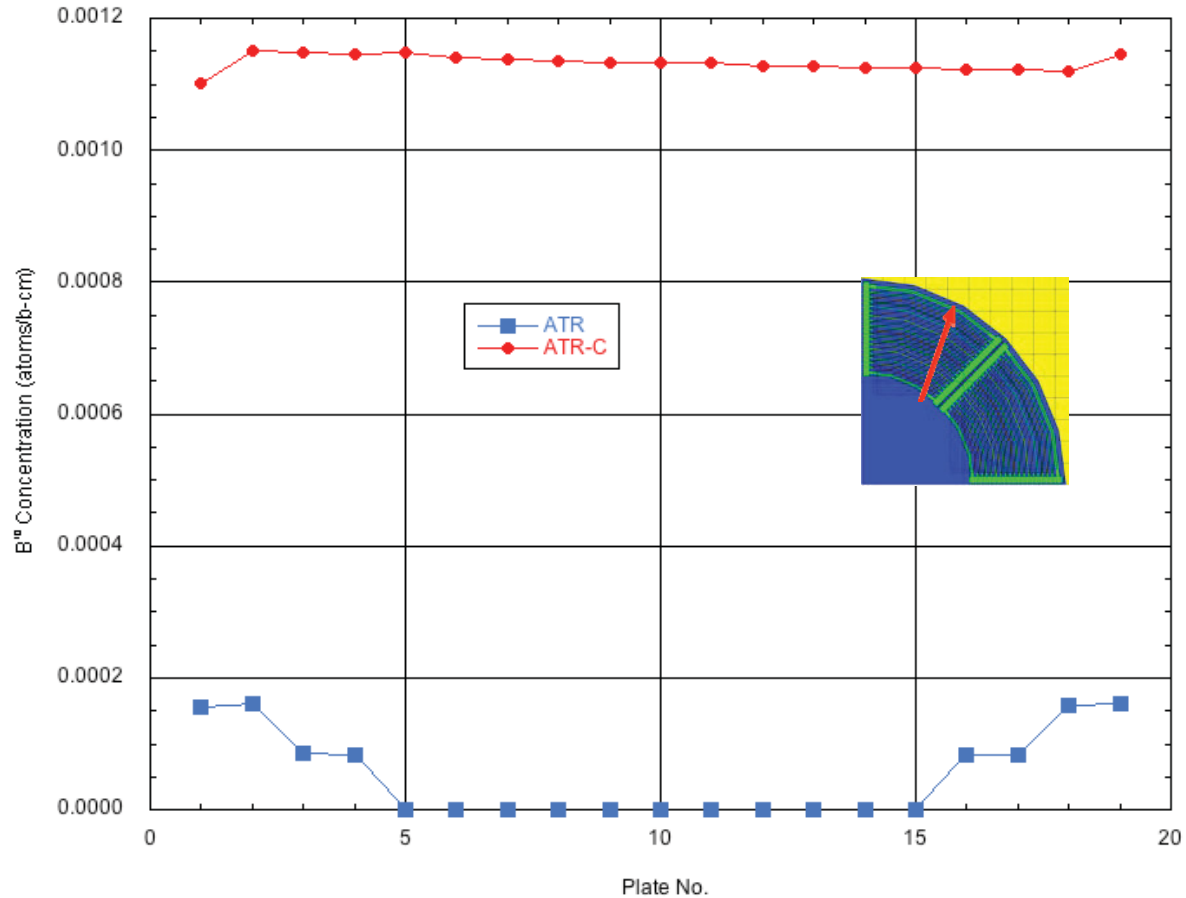


Figure 3-19.  $^{10}\text{B}$  distributions in ATR and ATRC fuel elements.

In the calculations described above, a core fully loaded with FE fuel elements was assumed in order to obtain the average power shape in the core. It is worth noting that the value of  $k_{\text{eff}}$  computed for this hypothetical configuration was  $0.97115 \pm 0.00056$ , indicating that the reactivity of the FE element is slightly less than that of the standard fuel. Ignoring uncertainties, the net reactivity loss is  $0.03202 \Delta k$  for the full core, which translates to  $0.0008 \Delta k$  per element. Thus, a very small reactivity decrease may be seen in the test core loaded with a single FE element. However, because this value is on the order of the uncertainty associated with these calculations, the difference may be hard to discern in KENO calculations.



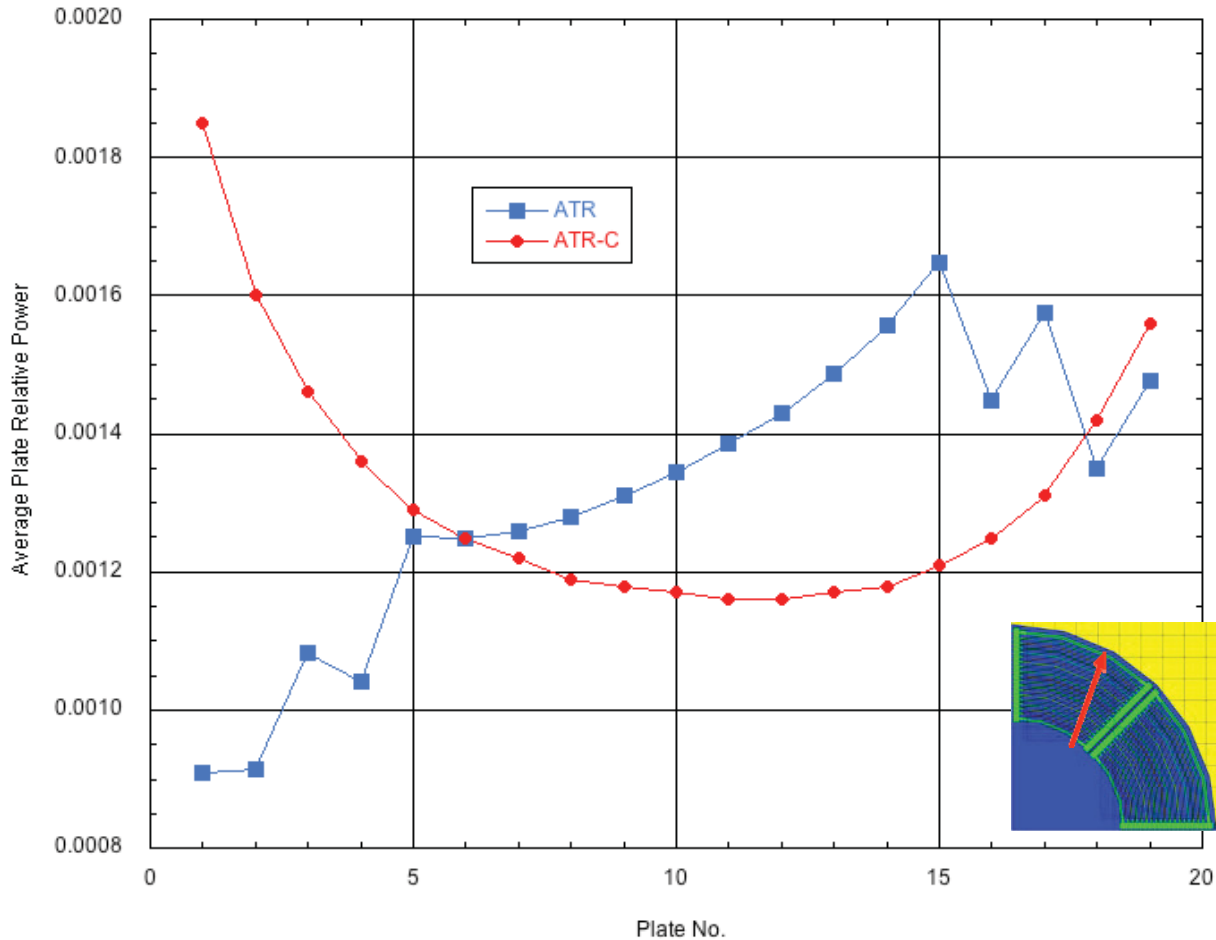


Figure 3-20. Calculated fission rate distributions in ATR and ATRC fuel elements (core averaged).

Now that an acceptable (albeit as yet unvalidated) ATRC model is available, it is appropriate to begin the process to evaluate the behavior of the core with the RERTF FE experiment loaded. However, before setting up core calculations, it was necessary to investigate resonance self-shielding calculations for the multigroup cross-section processing to be performed in KENO-VI calculations. (Note that although a continuous energy version of KENO-VI is available, the multigroup version is necessary for TSUNAMI calculations.)

An ATRC model was also developed using 39 standard ATRC fuel elements with the FE experimental element loading on position 38. This configuration is shown in Fig. 3-21; the FE location is shaded green to distinguish this element from the standard loading. Eigenvalue calculations have been completed for this configuration, to obtain a value for  $k_{\text{eff}}$  of  $1.00377 \pm 0.00077$ . As expected, the total system reactivity is statistically indistinguishable from the standard model. Further calculations with a larger number of histories would be needed to reduce uncertainties to the point where the reactivity change due to the FE element could be discerned.

The next step in this process will be to examine computed flux profiles to predict power distributions. Sensitivity methods, which are still being evaluated (see Sect 3.4) will be applied as appropriate in analysis of this configuration.

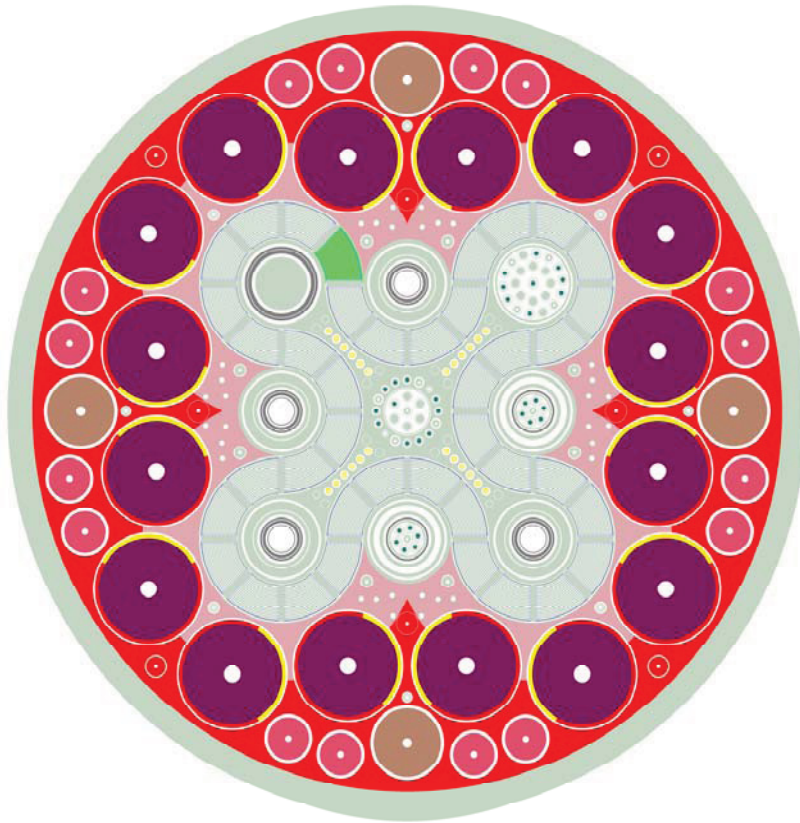


Figure 3-21. ATRC Model with experimental FE element (green) loaded in position 38.

### 3.4 ATRC/ATR Similarity Studies

Based on the approach described earlier, a TSUNAMI-3D-K6 calculation was performed for the ATRC configuration described above. Sensitivity data files from both ATR and ATRC calculations were provided as data for a TSUNAMI-IP calculation. Not surprisingly, a strong degree of similarity is found. The three similarity indices are calculated as:

$$\begin{aligned} c_k &= 0.9976, \\ E &= 0.9984, \\ G &= 0.9213. \end{aligned}$$

The  $c_k$  and  $E$  values indicate a virtually identical system. These two parameters are indicators of the correlated uncertainty for all reactions in all nuclides in the two systems: the former determined using sensitivity coefficients and covariance data, and the latter by a mathematical relationship (direction cosine) between vectors of sensitivity coefficients. Thus, we conclude that the ATR and ATRC as modeled here are highly correlated.

The  $G$  index, on the other hand, compares the sensitivity of two systems based solely on fission, capture, and scatter reactions, and the fraction of the sensitivity coefficient for the second configuration that is common with the sensitivity coefficient of the first system, for all nuclides and for the three reaction

types, normalized by the sum of the sensitivity coefficients of the first system, for all nuclides and for the three reaction types, and for all energy groups. Hence, the G index is a representation of the “coverage” of the uncertainty response of the first system by the uncertainty response of the second system [Goluoglu, 2003]. The concept of coverage and common sensitivity is illustrated in Fig. 3-22 [Bowman, 2009] – this is an illustrative example, and not representative of the ATR or ATRC. In this figure, the term “Application” refers to the first system analyzed, and “Experiment” the second. TSUNAMI-IP is actually designed to compare a number of experiments to particular application of interest in order to find a set of experiments that provide as complete coverage as possible. In the current work, we are simply trying to understand the similarity of two ATR-type designs, and ultimately develop a relationship that will estimate a priori uncertainties in an experiment in the ATR due to predetermined uncertainties in ATRC experiments (relative to calculations). Hence, the G index is less valuable at this point than the other two indices – coverage in terms of cross section validation is not our goal in this work.

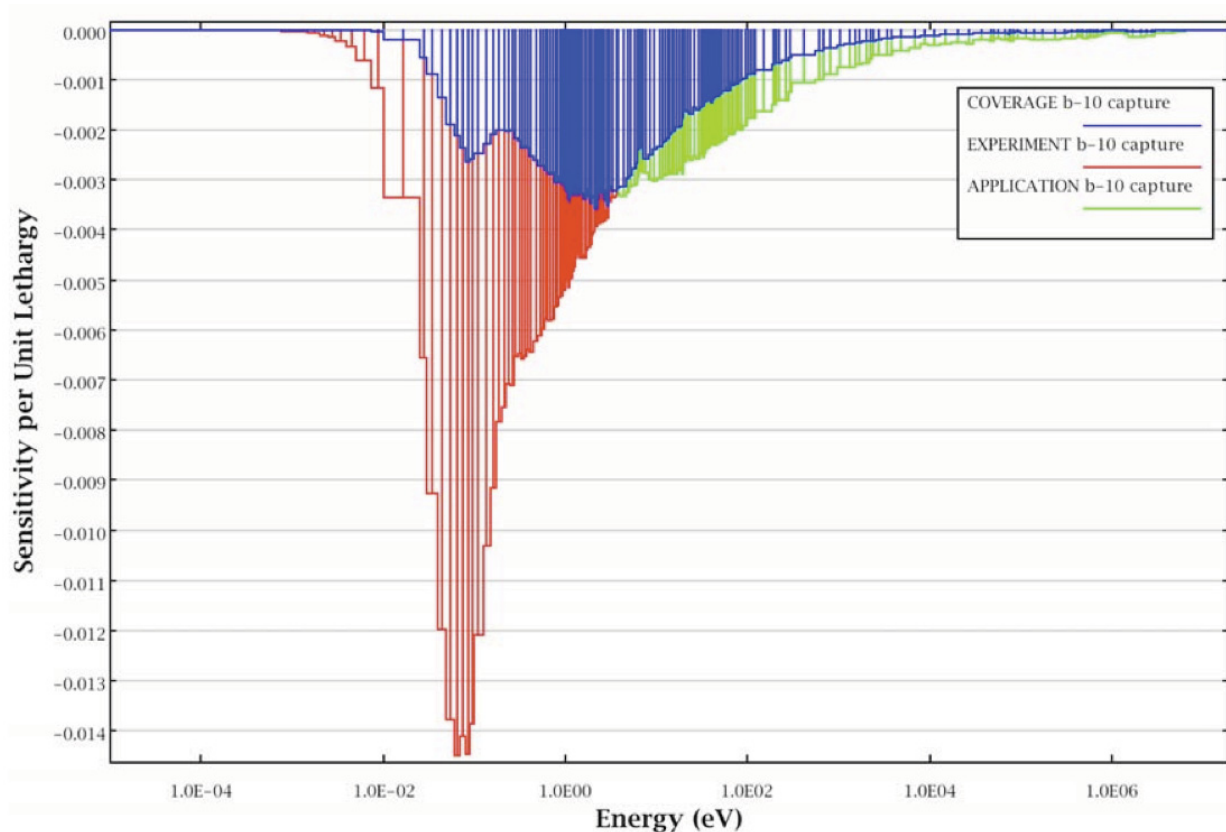


Figure 3-22. Example of coverage of one configuration’s uncertainty response relative to another.

Given sensitivity coefficients for the various nuclides and similarity indices, the challenge from this point will be to determine the method by which one can mathematically extend the knowledge of both systems to extrapolate errors from computations made with ATRC experiments to computations made for similar ATR experiments.

### 3.5 HELIOS ATRC Model Development

A HELIOS ATRC reactor model was also developed for future use, starting with the original ATR core model. The changes between the two models are focused on the penetrations into the beryllium reflector and the fuel design. This model is primarily intended to benchmark the models being developed for the other codes. The model may also be used as an independent method to evaluate ATRC reactivity measurements.

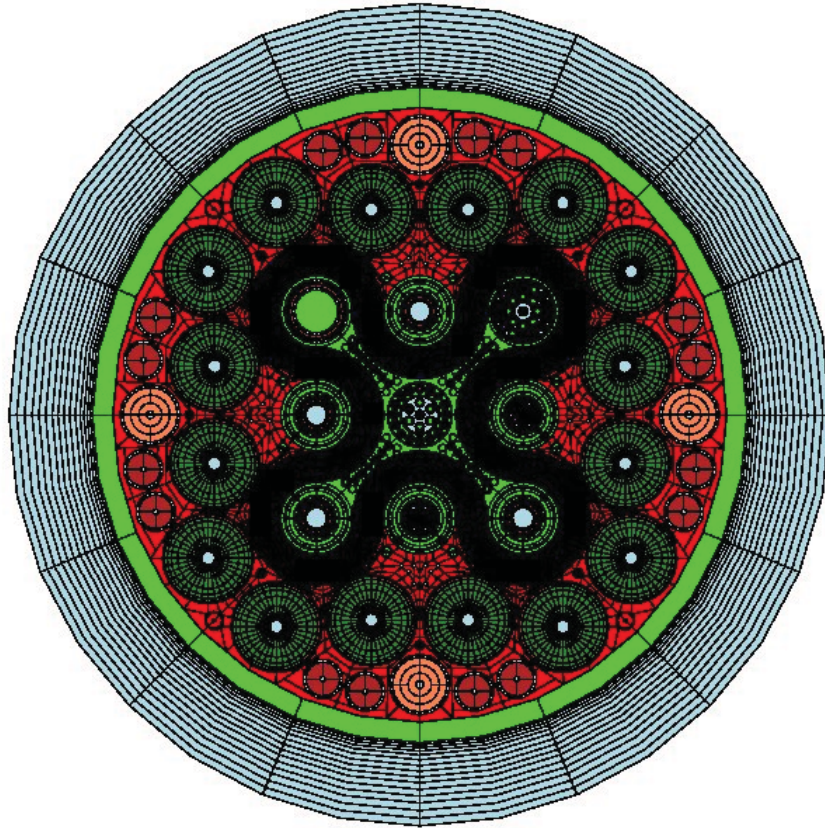


Figure 3-23 . HELIOS Model of ATRC

## 4.0 VALIDATION EXPERIMENTS IN THE ATRC

Validation protocols for the various computational models will be based on neutron activation spectrometry as described in this section and on post-irradiation burnup measurements for each fuel element as described in Section 5. In Fiscal Year 2010 some basic equipment for activation experiments in the Northwest Large In-Pile Tube and in the fuel elements was designed and fabricated, and initial scoping measurements were planned and approved for the ATRC. Over the course of the upgrade project additional equipment will be fabricated to enable activation measurements in at least one of the other flux traps and possibly in selected reflector experiment positions. Ultimately a complete set of experimental apparatus and associated standard measurement protocols for neutron activation spectrometry will be available for future code and model validation measurements as needed in both the ATRC and, when feasible, in the ATR itself. The work described here builds on extensive previous relevant INL experience at the ATR (e.g. Rogers and Anderl, 1995) as well as at other research reactor facilities worldwide.

It is also important to note that the ATR and the ATRC facilities currently lack real-time methods for directly detecting thermal neutron flux and fission reaction rates for irradiation capsules. However, recent technological developments offer the possibility for such direct measurements without resorting to complicated correction factors. In addition, it is possible to directly measure minor actinide fission reaction rates and to provide time-dependent monitoring of the fission reaction rate or fast/thermal flux during transient testing. Development of such real-time instrumentation is also of interest to the ATR Life Extension Program. Accordingly the validation measurements discussed in this section are being conducted in collaboration with a joint Idaho State University (ISU) /INL NSUF project that has been initiated to evaluate new real-time state-of-the-art in-pile flux detection sensors (Rempe et al., 2010)

Initially, the NSUF project is comparing the accuracy, response time, and long duration performance of French Atomic Energy Commission (CEA)-developed miniature fission chambers, miniature self-powered neutron detectors (SPNDs) developed by the Atomic Energy Commission of Argentina (CNEA), and specially-developed commercial SPNDs and back-to-back fission (BTB) chambers from Argonne National Laboratory (ANL). The detailed activation measurements described here will provide additional calibration data for the real-time sensors of interest in addition to high-quality benchmark neutronics data that will be useful for the LEP Methods and V&V Upgrade project. Collaboration with the NSUF project has also been very helpful in terms of improved efficiency of the INL administrative processes associated with planning and execution of experiments in the ATRC, since many of the required documents and safety analyses can be combined rather than performed separately for the two projects.

### 4.1 Methods and Materials

The basic principles of neutron activation spectrometry are reviewed in this section, followed by a description of the experimental apparatus and initial measurement protocols developed during FY-2010.

#### 4.1.1 Neutron Activation Spectrometry

Neutron activation spectrometry is based on the fact that different elements (and different isotopes of the same element) placed in a neutron field will capture and scatter neutrons selectively with respect to the incident neutron energy. Some elements are primarily sensitive to capture of thermal neutrons, others have strong capture resonances in the epithermal energy range, while others exhibit interaction energy thresholds for inelastic scatter, secondary neutron and charged particle emission, and fission, below which essentially no interactions occur. If the neutron interaction product for a particular nuclide is radioactive,



then the induced radioactivity of a sample of that nuclide placed in a neutron field will be largely proportional to the neutron flux at energies where interactions are most likely to occur in the sample. If different materials having different sensitivities to neutrons as functions of energy are activated in the same field it is ultimately possible to reconstruct a measured neutron spectrum from the induced activities. The level of spectral detail that can be reliably obtained generally corresponds to the number of different materials, and different interactions in the same materials, that are available.

As an example to illustrate the underlying physics of activation spectrometry, Figure 4-1 shows the capture cross section for  $^{197}\text{Au}$ , which has a relatively high thermal neutron capture component as well as a prominent capture resonance at about 5 electron volts (eV). Capture of neutrons in a small sample (typically a foil or wire) of  $^{197}\text{Au}$  produces  $^{198}\text{Au}$ , which undergoes beta decay with emission of a prominent 0.411 keV gamma ray. The strength of this gamma ray is proportional to the neutron capture rate, which is for the most part proportional to the flux of neutrons at thermal energies and at 5eV. If the sample is placed inside a cover made of cadmium, which absorbs essentially all incident thermal neutrons, then the interaction rate of the gold sample will be proportional to the neutron flux above thermal energies, primarily at 5 eV where the resonance occurs. The thermal and above-thermal neutron fluxes can then be separated by converting the measured induced activities to saturation activities (i.e. activation rates per atom), subtracting the activation rate of the cadmium-covered sample from that of the bare sample and computing the corresponding thermal-neutron and total neutron fluxes. This is the classic cadmium difference method and in effect it yields a two-energy group (thermal and above-thermal) spectrum. Elemental gold also exhibits several very useful and convenient threshold interactions for secondary neutron emission. These include (n,2n) up through (n,6n), covering the entire neutron energy range of interest for NCT as well as FNT, extending up to about 60 MeV (Nigg et al., 2000).

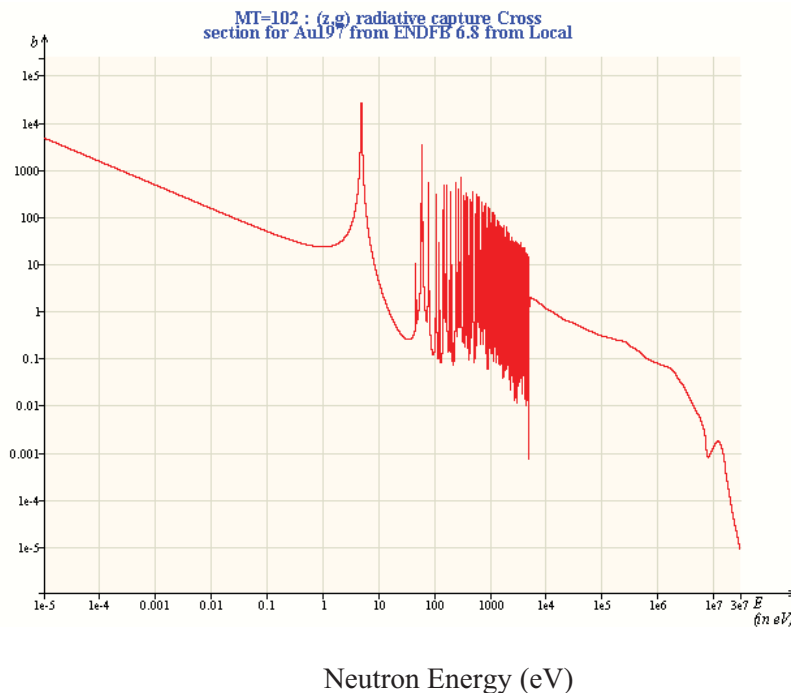


Figure 4-1. Capture cross section (barns) of  $^{198}\text{Au}$ . (Source: OECD Janis 2.1)

As another example, cross section data for  $^{115}\text{In}$  are shown in Figure 4-2. This nuclide (96% abundance in natural indium) captures thermal neutrons and it also has a strong neutron capture resonance at about 1 eV. In both cases neutron capture produces radioactive  $^{116}\text{In}$ , which emits three prominent gamma rays with energies of 416, 1097 and 1293 keV. In addition it will form an isomer by inelastic scatter of neutrons having energies above about 400 keV. This yields  $^{115\text{m}}\text{In}$ , which decays back to the ground state by emission of a 336 keV gamma ray. Hence the inelastic scatter rate (and thus the neutron flux above the 400 keV threshold) is proportional to the measured activity of the 336 keV gamma ray while the activities of the other three gamma rays, which are associated with a different half-life since they are emitted by a different radionuclide ( $^{116}\text{In}$ ) are largely proportional to the neutron flux at thermal energies and at 1 eV. If an indium foil is covered with cadmium, the thermal neutron capture rate is suppressed as described previously for gold. As a result, this single nuclide can be used to obtain information in three different energy ranges of the neutron spectrum of interest.

In the general case, a number of different activation responses (typically 8-12) are typically measured using a variety of nuclides having different sensitivities to neutrons in the thermal, resonance, and fast energy ranges. This permits the reconstruction of additional spectral detail in the unfolding process. Materials found useful for ATRC applications include gold and indium as described above as well as tungsten, manganese, cobalt, copper, and scandium for thermal and epithermal neutron measurements and several other materials having threshold interactions for fast-neutron measurements, as will be described later.

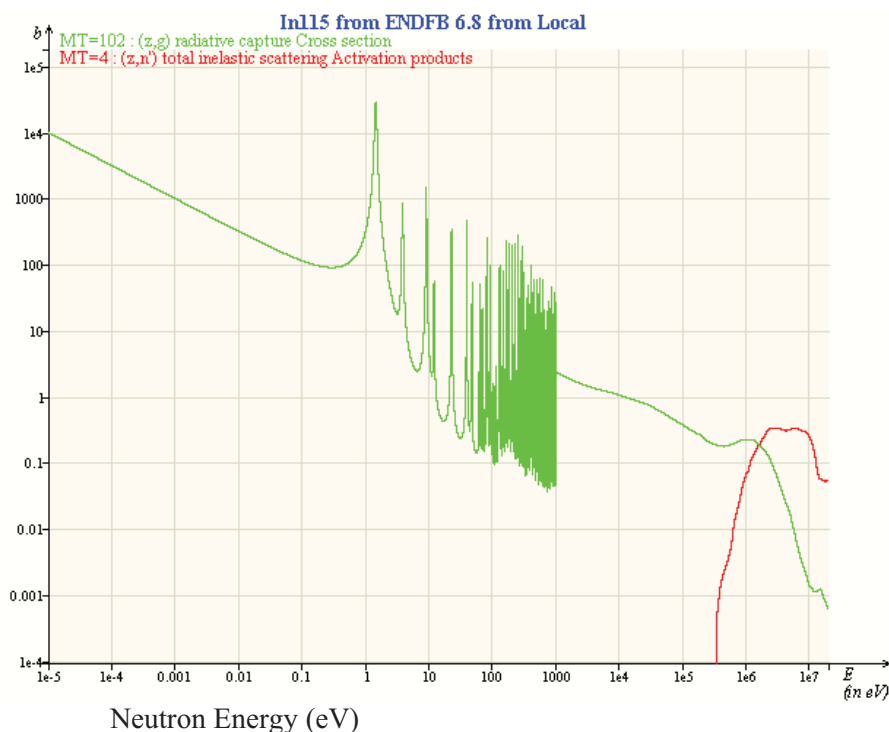


Figure 4-2. Capture (Green) and inelastic scatter (Red) cross sections (barns) of  $^{115}\text{In}$ . (Source: OECD Janis 2.1)



We now consider some essential mathematical details of neutron activation spectrometry. In general, the volume-average activation rate per atom for a foil or wire dosimeter placed in a neutron flux field may be calculated as:

$$R = \int_0^{\infty} \sigma_d(E) \Psi_d(E) dE \quad (1)$$

where  $\sigma_d(E)$  is the microscopic activation cross section of interest for the dosimeter material, as a function of neutron energy and  $\Psi_d(E)$  is the volume-average scalar neutron flux existing within the active dosimeter, again as a function of energy, and accounting for self-shielding effects, if any. Equation 1 can also be expressed as:

$$R = \int_0^{\infty} \sigma_d(E) \left( \frac{\Psi_d(E)}{\Psi(E)} \right) \Psi(E) dE = \int_0^{\infty} \sigma_d(E) P_d(E) \Psi(E) dE \quad (2)$$

where  $\Psi(E)$  is the unperturbed neutron flux that would exist at the measurement location in the absence of the flux perturbations caused by the dosimeter itself and any surrounding spectral modification devices and other structures placed in the field (Cd covers, foil and wire positioning devices, etc).

It may be noted here that, as a practical matter, the function  $P_d(E)$  in Equation 2 can be determined independently from  $\Psi(E)$  if desired since it is simply a flux ratio. In this case  $\Psi(E)$  on the far right hand side of Equation 2 can be any appropriate *a-priori* free-field unperturbed flux estimate that is then modified by the self-shielding function  $P_d(E)$ .

Equation 2 may be written as a summation rather than as an integral by partitioning the range of the energy variable into a number of discrete contiguous energy groups:

$$R = \sum_{j=1}^{NG} a_j \phi_j \quad (3)$$

where NG is the total number of energy groups, with

$$a_j = \frac{\int_{EL_j}^{EH_j} \sigma_d(E) P_d(E) \Psi(E) dE}{\int_{EL_j}^{EH_j} \Psi(E) dE} \quad (4)$$

and

$$\phi_j = \int_{EL_j}^{EH_j} \Psi(E) dE. \quad (5)$$

where  $EL_j$  and  $EH_j$  are the lower and upper energy limits of energy group  $j$ .

If additional dosimeter materials are placed in the field, or if a particular material exhibits more than one independent activation response (e.g. gold or indium as noted earlier) then Equation 3 may be written as a system of equations:

$$R_i = \sum_{j=1}^{NG} a_{ij} \phi_j \quad (6)$$

where  $R_i$  is the total activation rate for interaction  $i$  and  $a_{ij}$  is the activation constant from Equation 4 for reaction  $i$  due to neutrons in energy group  $j$ . There will be a total of  $NF$  equations, where  $NF$  is the total number of activation responses available.

Effective shielded cross sections  $\sigma_d(E)$  and the corresponding shielded and unshielded *a-priori* neutron fluxes suitable for computing the function  $P_d(E)$  in the above equations may be obtained by any of several well-established neutron transport modeling techniques and nuclear data libraries. A typical approach involves computation of application-specific cross sections and *a-priori* fluxes for each dosimeter in the neutron field using continuous-energy Monte Carlo techniques, e.g. MCNP. This is crucial if self-shielding or mutual shielding (as in a stack of foils) is significant. It is also sometimes possible to use highly-dilute foils (Auterinen et al., 2004) to avoid the need for shielding corrections, facilitating the direct application of standard dosimetry cross section libraries. The Monte Carlo calculations for dosimeter packages generally include only the dosimeters and surrounding support structure with a boundary condition that represents the incoming space, angle- and energy-dependent incident neutron source, precomputed using a Monte Carlo or deterministic computational model of the entire reactor. The global reactor computations may be done with MCNP, or with a standard multidimensional discrete-ordinates code such as DORT (Rhodes and Childs, 1988, Wheeler et al., 1990) or in the case of ATR, with any of the more advanced transport codes described in Section 2 of this Annual Report.

The system of activation equations, Eq. 6, may be written out in matrix form as:

$$\begin{bmatrix} a_{11} & a_{12} & a_{13} & \cdots & a_{1NG} \\ a_{21} & a_{22} & a_{23} & \cdots & a_{2NG} \\ a_{31} & a_{32} & a_{33} & \cdots & a_{3NG} \\ \vdots & \vdots & \vdots & & \vdots \\ \vdots & \vdots & \vdots & & \vdots \\ a_{NF1} & a_{NF2} & a_{NF3} & \cdots & a_{NFNG} \end{bmatrix} \begin{bmatrix} \phi_1 \\ \phi_2 \\ \phi_3 \\ \vdots \\ \phi_{NG} \end{bmatrix} = \begin{bmatrix} R_1 \\ R_2 \\ R_3 \\ \vdots \\ R_{NF} \end{bmatrix} \quad (7)$$

or, more compactly:

$$[A][\Phi] = [R] \quad (8)$$

Equation 7 is exact, provided that the reaction rates  $R_i$ , the activation constants  $a_{ij}$  and the group fluxes,  $\phi_j$  are all self-consistent. If experimentally measured reaction rates (as opposed to the *a-priori* reaction rates) for each interaction  $R_i$  are substituted into Equation 7, a solution of the resulting new system of equations for “measured” fluxes corresponding to the measured reaction rates may also be obtained under certain conditions.

If  $NF = NG$  in Equation 7 then the matrix  $[A]$  is square, its inverse will ordinarily exist, and the unknown flux vector may be obtained by any standard solution method that converges, provided that the rows of  $[A]$  are linearly-independent to a sufficient degree and the measured reaction rates are sufficiently precise. In physical terms the former requirement implies that the response functions (cross sections) for the activation interactions used in the measurement must be selected such that they have sufficiently different shapes as functions of energy. Spectral modification devices (e.g. cadmium covers) can also be used to force linear independence. It may be noted that positive fluxes are not guaranteed to result from this procedure, but if the elements of  $[A]$  are computed in a sufficiently valid, physically-realistic manner for the specific measurement configuration, and if the measured reaction rates are accurately determined, a positive solution will generally be obtained. In practice this situation ( $NF=NG$ ) is exemplified by the previously-noted cadmium difference method, which can readily be shown to be a special case of Equation 7, with only two rows in the matrix, one for the bare foil and one for the covered foil. It also typically occurs when measuring pointwise fluxes at resonance energies (Harker et al., 1992) using stacks of foils, and when measuring simple spectra using flux wires composed of alloys of two materials with different spectral responses, such as copper and gold (as is done in the present work), or manganese and gold.

There are two possibilities for the situation where  $NF$ , the number of available activation response functions, is not equal to  $NG$ , the number of energy groups for which it is desired to obtain unfolded fluxes. If  $NF < NG$  the problem is underdetermined and additional information must be introduced in some manner to permit a solution, as is done in the various types of “adjustment” and “iterative” techniques for spectrum estimation from activation data. These methods involve the numerical modification of an input *a-priori* spectrum by any of several well-developed algorithms to produce calculated responses that give the best overall quantifiable match to the measured responses. On the other hand, if  $NF > NG$  the problem is overdetermined and the “extra” information that is thereby available can be incorporated into the direct algebraic determination of a unique solution for the group fluxes and their propagated uncertainties by a least-squares procedure (Nigg et al., 2000). This “direct” unfolding method has an advantage in that it converges to a single unique solution.

The underdetermined methods for spectral unfolding allow the estimation of a spectrum having more energy detail than the number of linearly independent activation responses, but with one exception these approaches do not produce a unique solution – many solutions are possible from the same input data. A unique solution can be obtained only by the Generalized Least-Squares Method, which requires covariance information for all of the input parameters, including the input spectrum as well as the activation cross sections and the measured responses. This covariance information in effect constrains the solution to a single physically realistic optimum in a least squares sense. Several adjustment codes based on this approach have been developed. A popular example is the LSL code (Stallman 1986).

If the covariance information required for least-square adjustment procedures is not available, other somewhat more empirical iterative adjustment techniques are widely used, one popular example being the method described by Draper (1971), implemented as an option in the SAND-II code (McElroy and Berg, 1967). Effective use of such methods requires good physical insight and intuition, as the form of

the input *a-priori* spectrum and its assumed uncertainty, as well as the iteration strategy used to produce a solution can have a significant influence on the results.

Neutron activation spectrometry can be applied to any neutron field for which suitable activation responses can be measured. It is used on a regular, but somewhat limited, basis for flux characterization in most experiments irradiated in the ATR, generally using nickel and cobalt wires. A full spectral characterization of the ATR has not been done since 1986 (Rogers and Anderl 1995). The activation method is capable of high precision and accuracy ( $1\sigma < 5\%$ ) when uncertainties are carefully managed throughout every step of the process. Precautions to be taken include:

- Use of high-purity, accurately assayed dosimeter materials
- Careful weighing, preparation and handling of the foil packages to ensure accurate knowledge of the foil masses and to avoid contaminants
- Careful recording of the activation and post-irradiation decay times of the foils
- Irradiation at constant flux if at all possible, with appropriate corrections for any time-dependence of the flux.
- Accurate, reproducible calibration of gamma spectrometers used for measurement of the foil activities, using certified, traceable standards.
- Use of good techniques for the foil activity measurements in order to minimize uncertainties due to coincidence summing, counting geometry etc.
- Thoughtful selection and application of unfolding techniques
- Use of multiple unfolding techniques to verify consistency

It is also important to recognize that activation measurements for code validation, especially in the case of thermal neutron fields, must be planned interpreted very carefully due to the possibility of large flux gradients that can depend on the specific geometry of the reactor, which can change with time (e.g. as a result of shim rotation in the ATR). As a result, reproducibility can be an issue and self consistent comparison with the calculation being validated is crucial – i.e. be sure you are really calculating and measuring the same quantity.

#### **4.1.2 Summary Description of Experimental Apparatus**

In the initial phase of the experimental campaign of interest here, extending from late Fiscal Year 2010 through Fiscal Year 2011 various sets of activation foils will be irradiated in the Northwest Large In-Pile Tube (NW LIPT) of the ATRC at the axial core midplane for each of three critical outer shim configurations to determine detailed neutron spectral information at this location for benchmarking purposes. Measurements will be made for a balanced outer shim critical configuration as well as for two unbalanced configurations, one where the neutron flux is peaked in the northwest lobe and one where the flux is peaked on the opposite side of the core, in the southeast lobe. In the case of the balanced shim configuration measurements of the flux distribution in the fuel elements will also be performed, using standard flux wands placed in selected fuel elements to position flux wires at the core axial midplane. In a second phase of the validation protocol development measurements will also be conducted in one or

more of the other accessible flux traps and possibly in selected experiment positions in the beryllium reflector. More detailed fuel element flux distribution measurements will also be included. The end result will be a standard, repeatable, protocol with associated experimental apparatus for flux validation as noted earlier.

The foils to be used in the NW Flux Trap in the case of the balanced outer shim configuration (for which measurements began in late Fiscal Year 2010) are listed in Tables 4-1 through 4-3, grouped by the range of neutron energies to which each set of foils is sensitive. Some foils will be placed inside standard 40-mil (1 mm) cadmium foil covers or boron-10 spectral modification shields to enhance their response in the epithermal and fast neutron ranges, respectively as indicated in the tables. These foils are from a very well-characterized inventory of foils used at the INL over a period of many years. The foils will be supported inside of a standard ATRC NW LIPT insert. Figure 4-3 shows this insert, separated into its two components, as well as the Cd and B spectral shifters. The boron spectral shifting cover is a hollow sphere of sintered boron, enriched to approximately 90% in  $^{10}\text{B}$ , with an inside diameter of approximately 2.5 cm (1"), an outside diameter of 5 cm (2") and a nominal mass of 115 grams.

Table 4-1. Bare Foils for Thermal Flux Measurement

Foil ID	Mass	Neutron Interaction	Half-life of Product of Interest	Energy Range of Primary Response	Activation Gamma Energy of Interest (keV)
Mn/Cu-206	48.6 mg (80% Mn)	$^{55}\text{Mn}(n, \gamma)^{56}\text{Mn}$	2.578 Hours	Thermal	847
Mn/Cu-207	49.7 mg (80% Mn)	$^{55}\text{Mn}(n, \gamma)^{56}\text{Mn}$	2.578 Hours	Thermal	847
Au-105	64.0 mg	$^{197}\text{Au}(n, \gamma)^{198}\text{Au}$	2.694 Days	Thermal	412
Au-106	60.5 mg	$^{197}\text{Au}(n, \gamma)^{198}\text{Au}$	2.694 Days	Thermal	412

Table 4-2. Cd Covered Foils for Resonance Flux Measurement

Foil ID	Mass	Neutron Interaction	Half-life of Product of Interest	Energy Range of Primary Response	Activation Gamma Energy of Interest (keV)
In-60	25.9 mg	$^{115}\text{In} (n, \gamma) ^{116}\text{In}$	54 Minutes	1 eV Resonance	1293, 1097, 416
In-61	24.1 mg	$^{115}\text{In} (n, \gamma) ^{116}\text{In}$	54 Minutes	1 eV Resonance	1293, 1097, 416
Au-111	63.8 mg	$^{197}\text{Au} (n, \gamma) ^{198}\text{Au}$	2.694 Days	5 eV Resonance	412
Au-112	60.1 mg	$^{197}\text{Au} (n, \gamma) ^{198}\text{Au}$	2.694 Days	5 eV Resonance	412
W-R20-1-1	60.5 mg	$^{186}\text{W} (n, \gamma) ^{187}\text{W}$	23.9 Hours	18 eV Resonance	686
W-R20-1-2	61.5 mg	$^{186}\text{W} (n, \gamma) ^{187}\text{W}$	23.9 Hours	18 eV Resonance	686
Co-R20-3-4	64.8 mg	$^{59}\text{Co} (n, \gamma) ^{60}\text{Co}$	5.271 Years	132 eV Resonance	1333, 1173
Co-R20-3-5	64.3 mg	$^{59}\text{Co} (n, \gamma) ^{60}\text{Co}$	5.271 Years	132 eV Resonance	1333, 1173
Mn/Cu-204	48.4 mg (80% Mn)	$^{55}\text{Mn} (n, \gamma) ^{56}\text{Mn}$	2.578 Hours	340 eV Resonance	847
Mn/Cu-205	49.3 mg (80% Mn)	$^{55}\text{Mn} (n, \gamma) ^{56}\text{Mn}$	2.578 Hours	340 eV Resonance	847
Cu-510	140.9 mg	$^{63}\text{Cu} (n, \gamma) ^{64}\text{Cu}$	12.701 Hours	1 keV Resonance	511 (Positron)
Cu-511	141.0 mg	$^{63}\text{Cu} (n, \gamma) ^{64}\text{Cu}$	12.701 Hours	1 keV Resonance	511 (Positron)
501	52.2 mg	$^{45}\text{Sc} (n, \gamma) ^{46}\text{Sc}$	83.81 Days	4.5 keV Resonance	1120, 889
Sc 502	50.5 mg	$^{45}\text{Sc} (n, \gamma) ^{46}\text{Sc}$	83.81 Days	4.5 keV Resonance	1120, 889

Table 4-3. Foils in Boron Sphere for Fast Flux Measurement

Foil ID	Mass	Neutron Interaction	Half-life of Product of Interest	Energy Range of Primary Response	Activation Gamma Energy of Interest (keV)
Rh-104	45.0 mg	$^{103}\text{Rh}$ (n,n') $^{103\text{m}}\text{Rh}$	56.12 Minutes	0.15 MeV Threshold	39.8 (IT e <sup>-</sup> )
In-526	107.2 mg	$^{115}\text{In}$ (n,n') $^{115\text{m}}\text{In}$	4.486 Hours	0.5 MeV Threshold	336.3
Ti-1002	157.3 mg	$^{47}\text{Ti}$ (n,p) $^{47}\text{Sc}$ $^{46}\text{Ti}$ (n,p) $^{46}\text{Sc}$ $^{48}\text{Ti}$ (n,p) $^{48}\text{Sc}$	3.349 Days 83.81 Days 43.7 Hours	1.0 MeV Threshold 3.5 MeV Threshold 5.5 MeV Threshold	159.4 1121,889 984,1312,1038
Ni-1004	285.9 mg	$^{58}\text{Ni}$ (n,p) $^{58}\text{Co}$	70.88 Days	1.2 MeV Threshold	811
Zn-502	116.7 mg	$^{64}\text{Zn}$ (n,p) $^{64}\text{Cu}$	12.701 Hours	1.5 MeV Threshold	511 (Positron)
Fe-505	132.4 mg	$^{54}\text{Fe}$ (n,p) $^{54}\text{Mn}$ $^{56}\text{Fe}$ (n,p) $^{56}\text{Mn}$	312.2 Days 2.578 Hours	1.5 MeV Threshold 5.0 MeV Threshold	834.8 847
Cu-509	140.9 mg	$^{63}\text{Cu}$ (n, $\alpha$ ) $^{60}\text{Co}$	5.271 Years	4.0 MeV Threshold	1333, 1173
Nb-1005	267.9 mg	$^{93}\text{Nb}$ (n, 2n) $^{92\text{m}}\text{Nb}$	10.13 Days	6.0 MeV Threshold	935

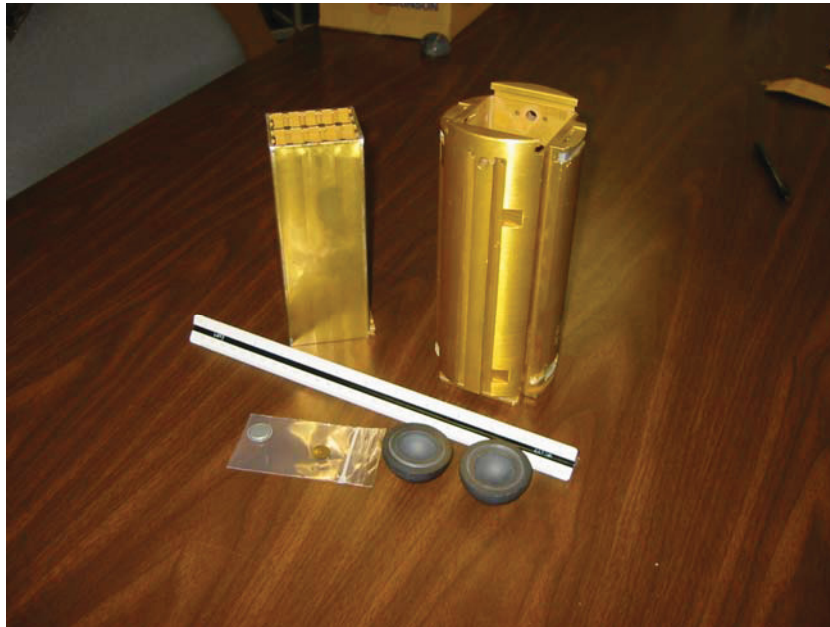


Figure 4-3. NW Flux Trap insert, cadmium foil cover, and boron spectral shaping sphere.



The foils are positioned within the ATRC NW LIPT insert using specialized insert fittings fabricated by the INL for this purpose. Foils used for thermal and epithermal neutron measurements are placed in covered aluminum strips (Figure 4-4) that fit into the square holder shown on the left-hand side of Figure 4-3. This holder fits, in turn, into the square cavity in the cylindrical LIPT insert on the right hand side of Figure 4.3. A second fitting (Figure 4-5) that goes directly into the square cavity of the cylindrical insert is used to hold the boron sphere, which contains the foils used for the fast-neutron spectral range. The insert fittings shown in Figures 4-4 and 4-5 have O-rings around their cavities to keep the contents out of contact with the reactor water. The insert fittings are fabricated from aluminum under INL Quality Level 2 requirements. Co-normalization of flux from separate reactor runs is accomplished using the measured activation of standard INL copper/gold (1.55% Au by weight) flux wires at specific locations within the insert fittings as shown in Figures 4-4 and 4-5 and in the circled position (see Figure 4-6) between Fuel Plates 10 and 11 (referred to as “Wire Position 10”) at the axial core midplane of the four even-numbered elements surrounding the NW flux trap (Elements 32, 34, 36, 38). These wires are 1 mm in diameter. The copper mass per unit length of the wire stock is 70 milligrams per centimeter and the gold mass is approximately 1.1 milligrams per centimeter. The segments to be placed in the core fuel elements at the midplane are approximately 0.635 cm (0.25”) in length and will therefore contain approximately 45 milligrams of copper and 0.7 milligrams of gold.

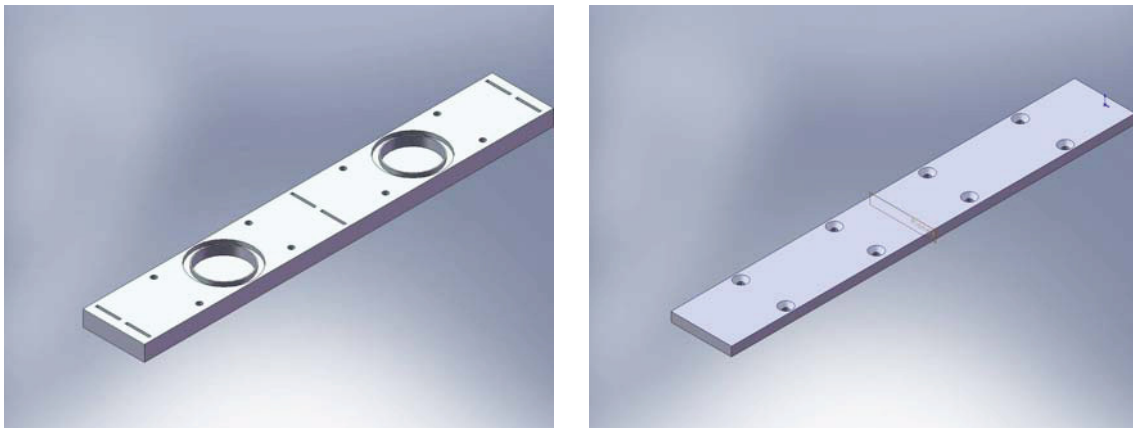


Figure 4-4. Aluminum strip (L) with cover (R) used for holding thermal and epithermal activation foils. Foils are placed in the circular indentations shown in the diagram on the left. Duplicate flux wires are placed in the indented slots at each end and in the middle of the strip shown in the diagram on the left.

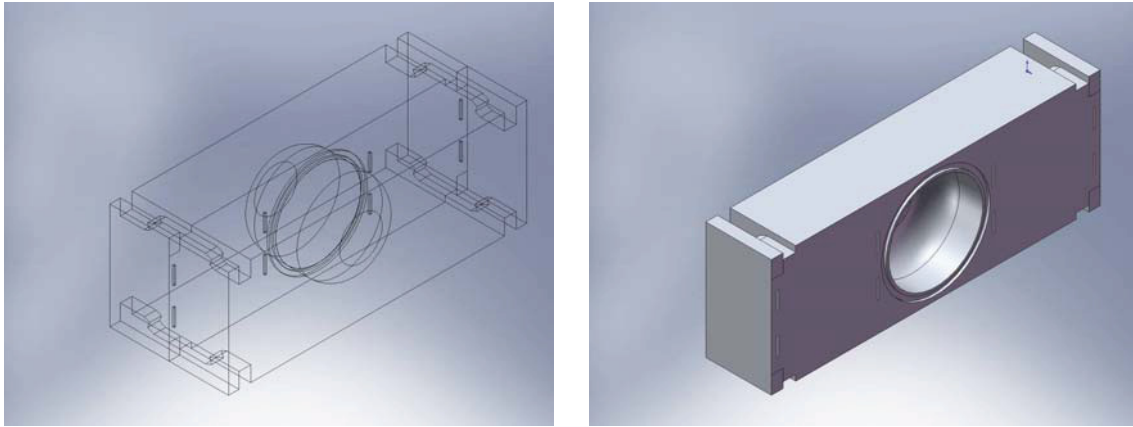


Figure 4-5. Fitting for positioning of boron sphere. Both halves are shown on the left. Detail of one half is shown on the right. The boron sphere fits into the central cavity. Duplicate flux wires are placed in the indented slots at each end and in the central region of the left half of the fitting as shown in the diagram on the left.

In addition to the foil measurements described above, activation measurements for the balanced outer shim critical configuration will be made with standard ATRC uranium/aluminum flux wires mounted at the axial midplane of all odd-numbered (1,3,5, etc.) fuel elements using standard plastic wands to determine the fission rate distribution throughout the ATRC core in the usual manner. Odd numbered elements 1-39 will have wires only in the three circled positions shown in the Figure 4-6. In addition, the four even-numbered elements surrounding the NW flux trap (Elements 32, 34, 36, 38) will be instrumented with standard INL copper/gold (1.55% Au by weight) flux wires in the three positions of interest shown in Figure 4-6 to determine two-group neutron spectra at these locations. The standard fitting shown in Figure 4-3 will be placed in the NW LIPT, with the foil holding strips (Figure 4-4) in place, with Cu/Au normalization wires but without foils for this irradiation. The U/Al flux wires used in these measurements will be standard approved wires. The Cu-Au wires will come from the same INL stock as before.

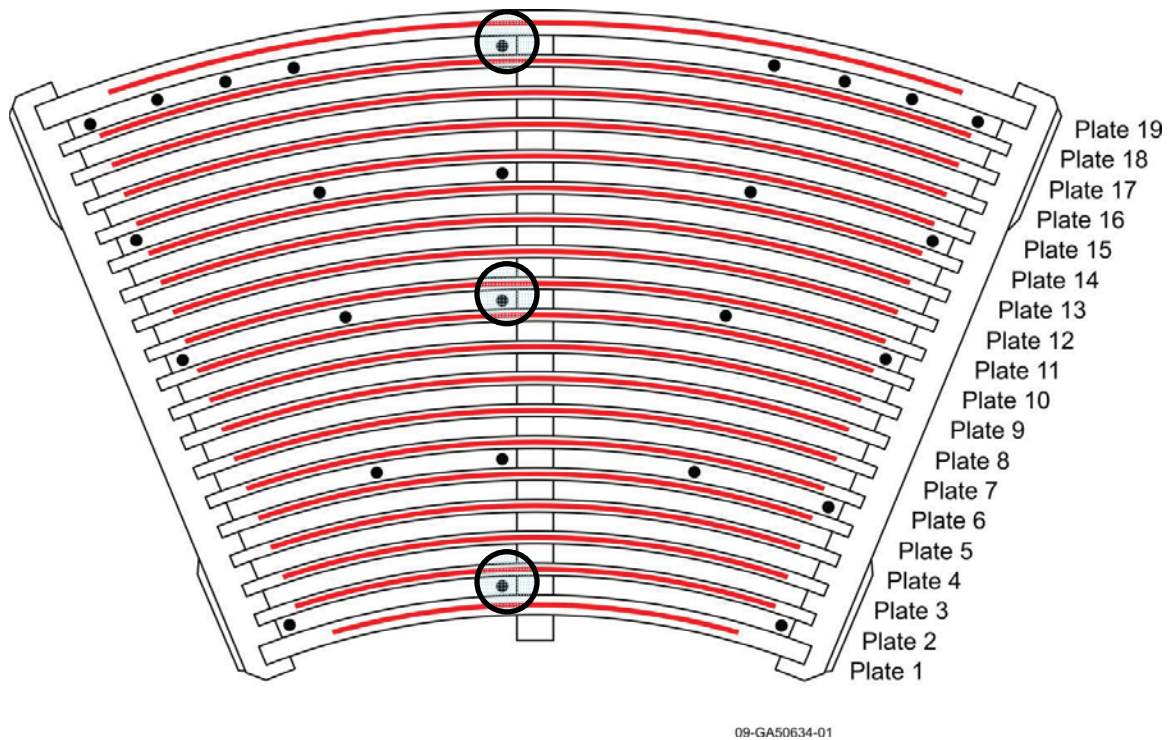


Figure 4-6 ATRC Fuel Element showing available flux wire positions. The circled positions are discussed in the text.

The typical experimental arrangement for the NW LIPT, referred to as a Test Train, consists of several standard approved aluminum sample holders that are assembled together and then put inside of an aluminum shroud that fits inside of the NW LIPT. Testing in the NW LIPT will employ existing LIPT hardware that will house the specially-designed inserts depicted in Figures 4-4 and 4-5. Figure 4-7 illustrates how the test train is assembled and positioned in the NW LIPT. The LIPT Test Train rests on the bottom of the LIPT at an axial height of -28 inches from core mid-plane. The height of the test train is adjusted with a nosepiece that is adjustable from 2-4 inches.

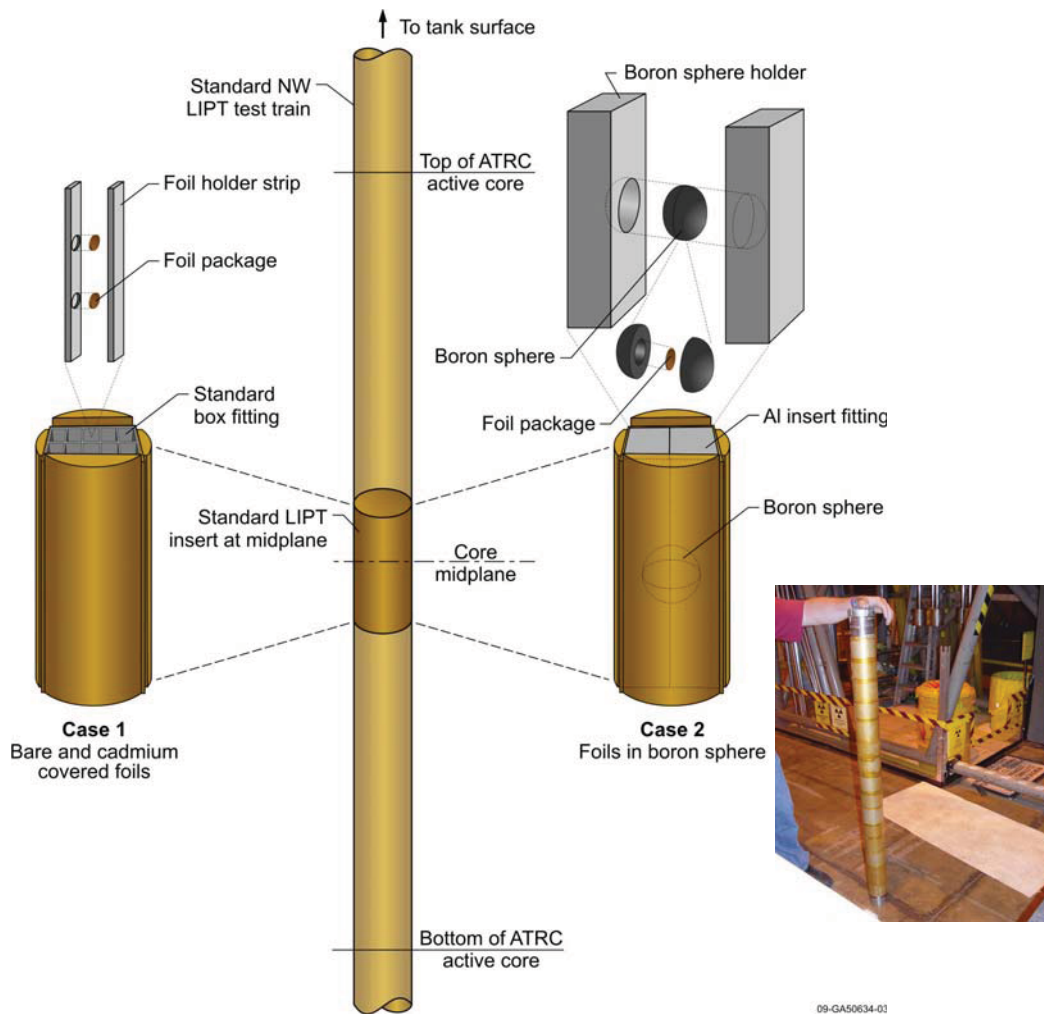


Figure 4-7 Positioning of test train components in the ATRC Northwest Large In-Pile Tube. The inset photo shows the entire assembled test train.

Three 20-minute ATRC reactor runs, each at a power in the range of 120 watts average power per lobe (600 watts total core power) are required to complete a set of activation measurements in the NW Flux Trap for the balanced outer shim configuration. The first reactor run is for irradiation of duplicate sets of bare and cadmium-covered foils in the aluminum strips shown in Figure 4-4. The strips are positioned in the square fitting that goes into the cylindrical LIPT insert as described. The second run is for the same setup but without the foils (i.e. with only the Cu/Au flux wires in the strips), to characterize the unperturbed condition required in the spectral deconvolution procedure. The third run is for irradiation of the foils in the boron sphere positioned using the insert fitting shown in Figure 4-5. In the case of the balanced shim configuration, a fourth 20-minute run is required for the core fuel element flux characterization as described earlier. The core flux distribution measurement for the balanced shim position is conducted using standard ATRC core flux run procedures, with the exception that Cu/Au flux wires are substituted for standard U/Al wires in selected fuel elements surrounding the NW LIPT, again as described previously.

The reactor power and irradiation times for the foils are estimated based on previous extensive INL experience with the same foils and wires in various other research reactor-based and accelerator-based neutron measurements at Washington State University, the University of Washington, the University of Missouri, and the Studsvik research reactor at their facility in Nyköping, Sweden, all scaled to the desired thermal flux in the ATRC NW flux trap of approximately  $10^9$  n/cm<sup>2</sup>-s. These estimated times may be adjusted for repeat runs based on experience. The masses of the foils in the boron sphere may also be adjusted for any repeat measurements that may be needed.

Handling of the irradiated foils and wires is done under an approved job-specific Radiation Work Permit. Radiation levels from the foils and wires at the time of discharge from the reactor are anticipated from previous relevant experience in neutron flux fields of the same approximate magnitude to be in the approximate range of 5 millirems per hour or less per foil or wire at a distance of 30 cm (1 ft). All foils and wires are transferred after irradiation to the nearby Radiation Measurements Laboratory for detailed gamma spectrometry to obtain the measured saturation activities required for the spectral deconvolution procedures.

## **4.2 Experimental Procedure and Results**

All of the required hardware for the NW LIPT activation measurements was fabricated during FY-10 and near the end of the year the complete test train inserts for the first three irradiations were assembled. Because of various factors affecting ATRC availability, only the first two irradiations described previously were conducted in FY-10, however. The third and fourth irradiations for the balanced shim configuration will be conducted in early FY-11.

### **4.2.1 Final Assembly of Apparatus**

The NW LIPT foil and wire insert fittings described in previous sections were fabricated to INL Quality Level 2 standards by the INL Prototype Shop. Final assembly of the experimental components was

conducted at the INL Radiation Measurements Laboratory at the Advanced Test Reactor Complex. Figure 4-8 shows the foil positioning strips for the first irradiation. Duplicate bare and cadmium-covered foil packages (Tables 4-1 and 4-2) were placed in both strips, with the Cd-covered package in the upper position in the first strip and in the lower position in the second strip. The upper and lower positions are reversed for the bare foil packages. This will allow quantification of flux differences that that may exist between the upper and lower positions due to axial gradients. Cu-Au flux wires are also inserted in the upper, middle and lower indentations as shown. This will allow additional quantification of flux gradients.



Figure 4-8. Foil positioning strips for the bare and cadmium-covered foil packages, with foils and normalization wires in place

Figure 4-9 shows the foil positioning strips prepared for the second irradiation, with flux wires in the various positions as before, but without foil packages. This arrangement represents the assumed “unperturbed” LIPT configuration, which is required in the unfolding process. Figure 4-10 shows the foil positioning strips as they mounted in the standard NW LIPT test train inserts that are used for all of the irradiations. The insert also contains “dummy” strips in the other eight positions as shown. These dummy strips are designed so that the fully-assembled insert will have the same metal to water ratio as it will have in the case of the third irradiation, where the boron sphere positioning device is substituted in the place of the foil holding strips and dummies used in the first and second irradiations. Final assembly of the foil positioning strips consists of fastening the cover strips in place using aluminum machine screws.



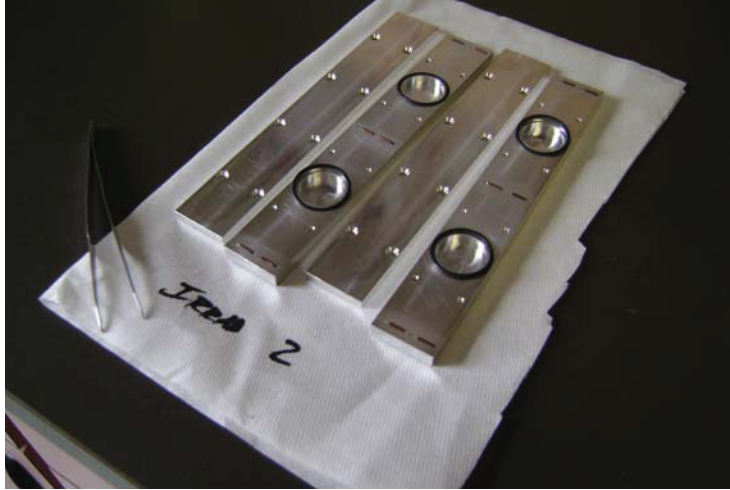


Figure 4-9. Foil positioning strips for the unperturbed flux configuration, with normalization wires in place.



Figure 4-10. Foil positioning strips and dummy strips mounted in the standard NW LIPT test train insert.

Finally, Figure 4-11 shows the insert fitting used to position the boron sphere, with the sphere loaded with its foil package (Table 4-3) and placed in the spherical cavity in the fitting. Final assembly of this fitting consists of bolting the two halves together using the aluminum cap screws seen on the right side of the illustration.



Figure 4-11. Boron sphere with enclosed foil package, mounted in its insert fitting.



Figure 4-12. Combined view of the various components of the NW LIPT Neutron Activation Spectrometry apparatus.

#### 4.2.2 Conduct of Irradiations

The first two irradiations described earlier were successfully conducted in late September 2010 at the ATRC. The activities of the foils and wires were measured at the INL Radiation Measurements Laboratory (RML) and the results were archived according to standard RML procedures. Irradiations 3 and 4 are planned for early November 2010, followed by detailed analysis of the data and reporting of the results for all four irradiations.

## 5.0 FEASIBILITY TESTING FOR ATR FUEL BURNUP MEASUREMENT SYSTEM

Computational models of the ATR will require information on the isotopic burnup of all irradiated fuel elements that are to be re-used in the reactor when the new modeling and simulation package is put into production use for ATR fuel management. Burnup Measurement is a confirmatory tool to compare the results with the existing records and model calculations. Feasibility measurements have been developed and carried out on some selected fuels in ATR canal to determine if it is possible to get a meaningful gamma-ray spectrum of very hot fuels, identify the fission isotopes, establish a method for burnup calibration for long cooling times (1-3 years) and investigate the best way to measure burnup for short cooling times (< 6 months) fuels. A combination of these two calibrations can be used to determine the burnup for fuels between these two cooling times (6-12 months). Burnup of ATR fuel elements will also be evaluated to support re-use of partially burned elements. Data collected during the evaluation will be used to establish a burnup for each element, and this will serve as the beginning point for core following calculations to be performed using an upgraded ATR modeling and simulation system.

### 5.1 Introduction

The absolute gamma-ray activity of a particular fission product, or the ratio of the particular isotopes, is used to measure the fuel burnup. This depends on the fuel element cooling time. No matter which technique is used, there is a linear relationship between the absolute isotope activity or isotopes ratio and the burnup value. The burnup calibration is obtained by measuring fuel elements with different burnup, well known irradiation history, and cooling times. The burnup is then plotted versus the absolute activity or isotopes ratio to obtain a linear burnup calibration curve. Finally, the burnup for unknown fuel element is simply derived from this calibration curve. For long cooling times fuels (> 9 months), the absolute activity of  $^{137}\text{Cs}$  or ratio of some fission product isotopes such as  $^{134}\text{Cs}/^{137}\text{Cs}$  or  $^{154}\text{Eu}/^{137}\text{Cs}$  is used. However, for short cooling time fuels (< 6 months), the absolute measurement of activity of  $^{95}\text{Zr}$ ,  $^{106}\text{Ru}$ ,  $^{144}\text{Ce}$ , or  $^{140}\text{La}$  may be required.

### 5.2 Measurement Setup

We need to emphasize here that all measurements were done with the detection system hanging with the crane and the detector position was controlled using ropes attached to the front and the back of detection system. This is done for the preliminary feasibility measurements reported here in order to avoid the expense of building a tower structure with motors to place the detection system at an exact location. The purpose was to determine whether the preliminary results are promising before committing to build an expensive tower structure. In this section, we describe the types of detectors used, waterproof housing and collimators of the detection system, and finally the measurement configurations.

#### 5.2.1 Detectors

Historically, detector of choice for very high-resolution gamma-ray spectroscopy has been Hyper-Pure Germanium detectors (HPGe). Another alternative is to use room temperature inorganic scintillation detectors. Among them the NaI detector is the most popular scintillator with advantages of ambient temperature operation, relatively low cost per unit mass, and its availability in large sizes for high efficiency detection. The energy resolution for this detector is about 7% at 662-keV line of  $^{137}\text{Cs}$ . The disadvantages of NaI detectors are fragile and likely to fracture due to thermal shock, gain change due to temperature change and poor energy resolutions of greater than 8% when a large size crystal is utilized. For fuel burnup measurements the detection system must be rugged, not very sensitive to environmental temperature extremes. It should preferably operate at room temperature if possible and must have a better

energy resolution than NaI detector. Within the last few years, several promising detector candidates have emerged that offer resolution between that of HPGe and NaI. In particular, two alternate room temperature detector types are now available as commercial detector products offering energy resolution in the range of 2.5% to 3.5% with acceptable efficiency for many applications. These are lanthanum bromide  $\text{LaBr}_3$  (Ce activator) scintillation detector and high pressure xenon (HPXe) detector. A commercial scintillation supplier (Saint-Gobain) recently reported the availability of a 3" x 3"  $\text{LaBr}_3$  scintillation detector with resolution of 2.8%. HPXe detectors of 1.75" diameter x 4" active length and 2.5% resolution are commercially available from Constellation Technology Corporation, as are detectors as large as 4.5" in diameter by 24" long. The HPXe detector energy resolution is better than other room-temperature detectors like NaI and CsI scintillators by a factor of 2.5 and also is a little better than  $\text{LaBr}_3$  detectors.

For our feasibility study of ATR fuel burnup measurement, we used three types of HPGe,  $\text{LaBr}_3$ , HPXe and detectors as shown in Figure 5-1. Two different sizes of HPGe detectors (40% efficient and 25% efficient) and two different sizes of  $\text{LaBr}_3$  (1"x1" and 2"x2") were utilized in our measurements. The performance of these detectors has been tested to determine which one is better suited for specific cooling times and burnup. In some cases like very short cooling time it is absolutely necessary to use an HPGe detector because of many close-by gamma rays that cannot be resolved using the other two detectors. However, for fuels with a long cooling time the less expensive  $\text{LaBr}_3$  or HPXe detector is more likely sufficient.

#### 5.2.1.1 HPGe Detector

HPGe detectors are used for high resolution gamma ray spectroscopy. A typical energy resolution is about 0.15% (2 keV) at 1332 keV line of  $^{60}\text{Co}$ . This superior energy resolution makes it possible to resolve gamma rays closely spaced in energy (<2 keV). Although, their superior energy resolution cannot be matched by other types of detectors, the HPGe detectors must be operated at cryogenic liquid nitrogen temperature. The requirement for cryogenic cooling of HPGe detectors and their overall size, limit their range of applications and complicate their implementation and precludes their use in in-situ measurements of spent fuel elements under the water. Also, the HPGe detector cannot be used in hostile environment such as in a high radiation field without adequate shielding. Recently, new mechanically-cooled HPGe detectors have been



Figure 5-1 Detectors used in this study.



developed based on Stirling-cycle cooler that eliminates the need to use liquid nitrogen for cooling. Much smaller footprint of this type of detector (LDM-100) was introduced by AMETEK-ORTEC Company that is more suitable for our application. This detection system includes a complete system of detector, digital signal processing, and software.

For our measurements we used two HPGe detectors with detection efficiencies of 45% and 25%. All measurements with these two detectors were performed above the water, which will be discussed later.

#### **5.2.1.2 LaBr<sub>3</sub> Detector**

The recently developed LaBr<sub>3</sub>(Ce) scintillator is becoming very popular for its use in gamma ray spectroscopy measurements due to its good timing resolution (few hundreds of pico seconds) and most importantly its energy resolution of 2.8-3.5% at 662 keV depending on its size and purity. This good energy resolution, in fact, makes this detector an alternative to HPGe and NaI in some applications. One major disadvantage is the inherent alpha- and gamma- contamination arising from decay of <sup>227</sup>Ac and <sup>138</sup>La impurities in the crystal that cannot be removed completely. These impurities, however, are very small and only affect the low-level gamma ray counting measurements. Another important factor to consider is the exposure of this detector to high gamma ray dose of radiation. The radiation effect induced by high gamma irradiation doses from a strong <sup>60</sup>Co source has been investigated using a 1"x1" detector. The most significant change of both yield and energy resolution takes place after the first irradiation with a 0.1 kGy dose. As much as 22% of the yield is lost, at the same time the resolution increases from 2.8% to 4.6%. Therefore, For the ATR fuel burnup measurements depending on gamma-ray field it is necessary to use sufficient shielding if a LaBr<sub>3</sub> detector is used. Another factor to consider in choosing LaBr<sub>3</sub> detector is its gain change at high count rates and temperature change. Temperature stability is important in applications where the detector temperature may change significantly on a daily and seasonal basis. One way of resolving this issue is to use internal calibration method for each spectrum taken. This can be done easily in our application because the energies of gamma-rays emitted from fission isotopes for short and long cooling times are very well known.

Currently, LaBr<sub>3</sub> detectors are expensive. This is because it is based on relatively new technology and cost of crystal purification to remove the impurities of <sup>138</sup>La and <sup>227</sup>Ac radioisotopes. The cost for 1/2"x1/2", 1"x1", 2"x2", and 3"x3" detectors are \$7K, \$15K, \$23K, and \$35K, respectively. In our measurements we used a 1"x1" and a 2"x2" LaBr<sub>3</sub> detector and supporting electronics system. For the former the conventional low-noise analog electronics plus ADC were used, whereas the latter was consisted of the detector attached to a DigiBase (photomultiplier and digitizer) that in turn is connected to a laptop computer through a USB cable. The Maestro software was used for data acquisition and the INL developed SPEX program was used for data analysis. The energy resolutions for 1"x1" and 2"x2" were measured to be 3.2% and 2.7%, respectively. These resolutions are better than manufacturer's claims.

Both detector was calibrated in the lab using several calibration sources including <sup>137</sup>Cs, <sup>60</sup>Co, <sup>152</sup>Eu, and <sup>226</sup>Ra. The relative efficiency calibration of the detectors was obtained using <sup>152</sup>Eu, and <sup>226</sup>Ra sources. This relative efficiency allows us to make correction for different gamma-ray energies. Next, the performance of the 2"x2" detector in a high gamma-ray field was measured using a strong 180  $\mu$ Ci <sup>137</sup>Cs source. The source to the detector distance was adjusted in order to achieve 90% dead time. Under this condition the energy resolution degraded only from 2.8% to 3.1%, which is very good.

The performance of the 1"x1" LaBr<sub>3</sub> detector was compared with measurements done with the 2"x2" detector to determine which one is more suited for burnup measurements. The measurements were performed with the same fuel element at the same distance in the water. The results showed the peak-to-Compton ratio (P/C) for the 662 keV Cs-137 peak is actually better for the smaller detector (1.4) than the larger detector (1.1). This is because the smaller detector sees less background due to the gamma rays going through the sides of shielding than the larger detector. Here, the size of the detector plays an important role. The smaller the detector means less background and consequently higher P/C ratio.

### 5.2.1.3 HPXe Detector

This detector can be used in harsh environment applications such as environmental monitoring stations, power reactor fuel measurements and bore-hole measurements at nuclear facility sites. It can be used for the energy range 0.1-2 MeV gamma rays. The unique properties of this detector such as good energy resolution, a wide operational temperature range, and long-term stability against radiation damage make it applicable in various fields of fundamental and applied research. In order to improve the resolution of this detector a grid electrode (called Frisch grid) must be placed close to the anode. This makes the detection system susceptible to acoustic influences in some application, which in turn degrades the detector resolution. Decreasing the microphonic sensitivity is necessary for improving the characteristic of these detectors. Recently, significant progress has been made to reduce this sensitivity to about 70 dB. Also, in the past, difficulties with obtaining sufficient xenon purity as well as the difficulties associated with developing the low-noise electronics necessary to extract useful information from small ionization signals have limited the use of this detector. Unlike LaBr<sub>3</sub>, the gain of this detector is quite stable and time variance of the gain is about 0.02% over a week. This stability is important in eliminating the need for periodic calibration. The detection efficiency is typically about ~3% at 662 keV and ~1% at 1332 keV. These low efficiencies to gamma rays are advantages in a high gamma-ray field that allow us to get the detector closer to the fuel element without saturating the detector and associated electronics. The detector energy resolution at 662 keV is about 2-2.5% and at 1332 keV is about 1.5-2%, which is far better than NaI detector and a little better than LaBr<sub>3</sub> detector. The main disadvantage of this detector is its small photo-peak efficiency (peak-to-Compton ratio; P/C) resulting of gamma rays not being able to deposit their full energies. This becomes more problematic at high energies (> 1 MeV) where only part of the energy will be deposited in the gas. In order to remedy this problem higher gas pressure, larger detector, or longer counting time will be required. However, these changes may not be possible in some applications. Overall, this detector is a potential alternate to LaBr<sub>3</sub> detector for short cooling time fuels where the radiation field is so high that the LaBr<sub>3</sub> detector cannot be placed close to the fuel element or cannot be used at all due to saturation of electronics.

We used 1.5" in diameter and 4" long HPXe detector made by Constellation Technology. This detector consists of the ionization chamber filled with a Xenon gas plus 0.3% H<sub>2</sub> mixture at the density of 0.35 g/cm<sup>3</sup> and gas pressure of 650 psi (44 atmospheres). This detector has energy resolutions of 2.7% and 2.0% for the <sup>137</sup>Cs 662-keV peak and the <sup>60</sup>Co 1332-keV peak, respectively.

### 5.2.2 Waterproof housing and shielding collimators

Figure 5-2 shows the waterproof housing, collimators, and detector holder used in the measurements. The housing is made of aluminum and is 9" in diameter and 16" long. It consists of cylinder attached to the front and back plates. The back plate has a cables port, which attached to the PVC tube for sending HV, preamplifier and signal cables through and then to electronics modules outside the water. Other parts are support a rod made of stainless steel (attached to the front and back plates) and crane hook for lifting the housing. Inside the housing there is a collimators holder to make sure everything is centered along the housing cylinder axis. The collimator system is made of bismuth (Bi) that contains several different pieces for a multi-purpose functionality that can accommodate different types and sizes of detectors. This includes the 40% HPGe, 25% HPGe, 1"x1" LaBr<sub>3</sub>, 2"x2" LaBr<sub>3</sub>, and HPXe gas detectors used in this study. The collimator system consists of two 2"-thick Bi discs, collimator insert in the front, and one 1.5"-thick Bi cylinder in the back. Not shown in this figure, there is also an additional 0.5" Bi sleeve that can be inserted inside the bigger cylinder when smaller detectors are used to provide more shielding around the detector. In fact, this Bi sleeve was used in all of our measurements. Different collimator inserts with different shape and sizes were used to determine which ones deliver the best results under different measurement scenarios.



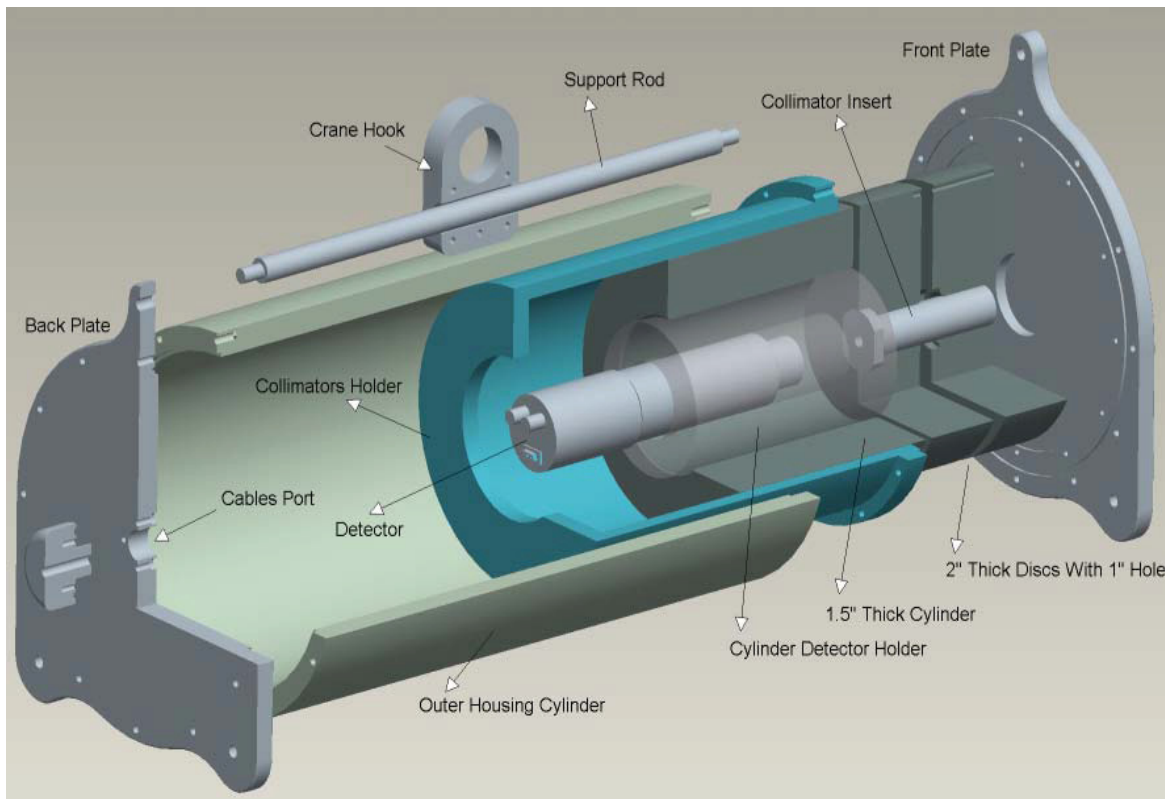


Figure 5-2. Waterproof housing and collimators.

The detector holder made of Nylon or Delrin is used to fill the gap between the detector and Bi collimator and more importantly to electrically isolate the detector from the housing for eliminating the noise signal. Different sizes of this holder were made to fit different sizes of detectors used in our measurements.

### 5.2.3 Measurement Configurations

The measurements for  $\text{LaBr}_3$  and  $\text{HPGe}$  detectors were performed both in and above the water. Because of the limitations due to the cooling of the  $\text{HPGe}$  detectors, the measurements with these detectors were carried out above the water. In both configurations the fuel elements were placed inside the turning table vertically, with the plate number 19 facing the detector. The detector was viewing a small section of the fuel assembly allowed through small aperture in the collimator insert.

For under the water measurements shown in Figure 5-3, the detection system was lowered with the crane to the desire position and ropes attached to the front and back of the lifting rod controlled the position of the detection system. The PVC tube attached to the back plate was used to send the cables from the detector to the electronics outside the water. In this configuration, it is important to make corrections due to the energy-dependent attenuation of gamma rays in the water.

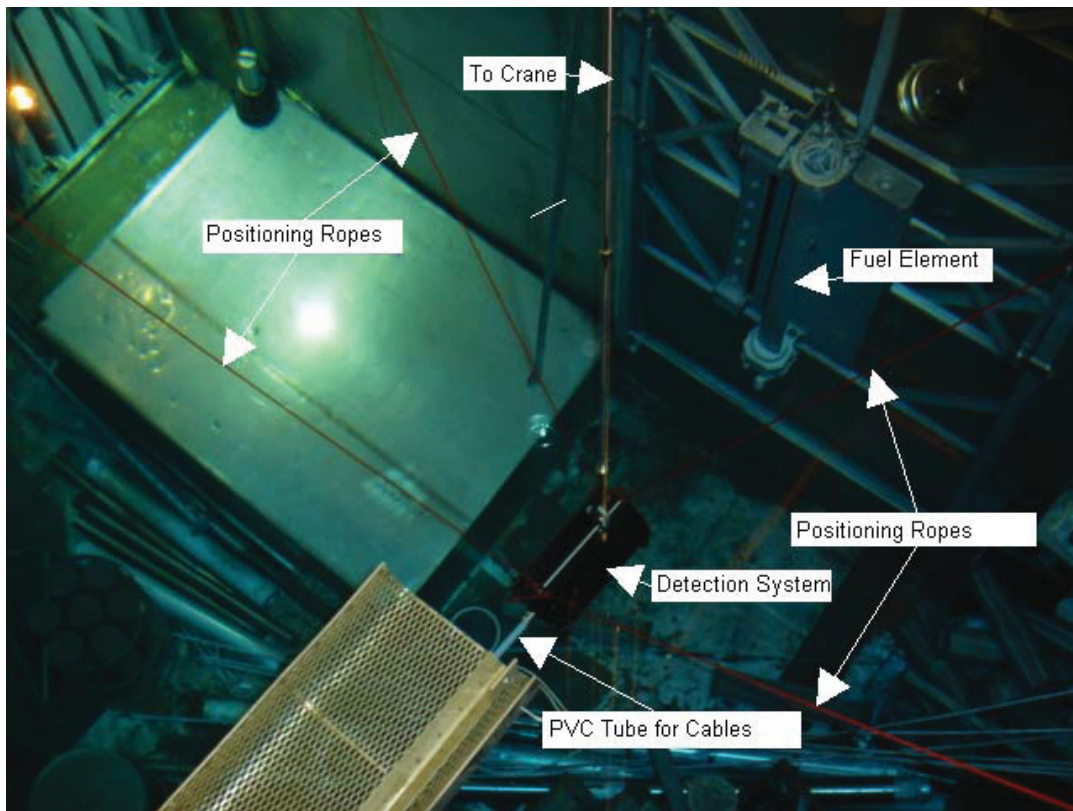


Figure 5-3. Under the water configuration.

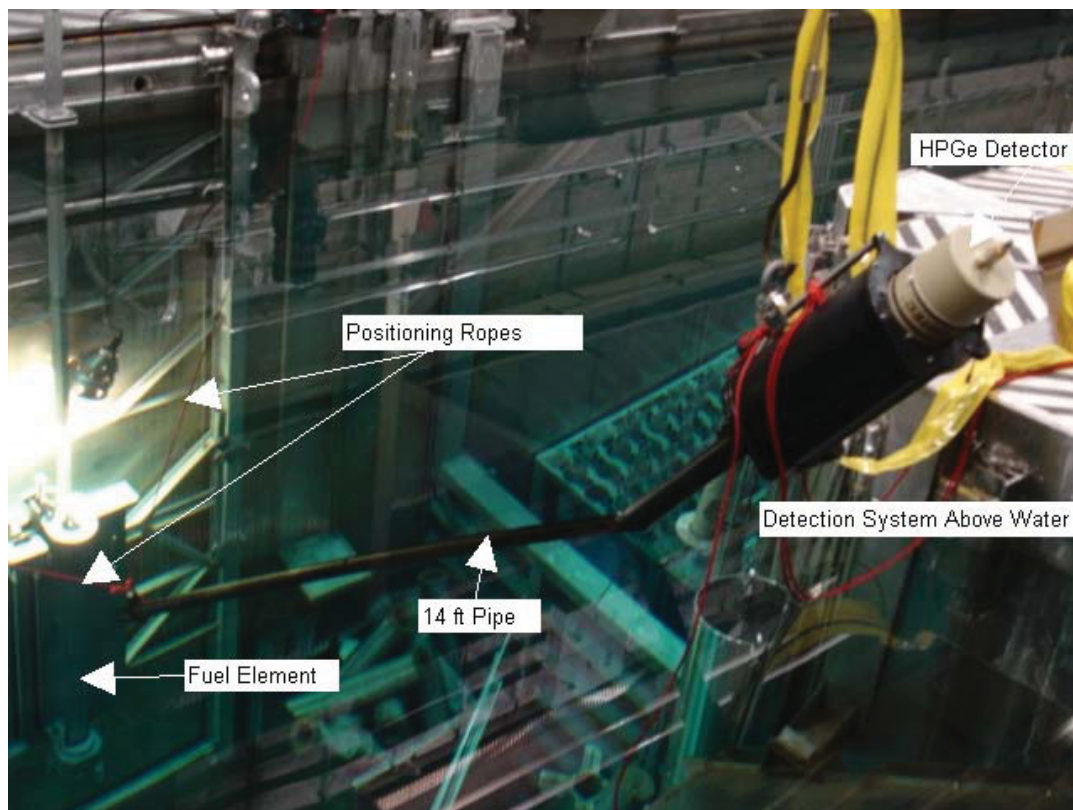


Figure 5-4. Above the water configuration.

The setup for the above the water measurement is shown in Figure 5-4. In this configuration a long 14-foot pipe with the 2.5" inches in diameter was attached to the front of detection system housing. This pipe was water-sealed with air inside. Inside the pipe at the end additional collimation system made of Bi was added in order to collimate gamma rays emitted from the fuel element through the pipe. Here again, collimator inserts with different aperture were utilized to decrease or increase the gamma-ray flux going through the pipe. For example, the collimator pipe with a small collimator insert hole allows the detector to view small section of the fuel assembly and therefore the pipe can be moved closer to the fuel element. Like the previous configuration, the detection system was hanged from the crane and the ropes were used to position the end of the pipe at the desired position.

### **5.3 Model Calculations**

#### **5.3.1 ORIGEN Program Description and Version Used**

ORIGEN 2.2 (Croff et al., 1980) is a point depletion and decay computer code used to simulate nuclear fuel cycles. The original code was developed in the late 1960's and early 1970's by the Chemical Technology Division at Oak Ridge National Laboratory. Currently the Radiation Safety Computational Center is in charge of developing and maintaining the most recent ORIGEN code. The code uses the matrix exponential method to solve a large system of coupled, linear first-order ordinary differential equation with constant coefficients in order to obtain build up, decay, compositions and radioactivity of fission products. The code also includes extensive nuclear data libraries that are used as inputs.

##### ***5.3.1.1 Burnup estimates and Corrections using PDQ calculations***

In our study the ORIGEN 2.2 computer code was used to calculate burnup and depletion rates along with fission products isotopes activities of ATR fuel elements. The objective was to correlate experimental isotopic activity or isotopic ratios with ORIGEN fuel burnup values to create calibration curves that would create a tool to predict fuel burnup of ATR fuels. Correlations are necessary because determining burnup directly from gamma spectroscopy is a difficult task.

Correlations between fission products activities or ratios with burnup of different types of fuel (mainly long cooling times) have been the topic of several studies. Based on those studies, numerous calibration curves using ORIGEN 2.2 burnup results in combination with experimental fission products absolute and isotopic ratio activities were created. Establishing the consistent relationships between activity measurements and burnup will ultimately allows us to experimentally determining ATR fuel elements burnup without the need of previous irradiation history or computer calculations.

In some instances ORIGEN 2.2 calculated amount of  $^{235}\text{U}$  differs from the results obtained from PDQ calculations. PDQ is a two dimensional group diffusion computer code that employs continuous slowing of neutrons and is the standard code for operations at the Advanced Test Reactor Facility. In order to be consistent adjustments in the number of effective power days were made to the ORIGEN input to obtain a result that eliminate the difference in amount of  $^{235}\text{U}$  with PDQ code.

### **5.4 Measurement Techniques**

An efficient and reliable fuel management program requires having on-site accurate information concerning fuel elements without having to completely rely on computer codes. An integral part of any on-site fuel management system has to involve non-destructive techniques that can provide burnup and cooling time information of fuel elements without the need of expensive destructive chemical tests. Non-

destructive methods are a more attractive tool than chemical tests because they are faster, cheaper and most importantly they preserve the integrity of the fuel.

The use of gamma-ray spectrometry for the passive, non-destructive determination of spent fuel burnup and cooling time has been common in domestic and international safeguards for decades (Reily et al, 1991; Ramalho and Payne, 1979; Phillips et al., 1980; Lebrun and Bignan, 2001). These techniques usually rely on ratios of various fission products rather than absolute concentration measurements. This is because ratios is geometry-independent and can generally be determined more accurately. Also, the fission product ratios measured by gamma-ray spectrometry can be directly compared with those computed by a validated isotope build up and model calculations code such as ORIGEN. This code uses the data provided with either the operator-declared irradiation and cooling history, or a generic set of irradiation and cooling times to confirm the irradiation history.

Two of the most important parameters for fuel management are burnup and time since discharge of fuel assemblies. Burnup of the fuel is among the most valuable piece of information that ideally can be obtained by knowing the initial material composition and comparing it to the amount of fissile material left in the fuel at the end of the reactor power cycle. However, performing a procedure that can effectively and directly measure the leftover material is very difficult. The  $^{235}\text{U}$  content cannot be directly measured because gamma rays from the fission products dominate the spectrum by roughly 7 orders of magnitudes, which mask the  $^{235}\text{U}$  gamma rays. One of the feasible and simpler ways is to use gamma-ray spectroscopy to indirectly estimate burnup by using the spontaneous emission of gamma-rays emitted from the fission products.

A simplified set of equations applicable only for direct fission products produced in a single continuous irradiation can be used to illustrate the correlation of measured gamma-ray spectral results to burnup and cooling times (Phillips et al., 1980). Gamma-ray signatures of irradiated fuel assemblies originate from the fission products in the fuel, the activation products of the cladding, and associated structural material. The gamma-ray spectra can be analyzed to compute the fission product activities at the time of measurement. From the counting rate in the  $j^{\text{th}}$  photopeak of a fission-product isotope  $i$ , the total number of atoms present in the fuel assembly at the time of measurement as well as at the end of irradiation exposure can be calculated by using the following equations.

$$N_i = \frac{A_{ij}}{\lambda_i \epsilon_j B_{ij}} \quad \text{and} \quad N_i^0 = N_i e^{\lambda_i T_c}$$

where:  $N_i$  = the number of atoms of the  $i^{\text{th}}$  isotope at the time of measurement

$A_{ij}$  = the peak count rate of the  $j^{\text{th}}$  gamma ray from the  $i^{\text{th}}$  isotope

$\lambda_i$  = decay constant of the  $i^{\text{th}}$  isotope

$\epsilon_j$  = detection efficiency for the  $j^{\text{th}}$  isotope, including all absorption corrections

$B_{ij}$  = the emission probability of the  $j^{\text{th}}$  gamma ray in the decay of the  $i^{\text{th}}$  isotope

$T_c$  = time since end of irradiation (cooling time)

$N_i^0$  = the number of atoms of the  $i^{\text{th}}$  isotope at the end of the irradiation

The parameters  $\lambda_i$  and  $B_{ij}$  are physical constants,  $A_{ij}$  is measured, and  $\epsilon_j$  value is obtained from the detector efficiency calibration.

Defining burn up as number of fissile atoms fissioned per 100 fissile atoms initially present (at%), the fuel burn up can be calculated as:

$$\text{at\%} = (100) \left( \frac{N_i^0}{Y_i U} \right)$$

where: at% = the fuel burn up

$Y_i$  = the fission yield of the  $i^{\text{th}}$  product

$U$  = the number of initial uranium atoms

For a single isotope, the following relates the cooling time ( $T_c$ ) to  $N_i$ .



$$T_C = \lambda_i^{-1} \ln \left( \frac{N_i^0}{N_i} \right)$$

and by extension to two isotopes:

$$T_C = (\lambda_2 - \lambda_1)^{-1} \ln \left( \frac{N_1 N_2^0}{N_2 N_1^0} \right)$$

Basically if the irradiation history is known then the cooling time can be determined from the gamma-ray spectral data. Conversely, if the cooling time is known, the burnup can be computed from quantitative gamma-ray spectrometry. The cooling time can be determined from measured activity ratios rather than absolute activity values. Ratio determinations require only relative efficiency and sample attenuation corrections that are more easily and accurately measured than absolute values. In fact, if several gamma-ray peaks from the same nuclide are detected in a given measurement, the required corrections can be derived directly from the spectral data.

In principle, the greater the number of fission product isotopes detected during non-destructive assay of a given fuel element, the better the fuel burnup and cooling times can be predicted. Also, the more gamma-rays detected from each individual multi-gamma-ray emitting nuclide, the better the relative detection efficiency and source attenuation can be quantified.

There are about 10 major isotopes produced in fission process that can be measured after fuel discharge. Table 5-1 lists these dominant isotopes, along with their half-lives and gamma rays. Only strong gamma rays are listed. In this table, the decay half-life, fission yields (per 100 fission disintegrations), Gamma-ray relative intensity (in black) and gamma-ray emission probability (in red) are reported. In addition to the fission product gamma rays, gamma rays from the activation of fuel cladding and structural materials such as <sup>54</sup>Mn, <sup>58</sup>Co, and <sup>60</sup>Co may be also present depending on type of reactor, type of fuels, and etc.

Either absolute gamma-ray spectroscopy that measures the activity of one or more fission product isotopes, or relative measurements that determine the ratio of activities of two certain isotopes can be used to measure the fuel burnup. Absolute activity measurements require the careful and precise determination of the detection system efficiency calibration that is energy dependent. This means that being able to position the detection system at precise position all the time in order to obtain accurate results. Unfortunately, this was not possible with the crane system used in this study. However, with the proposed permanent system (discussed later) capable of positioning the detection system within 1/1000" accuracy, absolute measurements is easily achievable.

Table 5-1. Fission Fragments in Fuel Assemblies with their half-lives and associated main gamma rays from their decay. The % relative intensities are in black and the gamma-ray emission rates per 100 fission decays are in red. Only strong gamma rays are listed in this table.

Isotope	Half-Life	Fission Yields (%)	Main gamma rays (keV)
$^{140}\text{Ba} \rightarrow$ $^{140}\text{La}$ $^{140}\text{La} \rightarrow$ $^{140}\text{Ce}$	12.75 d 1.68 d	6.2	537.26 (100%, 24.4%) 328.8 (19.6%, 20.3%), 487.0 (44.7%, 45.5%), 815.8 (24.2%, 23.3%), 925.2 (7.2%, 6.9%), 1596.2 (100%, 95.4%), 2521.4 (3.59%, 3.5%)
$^{95}\text{Zr}$	64.02 d	6.5	724.2 (80.6%, 44.2%); 756.7 (100%, 54.5%)
$^{95}\text{Nb}$	34.99 d	6.5	765.8 (100%, 99.8%)
$^{144}\text{Ce}$	284.5 d	5.5	133.5 (80.4%, 11.9%) 696.4 (100%, 1.3%); 1489.2 (21.4%, 0.3%); 2185.6 (57%, 0.7%)
$^{103}\text{Ru}$	39.27 d	3.0	497.1 (100%, 91.0%); 610.3 (7.4%, 5.8%)
$^{106}\text{Ru}$	1.02 yr	0.4	511.4 (100, 20.4%); 621.9 (48.8%, 9.9%); 873.5 (7.6%, 0.4%); 1050.5 (7.6%, 1.6); 1128.1 (1.98%, 0.4%); 1562.2 (0.8%, 0.2%)
$^{133}\text{Xe} \rightarrow$ $^{133}\text{Cs} + n \rightarrow$ $^{134}\text{Cs}$	2.06 yr	6.7 <sup>a</sup>	569.3 (15.3%, 15.4%); 604.7(100%, 97.6%); 795.8 (87%, 85.5%); 801.8 (8.8%, 8.7%); 1038.5 (1.1%, 1.0%); 1167.9 (2.0%, 1.8%); 1365.1 (3.3%, 3.0%)
$^{154-xn}\text{Eu} +$ $xn \rightarrow$ $^{154}\text{Eu}$	8.59 yr	1.6 <sup>b</sup>	123.0 (100%, 40.6%); 247.9(16.8%, 6.9%); 996.3(30.3%, 10.5%); 1004.8(50.5%, 17.9%); 1274.4 (95.0%, 35.0%)
$^{137}\text{Cs}$	30.07 yr	6.2	661.6 (100%, 85.1%)

<sup>a)</sup> Fission yield is for the  $^{133}\text{Xe}$  isotope.

<sup>b)</sup> Fission yield is for the  $^{153}\text{Eu}$  isotope.

Typically, a good burnup calibration can be achieved by selecting few fuel assemblies (4-5) with different exposures and well known irradiation history and cooling times. Then the burnup is plotted versus the absolute Cs-137 activity or isotopic ratio to obtain a linear calibration curve. Finally, the burnup for unknown fuel assembly is simply derived from this calibration curve.

#### 5.4.1 Ratio Measurements

The ratios of certain radioisotope activities such as  $^{134}\text{Cs}/^{137}\text{Cs}$  or  $^{154}\text{Eu}/^{137}\text{Cs}$  are directly related to the fuel element burnup. In a study of measurements on 14 PWR fuel assemblies the  $^{134}\text{Cs}/^{137}\text{Cs}$  ratio technique coupled with one destructive assay of burnup, provided burnup determinations with good accuracies and in some cases within 5% (Phillips et al., 1980). The  $^{137}\text{Cs}$  isotope is a direct fission product and its concentration in the fuel is directly proportional to the integrated fluence. However,



$^{134}\text{Cs}$  and  $^{154}\text{Eu}$  have very low direct or chain fission yields, rather they are predominately produced by neutron capture of fission products  $^{133}\text{Cs}$  and  $^{153}\text{Eu}$ , respectively. Here, the  $^{134}\text{Cs}$  concentration within the fuel is approximately proportional to the square of the integrated flux. By dividing the concentration of  $^{134}\text{Cs}$  by the concentration of  $^{137}\text{Cs}$  the ratio becomes approximately proportional to the burnup. The  $^{134}\text{Cs}/^{137}\text{Cs}$  isotopic ratio has worked well for determining the burnup of both light-water-reactor and fast-breeder-reactor. The  $^{154}\text{Eu}/^{137}\text{Cs}$  isotopic ratio also has a fairly linear dependence on exposure. The use of isotopic ratios requires correcting for the decay of the isotopes. This correction is important for the  $^{134}\text{Cs}/^{137}\text{Cs}$  ratio because of the short 2.06-yr half-life of  $^{134}\text{Cs}$ . For the  $^{154}\text{Eu}/^{137}\text{Cs}$  isotopic ratio the 8.5-yr half-life of  $^{154}\text{Eu}$  and the 30.2-yr half-life of  $^{137}\text{Cs}$  make the correction less important. For ratio measurements only relative detector efficiencies must be known. However, it is still necessary to correct for changes in detection efficiency with gamma-ray energy. This is because the  $^{134}\text{Cs}$ ,  $^{137}\text{Cs}$ , and  $^{154}\text{Eu}$  gamma rays have different energies and therefore different detection efficiencies. These isotopes are used for very long exposure and greater than six months cooling time. Other burnup monitors like  $^{95}\text{Zr}$ ,  $^{106}\text{Ru}$ ,  $^{144}\text{Ce}$ , and  $^{140}\text{La}$  should be considered for short cooling time of less than 6 months. Each is selected based on amount of burnup and cooling time.

#### 5.4.2 Absolute Measurements

The absolute measurement of  $^{137}\text{Cs}$  fission product is widely accepted indicator of fuel burnup. This is because this isotope requires no knowledge of fuel composition or irradiation history. In addition, the  $^{137}\text{Cs}$  neutron absorption cross-sections are negligible and its 30-yr half-life makes a correction for reactor power history unnecessary. The only disadvantage is the requirement for absolute energy and efficiency calibration of the detection system and precise control of its geometry. This method has been shown to be consistently predicted by the different calculation codes such as ORIGEN and also validated by destructive analysis, provided the measurement geometry and detection efficiency are well known and reproducible. Therefore, the key here is to ensure that no changes occur between calibration conditions and measurement conditions. Also, there are several corrections such as background correction, energy-dependent relative efficiency correction, and self-attenuation correction that need to be implemented. For short cooling time (< 6 months) fuels, the absolute activity measurement of  $^{95}\text{Zr}$ ,  $^{140}\text{La}$  should be investigated.

#### 5.4.3 Fuel Selections

The selection on the fuel was based on an analysis from results of exploratory studies made with ORIGEN 2.2. The exploratory studies performed with ORIGEN were the main tool to efficiently and effectively determine how many and which ATR fuel elements to measure. The selection was based primarily on analyzing ORIGEN results from several calculations performed on a series of elements with a wide range of cooling times and irradiation histories. The ORIGEN Calculations told us which fission products isotopes to expect, their relative strength and their capability to correlate with burnup and cooling times.

Ultimately, the main objective of the feasibility study was to find correlations between experimental measurements and burnup. Figure 5-5 shows a burnup calibration curve created solely with ORIGEN results. The calibration curve includes elements that were in the ATR for one, two, and three cycles. The linear fit clearly shows the relationship between burn up and activity ratio as calculated by the code.

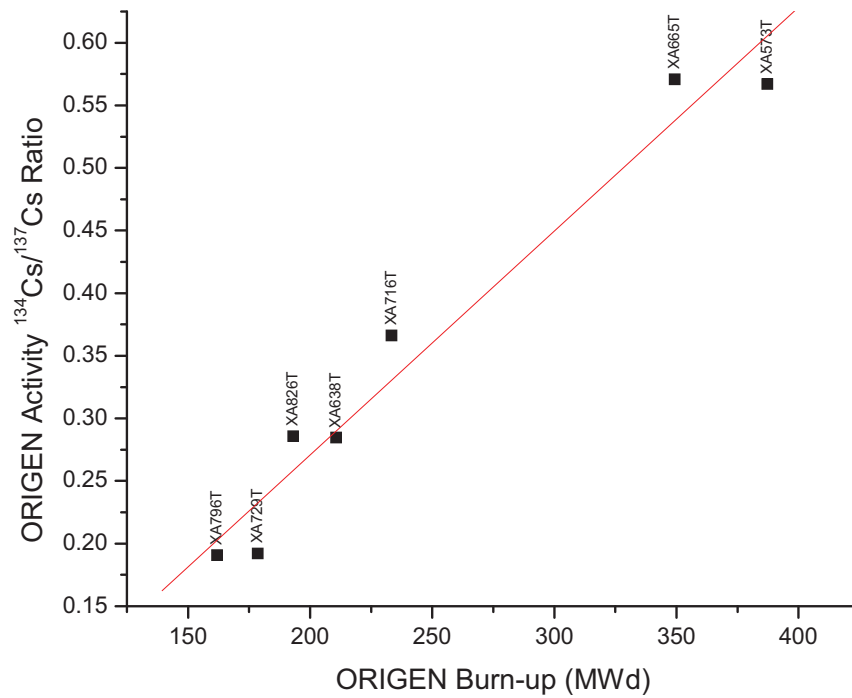


Figure 5-5. Plot of ORIGEN activity ratio versus ORIGEN burnup calculations.

Table 5-2 contains data generated with ORIGEN for seven ATR fuel elements. The table shows results for ten fission products isotopes that were used as monitors. These ten isotopes along with burn up rates and cooling times were the main factor in selecting ATR fuels for measurements. The effective and efficient selection of elements was a crucial part of the feasibility study because time constraints will not permit measuring a large number of ATR fuel elements in the canal.

Table 5-2. ORIGEN calculated activities of the fission product isotopes for 7 fuel elements selected for this study. The last two rows are for calculated burnup and cooling times, respectively.

<b>Isotope</b>	<b>XA729T Activity (Ci) Jun-17-10</b>	<b>XA796T Activity (Ci) Jun-17-10</b>	<b>XA826T Activity (Ci) Jun-17-10</b>	<b>XA638T Activity (Ci) Jun-22-10</b>	<b>XA716T Activity (Ci) Jun-22-10</b>	<b>XA573T Activity (Ci) Jun-17-10</b>	<b>XA665T Activity (Ci) Jun-17-10</b>
<sup>140</sup> Ba	1.179E-08	2.210E-05	6.903E-01	1.325E-05	3.431E-03	9.152E-09	2.123E-05
<sup>140</sup> La	1.357E-08	2.548E-05	7.945E-01	1.525E-05	3.948E-03	1.053E-08	2.443E-05
<sup>95</sup> Zr	1.854E+02	7.773E+02	6.974E+03	8.127E+02	2.557E+03	2.791E+02	1.177E+03
<sup>95</sup> Nb	4.092E+02	1.691E+03	1.385E+04	1.773E+03	5.442E+03	6.167E+02	2.569E+03
<sup>103</sup> Ru	2.817E+00	3.088E+01	9.903E+02	2.869E+01	1.771E+02	3.570E+00	4.027E+01
<sup>106</sup> Ru	3.974E+02	4.693E+02	7.969E+02	5.896E+02	7.836E+02	8.250E+02	9.655E+02
<sup>134</sup> Cs	1.071E+02	9.722E+01	1.758E+02	1.886E+02	2.704E+02	6.837E+02	6.267E+02
<sup>137</sup> Cs	5.577E+02	5.100E+02	6.154E+02	6.624E+02	7.384E+02	1.206E+03	1.098E+03
<sup>144</sup> Ce	4.738E+03	6.064E+03	1.138E+04	7.483E+03	1.045E+04	9.361E+03	1.191E+04
<sup>154</sup> Eu	7.262E+00	5.985E+00	9.393E+00	1.130E+01	1.488E+01	4.683E+01	3.813E+01
<b>Element Burnup (MWd)</b>	<b>1.786E+02</b>	<b>1.619E+02</b>	<b>1.931E+02</b>	<b>2.106E+02</b>	<b>2.333E+02</b>	<b>3.872E+02</b>	<b>3.493E+02</b>
<b>Cooling Time (Days)</b>	<b>563</b>	<b>423</b>	<b>228</b>	<b>423</b>	<b>353</b>	<b>563</b>	<b>423</b>

#### 5.4.4 Calibration Method

Gamma-ray spectroscopy is a well research and reliable nondestructive method that can be used to estimate fuel element burnup and cooling time for fuel assemblies with short to long cooling times. This technique uses the measured gamma-ray signatures and correlates absolute or isotopic ratio of fission products from the irradiated fuel elements with known values for burnup and cooling times. Choosing between absolute or ratio measurements depend on the type of fuel, cooling time, geometry, and efficiency of the detector.

The method to provide a relationship between burnup and cooling times with experimental isotopic activity from fission products is to create calibration curves. There are two techniques to built calibration curves that can be used to predict burnup and cooling time from experimental isotopic information. The two methods have been proven reliable and are based on measuring burnup and cooling time indicators from fuel elements with well defined irradiation histories. The first method is to create a calibration curves using experimental information and declared operator values. The second technique is to build calibration curves based on experimental isotopic measurements and values calculated from a computer code. In order to have an integral study computer codes that are well established and validated should be

used to provide confirmation and enhanced assurance on operator declared values. Computer codes also provide vast information regarding inventories of fission products and actinides present in fuel elements.

#### **5.4.5 Burnup and Cooling Time Calibrations using Activity Ratios**

As mentioned before, quantitative characteristics of nuclear material in fuel cannot be measure directly from gamma radiation. Characteristics for determining burnup and cooling time have to be estimated indirectly using indicators based on radiation from fission products. The basic approach is to correlate burn up and cooling time with absolute activity, or activity ratios from long-lived fission product isotopes to indirectly determine the quantitative attributes of the fuel element.

The key to success of any approach to indirectly calculate quantitative characteristics from fission products indicators relies on being able to have dependable measurements along with accurate cooling time and burnup values from operations or depletion codes. Reliability in absolute activity measurements depends heavily on the geometry of the system. For systems were the geometry cannot be kept constant or measured accurately, fission product activity isotopic ratios can be used to determine burnup or cooling times.

The intrinsic calibration method has been topic of several scientific papers in which a few ratios have been found to have consistent relationships with cooling times and burnup of nuclear fuel. Table 5-3 shows several ratios used for calibrations along with some advantages and disadvantages. From the ratios included in this table  $^{134}\text{Cs}/^{137}\text{Cs}$  has been reported in several scientific articles to be the most effective and constant as an isotopic ratio burnup monitor for elements with a wide range of cooling times and fuel enrichments. For cooling times the options are broader and most ratios included in this table have been reported to be good predictors.

It is important to mention that  $^{134}\text{Cs}/^{144}\text{Ce}$  ratio has not been reported as an isotopic activity monitor in any of the scientific articles consulted, but in this feasibility study we found that it consistently has a linear relationship with burnup. Finding an isotopic activity ratio to predict burnup for elements with short cooling time (0-3 months) is an area where further investigation is needed.

Table 5-3. Advantages and Disadvantages of various fission product isotopes used in burnup and cooling times characterization techniques.

TECHNIQUE	ADVANTAGES	DISADVANTAGES
Absolute count rate of the 662 keV gamma ray from $^{137}\text{Cs}$ (Half life of 30 years)	Simple linear relationship between $^{137}\text{Cs}$ and burnup. Insensitive to variations in reactor power rating and dwell time.	Absolute measurement requires a well defined and reproducible geometry between the detectors and the fuel assembly.
The nuclide activity ratio: $^{134}\text{Cs} / ^{137}\text{Cs}$ and $^{154}\text{Eu} / ^{137}\text{Cs}$	The ratio method makes it insensitive to geometry.	2.2 year half life requires significant decay correction and can only be applied to fuel with cooling time < 20 years. Burnup correlation is dependent on initial enrichment and power rating.
The nuclide activity ratio: $^{106}\text{Ru} \times ^{137}\text{Cs} / (^{134}\text{Cs})^2$	Insensitive to geometry. Independent of enrichment and rating.	Only useful for fuel < 9 years cooling time ( $^{106}\text{Ru}$ has a 372 day half life).
The nuclide activity ratio: $^{144}\text{Ce} / ^{137}\text{Cs}$	The ratio method makes it insensitive to geometry.	Peaks in short cooling times spectra are hard to resolve.
Absolute $^{95}\text{Zr}$	$^{95}\text{Zr}$ good monitor for locating relative positions of fuel material. Peaks are easily resolvable	$^{95}\text{Zr}$ has a short half-live Decrease of atomic density as burnup increases Absolute measurement requires a well defined and reproducible geometry between the detectors and the fuel assembly
Absolute $^{134}\text{Cs}$	$^{134}\text{Cs}$ relatively independent of fission source. Easily resolvable gamma peaks.	$^{134}\text{Cs}$ Absolute measurement requires a well defined and reproducible geometry between the detectors and the fuel assembly.
Absolute $^{144}\text{Ce}$	Easily resolvable gamma-peaks	For long irradiations half-life becomes a disadvantage, because atomic density reflects more recent exposure.

#### 5.4.6 Burnup and Cooling Time Calibrations using Absolute Measurements

Another method for determining fuel characteristics is by absolute activity measurement of fission product isotopes. This approach can be used to predict burnup and cooling time from a single radionuclide very accurately and fast way. Table 5-3 also contains isotopes that have been reported in several scientific studies as effective monitors to help predict cooling time and burnup. From the isotopes shown in the table the most widely used as a burnup monitor is  $^{137}\text{Cs}$ . This isotope is preferred because it has easily resolvable gamma peaks, it is independent of fuel composition and it has a long half life that allows it to be a consistent tool for fuel prediction for a variety of discharge times.  $^{144}\text{Ce}$  isotope has been proven to be a consistent cooling time predictor and has shown some promise as a burnup monitor.  $^{95}\text{Zr}$

and  $^{95}\text{Nb}$  isotopes are good monitors for predicting cooling times but because of their short half lives they can only be used for a limited time after discharge.  $^{95}\text{Zr}$  has also been reported as possible option to predict burnup for fuel elements with short cooling times (0-3 months), however questions about accuracy and consistency are a concern for this monitor. In general isotopes that can be reliably used for burnup prediction of fuel elements with short cooling times (0-3 months) have yet to be determined.

This study consisted of seventy two measurements of fifteen different elements taken in thirteen different experimental dates. The elements cooling time vary from 38 days to 3.5 years with a burn up range from 100 to 500 MWd. The data were collected in two configurations mentioned before. Measurements with 1"x1" and 2"x2"  $\text{LaBr}_3$  detectors were performed under and above the water, while the other detectors shown in Table 5-4 were used for the above water measurements. The data for each measurement was collected for 1000 seconds. The spectra obtained from the fuel measurements at the ATR were analyzed using Spex software to identify isotopes, perform energy calibrations and to determine the total area of the peaks.

Table 5-4. Measurement dates and type of detectors and configurations.

Experiment Dates	Type of Detector	Type of Measurement
1/18/2010	1x1 $\text{LaBr}_3$	Underwater
1/21/2010	1 x1 $\text{LaBr}_3$	Underwater
3/17/2010	1x1 $\text{LaBr}_3$	Underwater
3/30/2010	2x2 $\text{LaBr}_3$	Underwater
4/28/2010	1x1 $\text{LaBr}_3$	Underwater
4/29/2010	1x1 $\text{LaBr}_3$ , HPGe 45%	Above water
5/6/2010	HPXe, 1x1 $\text{LaBr}_3$	Above water
5/11/2010	HPGe 45%	Above water
06/08/10	HPGe 25%	Above water
6/10/2010	HPXe, 1x1 $\text{LaBr}_3$	Above water
6/22/2010	HPGe 45%	Above water
6/28/2010	HPGe 45%	Above water
6/29/2010	HPGe 45%	Above water



Initial measurements were performed to establish the detector to fuel distance, collimator size using three different radiation detectors under different burnup and cooling time scenarios. This also determines whether or not more shielding is needed in the front and around the detector inside the waterproof housing. Burnup calibrations were obtained by measuring 4-7 fuel elements in the ATR canal with well known irradiation history, different burnup and cooling times (3 months to three years) for HPXe, LaBr3 and HPGe detectors.

The Measurements with the HPGe detector were performed with the detector placed in the waterproof housing above the water. The pipe attached to the waterproof housing was used only for above the water measurements. Comparison between measurements taken under and above the water showed the quality of spectra is much better for the latter. This is because the gamma rays emitted from the fuel are severely attenuated in the water. This attenuation becomes especially more important for low-energy gamma rays below 1 MeV.

## 5.5 Measurement Results

ATR uses uranium-oxide fuel, and its cycle times are relatively short. As a result, the fuel typically has little Pu buildup that could negatively impact radiation measurements. Additionally, ATR is typically operated at relatively constant power levels, so determination of fuel element power histories should be fairly straightforward. These will make the ATR burnup estimation process less complicated. The fuel elements measured were irradiated at the Advanced Test Reactor at the Idaho National Laboratory. Each element has 19 plates and approximately 1075 grams of  $^{235}\text{U}$ . The measurements were performed at the canal adjacent to the reactor using five different gamma detectors. The fuel elements were placed into a turn table fuel holder with plate number one facing towards the wall and the detector pointing at plate number nineteen.

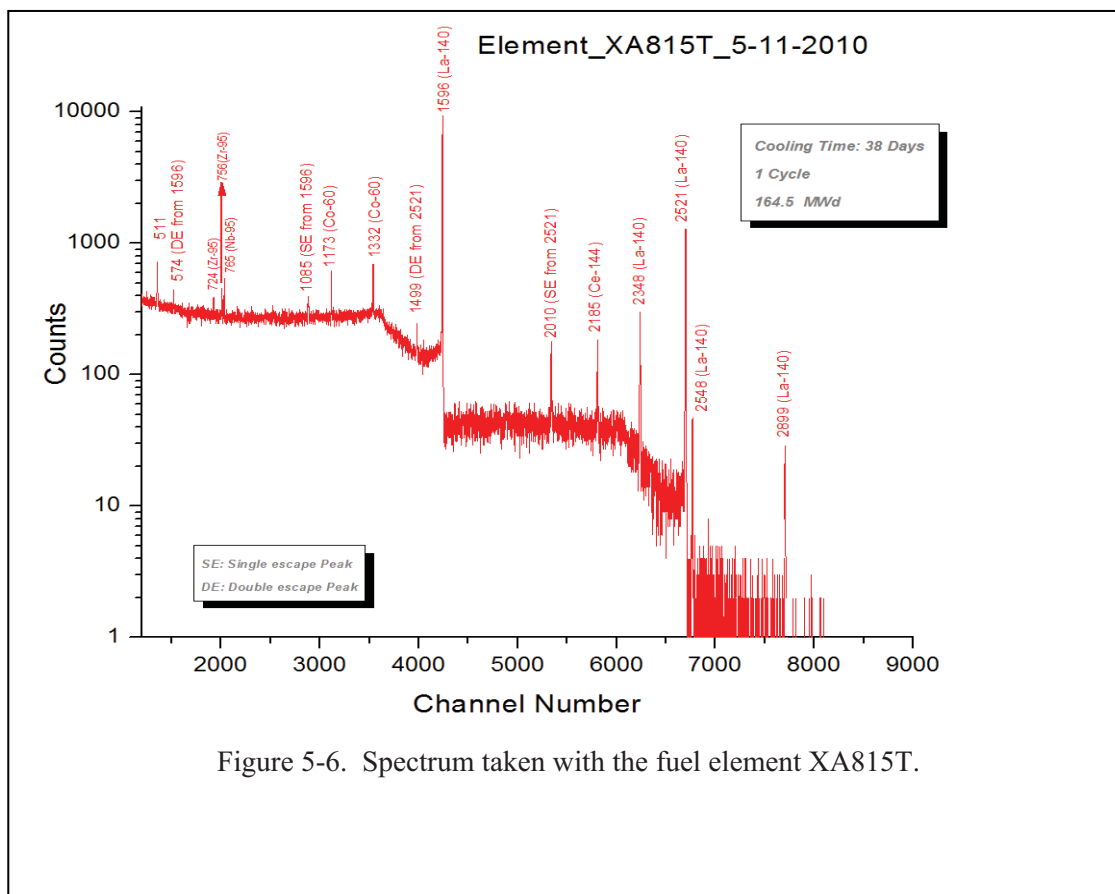
### 5.5.1 HPGe Detector Results

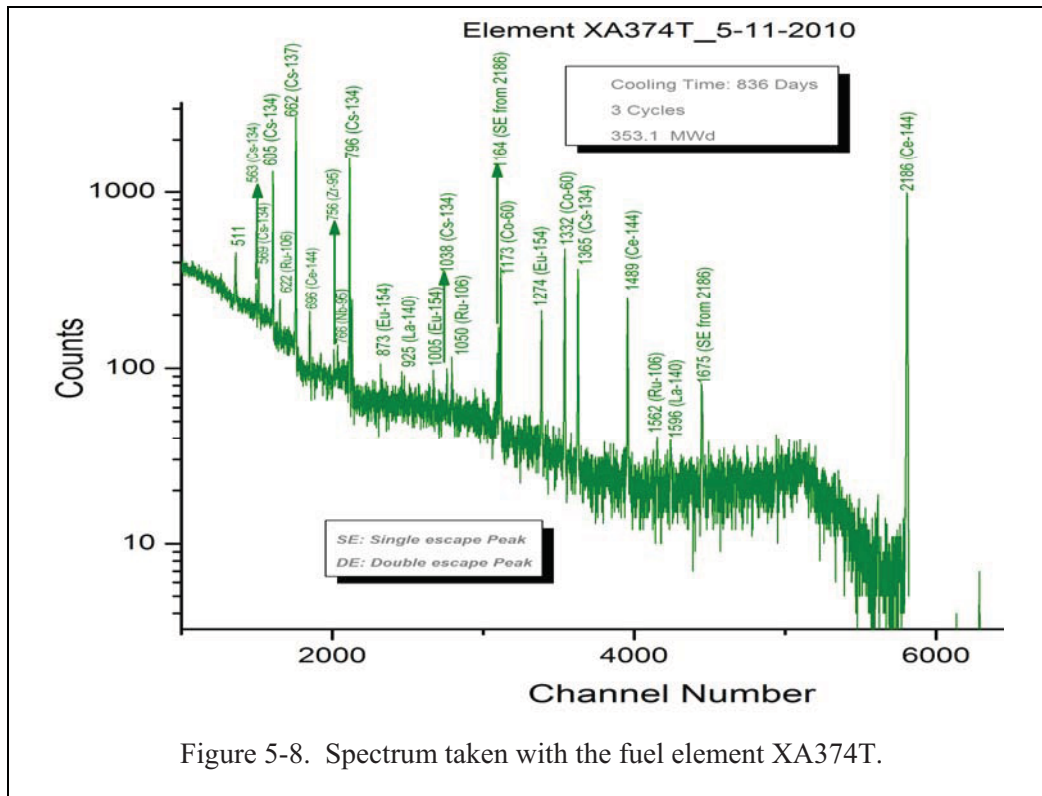
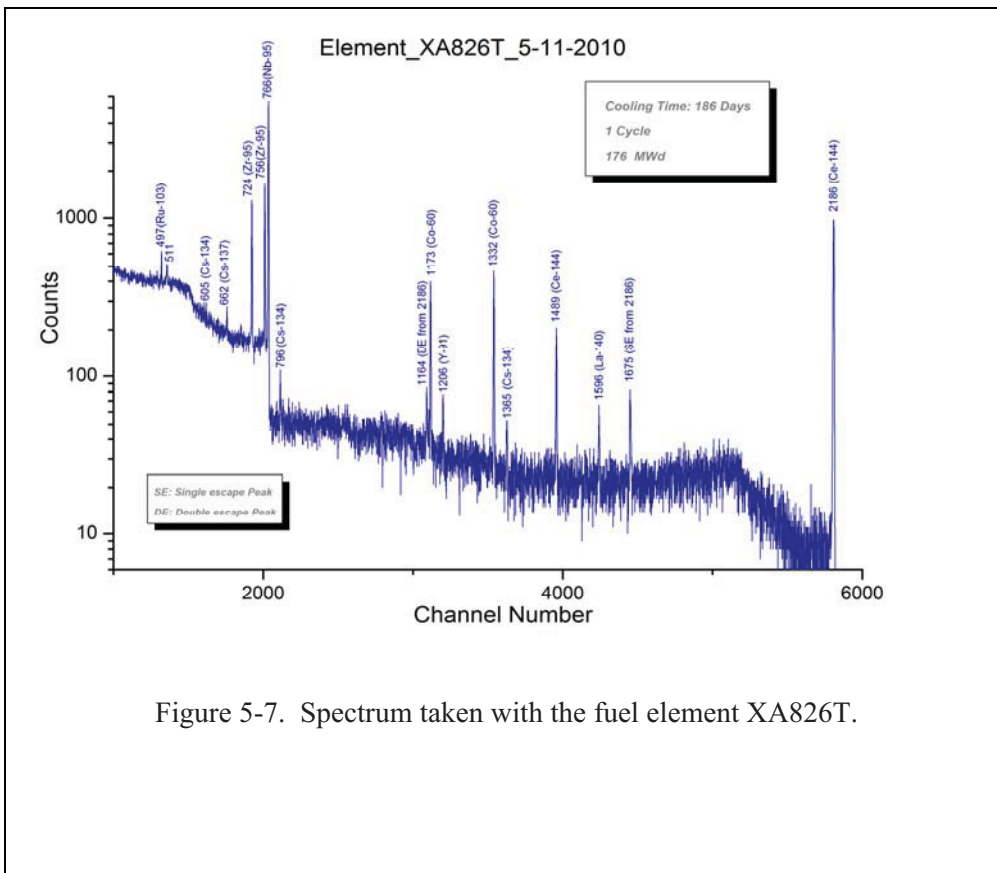
The results of the measurements taken with high purity germanium detectors were divided into three groups, based on their cooling time. The first group contains measurements made on element XA815T that was in the reactor for one cycle. Element XA815T was monitored with the high purity germanium detector for two months. Measurements were taken every two weeks to monitor the decay history of the fission product isotopes. Figure 5-6 shows a spectrum taken with a 45% efficient HPGe detector after 38 days of cooling time. Due to high resolution of the this detector the peaks of all the isotopes are very well separated. It can be seen that the spectrum is dominated by the gamma-ray emitted from the short-lived fission product isotope  $^{140}\text{La}$ . This figure also contains a couple of single and double escape peaks from full energy gamma-rays. These peaks are a result of pair production in the detector crystal. Pair production interaction in the detector occurs for gamma-rays that have energy greater than 1022 ( $2 \times 511$ ). In this process an electron-positron pair is created. The positron, which is the anti-particle of electron is not stable and consequently combines with the electron. Two particles disappear leading to the creation of two photons each with energy of 511 keV (annihilation radiation). The single escape happens when one of the annihilation gamma rays escape from the detector with no interaction. The single peak is produced at the energy of  $(E_\gamma - 0.511)$  MeV, where  $E_\gamma$  is the full energy photopeak. The double escape process happens when both photons created from the annihilation process escape from the detector with no interaction. The energy of the double escape peak is  $(E_\gamma - 1.02)$  MeV.

The second group of experiments consisted of measurements done on element XA826T, during a 5 month span. The element XA826T had been in the reactor for one cycle and the measurements with the high purity germanium detector started on March 17, 2010. Figure 5-8 is the spectrum of the element XA826T taken on May 10, 2010. On that day, the cooling time was 186 days. This spectrum when compared to Figure 5-7 shows the natural decay behavior of the fuel fission products. The spectrum is dominated by

the  $^{95}\text{Zr}$  and  $^{95}\text{Nb}$  peaks while the  $^{140}\text{La}$  peaks with a half-life of 12 days are mostly decayed away. It can also be seen that the long lived  $^{137}\text{Cs}$  and  $^{134}\text{Cs}$  are starting to show up in the spectrum. Another dominating peak is  $^{144}\text{Ce}$ , this peak was part of the XA-815T spectrum but due to the dominate role of  $^{140}\text{La}$  isotope it was relatively a small peak.

The third group of experiments consisted of measurements on several elements with longer cooling times (6 months- 3.5 years). Figure 5-8 shows the spectrum taken for element XA374T. If we compare it to the previous two groups spectra indicates that almost all the short lived isotopes ( $^{140}\text{La}$ ,  $^{95}\text{Zr}$ , and  $^{95}\text{Nb}$ ) have decayed away. Most of the peaks in Figure 5-8 are due to long-lived isotopes. The strongest peaks come from  $^{134}\text{Cs}$ ,  $^{137}\text{Cs}$ , and  $^{144}\text{Ce}$ . Also, in this spectrum the  $^{154}\text{Eu}$  gamma-ray peaks can be seen. From these spectra it is clear that all close-by gamma rays are easily resolved due to the high energy resolution.





The data analysis for the HPGe detector was focus on calibration curves made with experimental absolute activity or isotopic activity ratio and theoretical burnup and cooling times. These calibrations are the main goal of our study because they will allow us to create mathematical relationships to predict ATR fuel burnup. There were a number of calibrations curves created most of them based on results reported by various authors, but also some new curves were made based on trends we found when the data was being analyzed. Three activity ratios and two absolute activities were identified as consistent burnup and cooling time monitors for ATR fuel elements. It is important to keep in mind that calibration curves are highly sensitive to system geometry something that was hard to achieve with the current setup. The calibration curves created especially those using absolute activity values are highly dependent upon knowing the exact geometry of the system. The technique used to obtained the calibration curves when used correctly can be an effective tool to predict burn up from experimental measurements, however in order to reduce uncertainties a permanent detection system is needed. The permanent system will allow us to know the exact location of each measurement and take the data for longer period of time to reduce the overall uncertainty of the system.

The most consistent monitor was the activity ratio of  $^{134}\text{Cs}/^{137}\text{Cs}$ . The results can be seen in Figure 5-9, where experimental isotopic ratios for five long cooling time elements were plotted against burnup calculated with ORIGEN. In this figure, it can be seen that data points together with their uncertainties fall into the linear trend. The other activity ratio that was consistent when used as a burnup monitor was  $^{134}\text{Cs}/^{144}\text{Ce}$ . This ratio was not previously reported in any of the scientific articles we consulted. This was corroborated with other set of data we measured. The results for the  $^{134}\text{Cs}/^{144}\text{Ce}$  activity ratio as a burnup monitor are shown in Figure 5-10. Again, all data points uncertainties fall inside the line. Finally, the plots using absolute activities of  $^{134}\text{Cs}$  and  $^{137}\text{Cs}$  isotopes as burnup monitors are shown in Figures 5-11 and 5-12 that indicate a linear relationship between absolute activity and burnup. However, not all points fall exactly on the line.

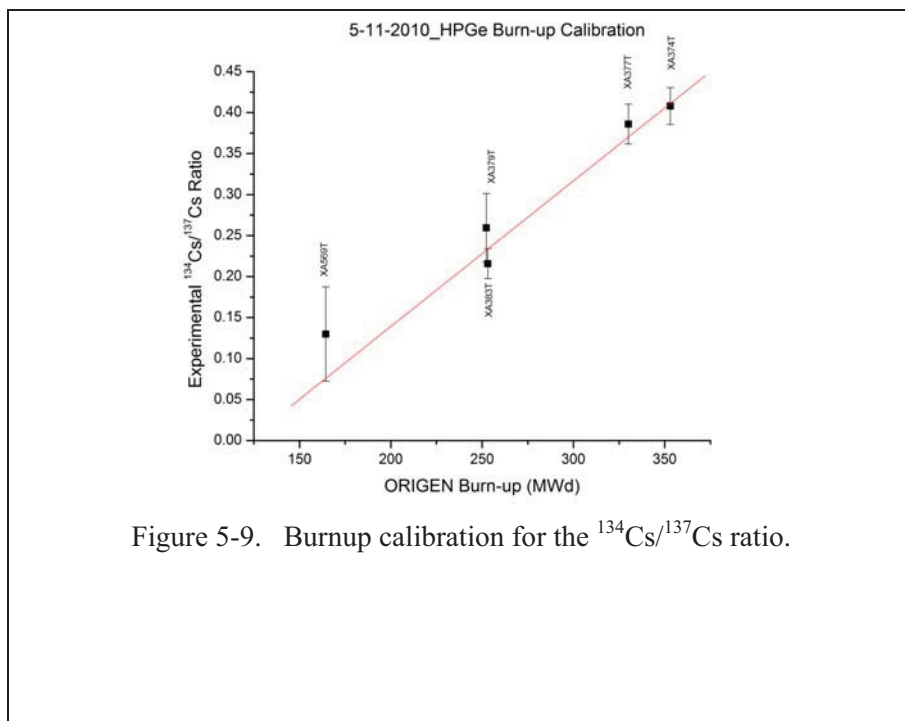
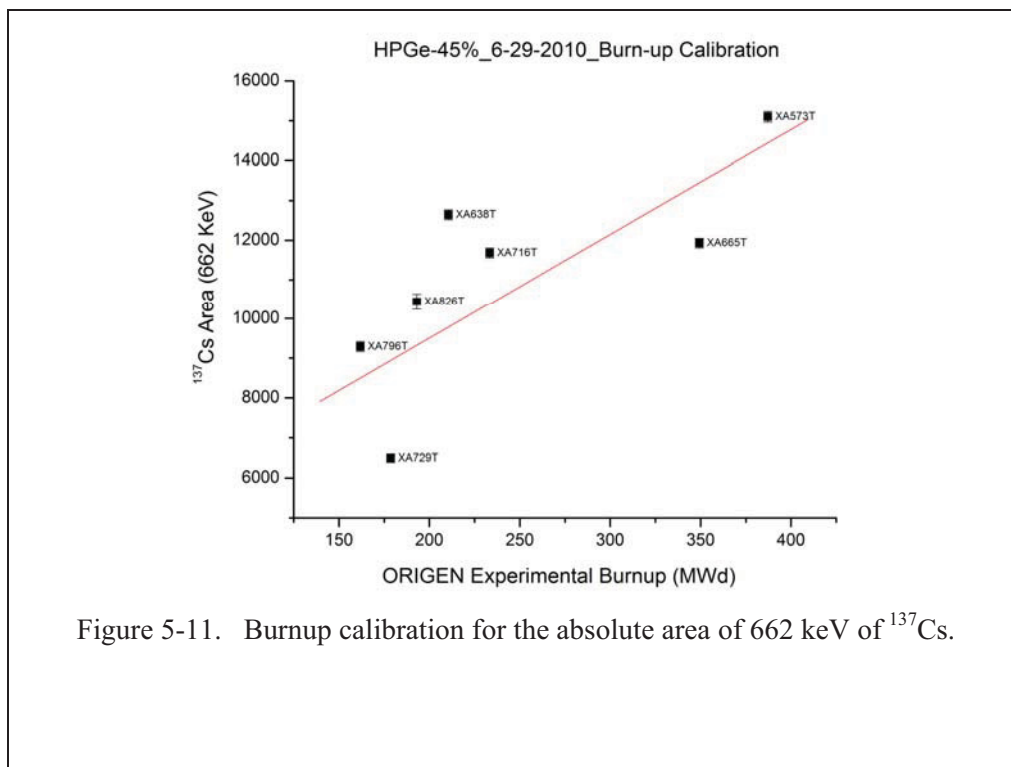
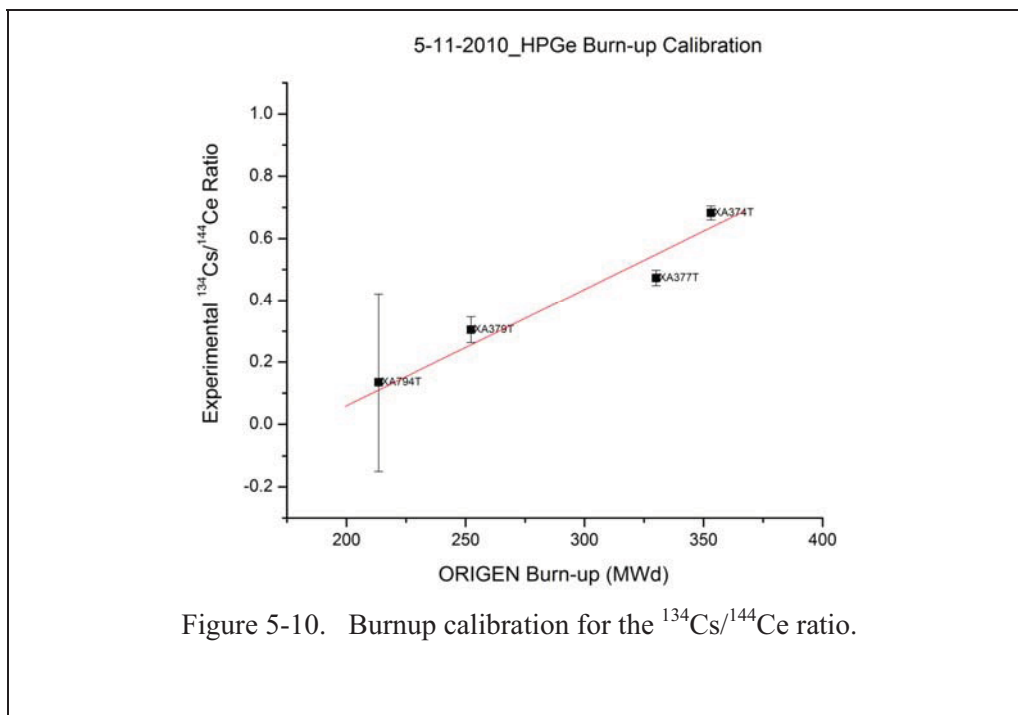
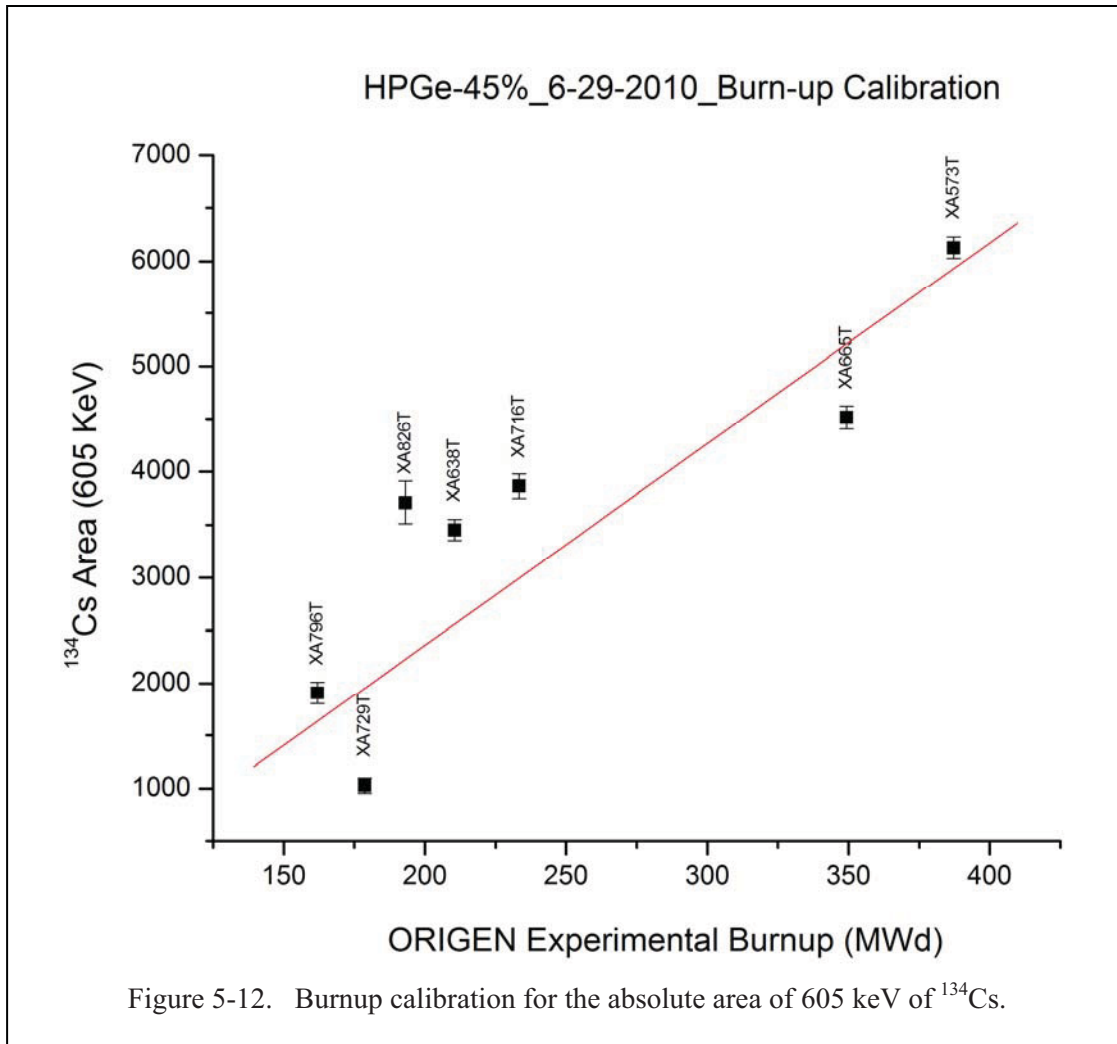


Figure 5-9. Burnup calibration for the  $^{134}\text{Cs}/^{137}\text{Cs}$  ratio.



The correlation of the absolute activity of  $^{137}\text{Cs}$  with fuel burnup has been reported previously in various scientific articles. But, the same correlation for the  $^{134}\text{Cs}$  isotope has never reported before. In order to confirm this finding more measurements are needed.



We also investigated the possibility of using experimental absolute activity or isotopic ratios as cooling time monitors. Among them, using  $^{144}\text{Ce}/^{137}\text{Cs}$ ,  $^{95}\text{Zr}$  and  $^{144}\text{Ce}$  were found to be good cooling time predictors. The  $^{144}\text{Ce}/^{137}\text{Cs}$  activity ratio was the most consistent and efficient when correlated with ATR operator declared cooling time. Figure 5-13 shows the results of  $^{144}\text{Ce}/^{137}\text{Cs}$  ratio as a function of cooling time in log scale. It is clear that all points representing ATR fuel elements measured and their uncertainties fall on the line. Finally, Figures 5-14, and 5-15 show the correlations between the other two monitors  $^{95}\text{Zr}$  and  $^{144}\text{C}$  activities and operator declared cooling times values. It can be seen that in all three plots points representing ATR fuel elements with different burnup and cycles in the reactor follow the linear trend. In addition, we also looked at the  $^{95}\text{Nb}$  isotopes and the results show exactly the same trend as  $^{95}\text{Zr}$  isotope. We believe that with the permanent system the uncertainties can be reduced substantially and all data points will be much closer to the line.



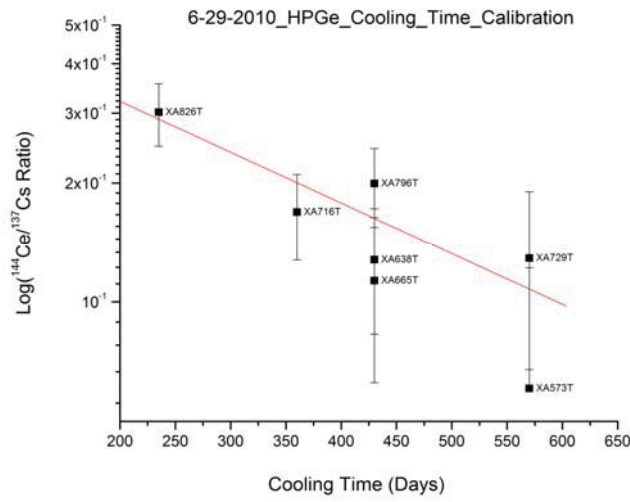


Figure 5-13. The  $^{144}\text{Ce}/^{137}\text{Cs}$  ratio versus cooling time in Log scale.

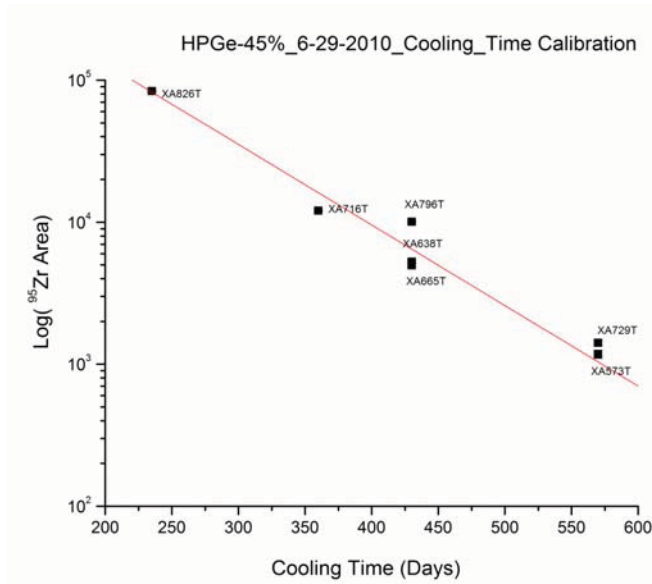


Figure 5.14. The absolute area of  $^{95}\text{Zr}$  versus cooling time in Log scale.

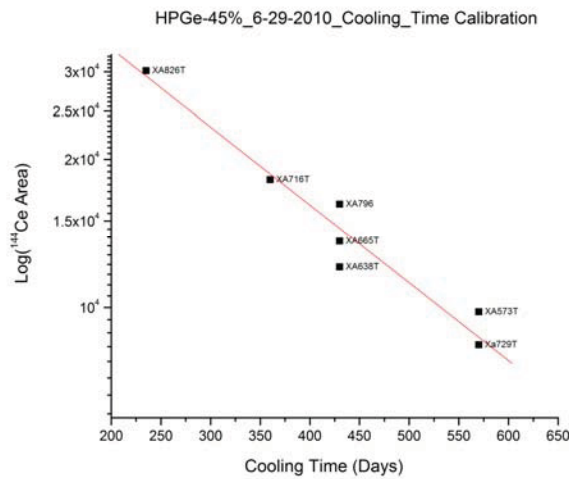


Figure 5-15. The absolute area of  $^{144}\text{Ce}$  versus cooling time in Log scale.

### 5.5.2 LaBr<sub>3</sub> Detector Results

Underwater and above water measurements were made using the LaBr<sub>3</sub> detectors. The main goal of these measurements was to determine which set up (underwater or above the water) would be a better choice for the permanent system. The LaBr<sub>3</sub> detector was chosen as the selection tool because it was not possible to place the HPGe detector in the water due to the high pressure nitrogen cooling tank attached to it. The decision was based on analyzing and comparing above water and underwater data. The analysis was focus on determining which detector configuration provides better results. Figures 5-16 and 5-17 are spectra of element XA374T taken with the same detector in two different configurations of above and under the

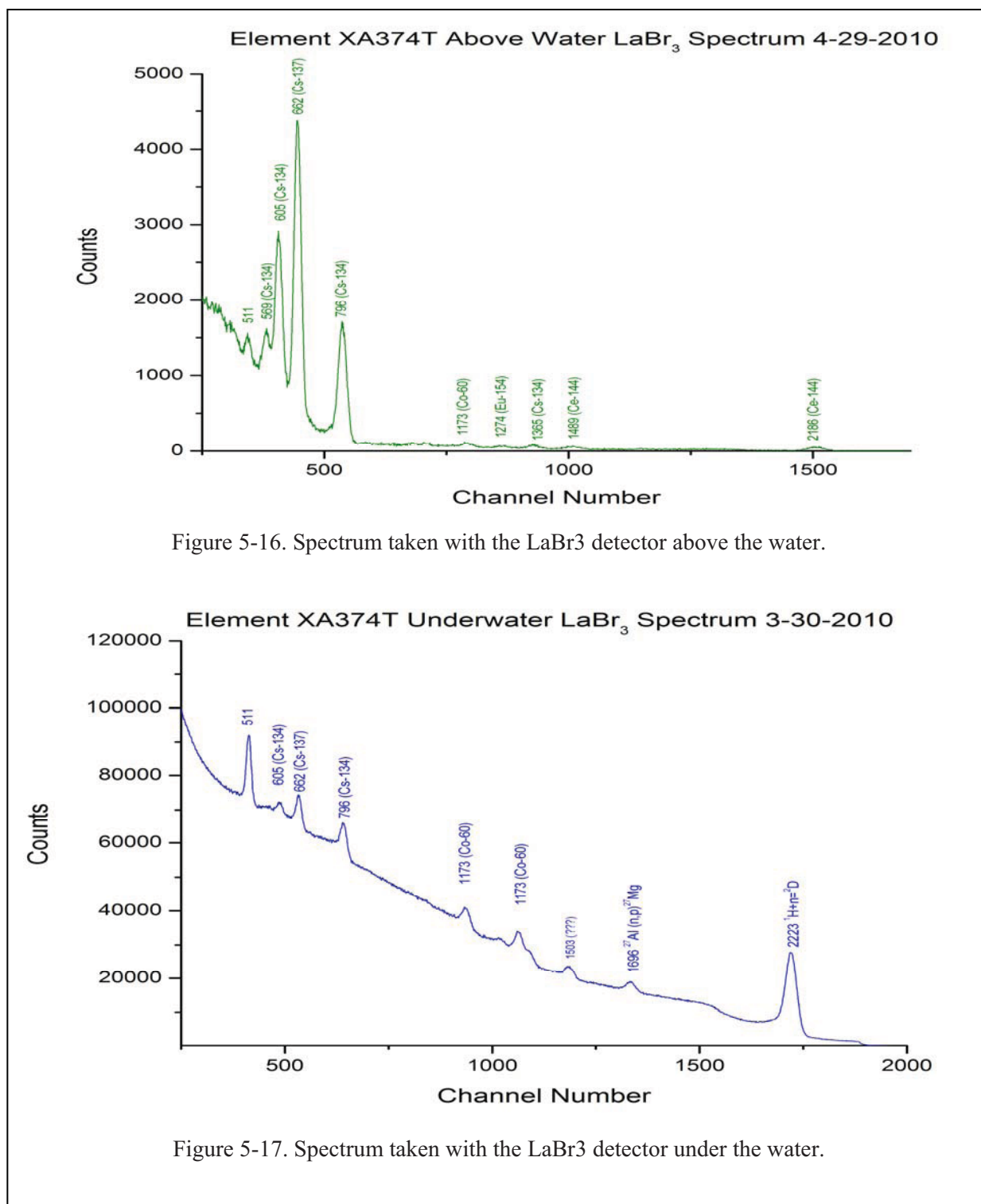


Figure 5-16. Spectrum taken with the LaBr<sub>3</sub> detector above the water.

Figure 5-17. Spectrum taken with the LaBr<sub>3</sub> detector under the water.

water, respectively. The detection system in the under the water measurements was placed at 4.0 ft from fuel element XA374T. The spectrum in Figure 5-17 was taken with the detection system above the water with the 14 feet pipe attached to the front of it and the end of the pipe was 6 inches from the fuel element. By comparing the two spectra it is very clear that quality of spectrum regarding the P/C ratio is much better for the above the water measurements, especially for low energy gamma rays like 605 KeV of  $^{134}\text{Cs}$  and 662 keV of  $^{137}\text{Cs}$  peaks. This is mainly due to the fact that gamma rays are severely attenuated going through the water in the under-water measurement. Gamma attenuation is higher in the underwater detector setup due to 4 feet of water that gamma rays have to travel before reaching the detector. While in the above the water setting gamma rays need to travel only 6 inches of water. Another important distinction between these two spectra is the existence of the hydrogen neutron-capture peak at 2223 keV in the under the water measurement (see Figure 5-17). This peak was not observed in the above water spectrum due to the shorter distance between the fuel element and pipe (less water between), and also due to the long 15 feet of air within the collimated pipe that this gamma ray has to travel to reach the detector.

### 5.5.3 LaBr<sub>3</sub> Calibration Results

One isotopic activity ratio was used as a monitor to create calibration curves using experimental data taken with LaBr<sub>3</sub> detector. The reason for only using one ratio as a burn up monitor was the high uncertainty bars associated to other possible activity monitors due to the lower resolution of the LaBr<sub>3</sub> spectra. The calibration curves were created by plotting experimental measurements against ORIGEN calculated burn-up Figure 5-18 shows the  $^{134}\text{Cs}/^{137}\text{Cs}$  calibration curve. This plot shows the linear fit of four elements and their uncertainties with fuel burn-up.

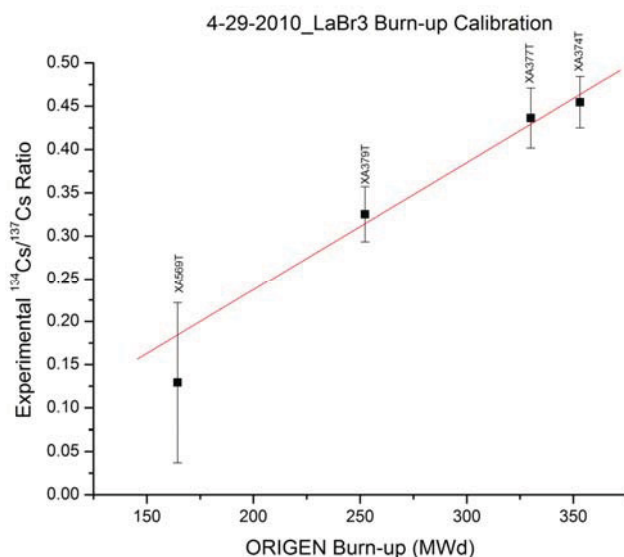


Figure 5-18. Burnup calibration using the 1"x1" LaBr<sub>3</sub> detector the  $^{134}\text{Cs}/^{137}\text{Cs}$  ratio.

### 5.5.4 Comparison Between HPGe and LaBr<sub>3</sub> Results

There were two differences used to compare the performance between the HPGe and LaBr<sub>3</sub> detectors. The first one involves comparing their energy resolutions. By comparing spectra shown in Figures 5-8 (HPGe) and 5-16 (LaBr<sub>3</sub>) taken with the same element it is clear that the high purity germanium spectrum has a far better energy resolution than the LaBr<sub>3</sub> spectrum. The better energy resolution of the HPGe detector makes it possible to resolve close-by peaks. This becomes very important for short cooling time fuels. In addition, the P/C ratio is much better for the HPGe detector resulting in a better area definition and reducing the measurement uncertainties.

The second difference was to compare the uncertainties on burn-up and cooling time. The results from calibration curves made with the two detectors for the same set of fuel elements are shown in Figures 5.9 and 5.18. Comparison between these two spectra indicates that uncertainties for HPGe data are much smaller than LaBr<sub>3</sub> data. The quality of the spectrum obtained using the HPGe detector is better due to high energy resolution. For the reasons stated above and also because we are going to use above the water configuration only, the HPGe detector was selected as a primary detector for the permanent system. However, we are planning to use the 1"x1" LaBr<sub>3</sub> detector for longer cooling time fuels (1-3 years) as well. This detector is a less expensive alternative to HPGe detector that works also well for the longer cooling time fuels.

### 5.5.5 HPXe Gas Detector Results

A high pressure xenon detector was also used in this study; this detector was selected because it can be placed very close to the fuel (< 2 inches) and it also has the capacity of being positioned under or above the water. The disadvantage of the HPXe detector is that it has very low detection efficiency than the other types of detector. In addition because majority of gamma-rays interactions occur through the Compton scattering, only few interactions contribute to the full-energy peaks. Therefore, the peak-to-Compton (P/C) ratio is very small and weaker peaks will be buried in Compton background and very hard to resolve as it can be seen in Figure 5-19. The calibration curve was made by plotting the <sup>134</sup>Cs/<sup>137</sup>Cs experimental activity ratio of five elements against burn-up calculated by ORIGEN. Figure 5-20 shows the calibration curve made with HPXe detector data. The uncertainties on the data are very large due to counting time limitation. Longer counting time will definitely lower these uncertainties.

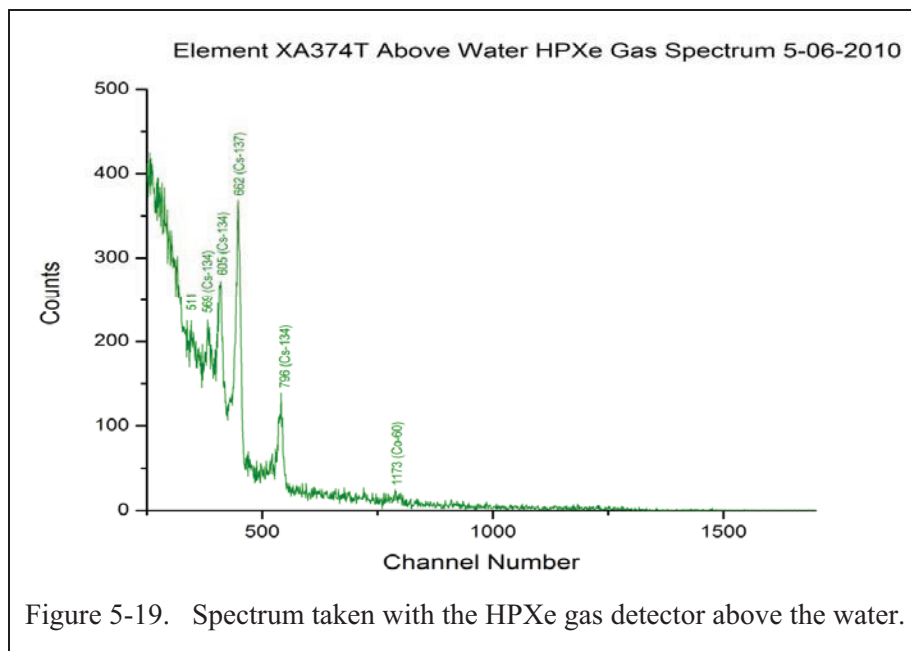
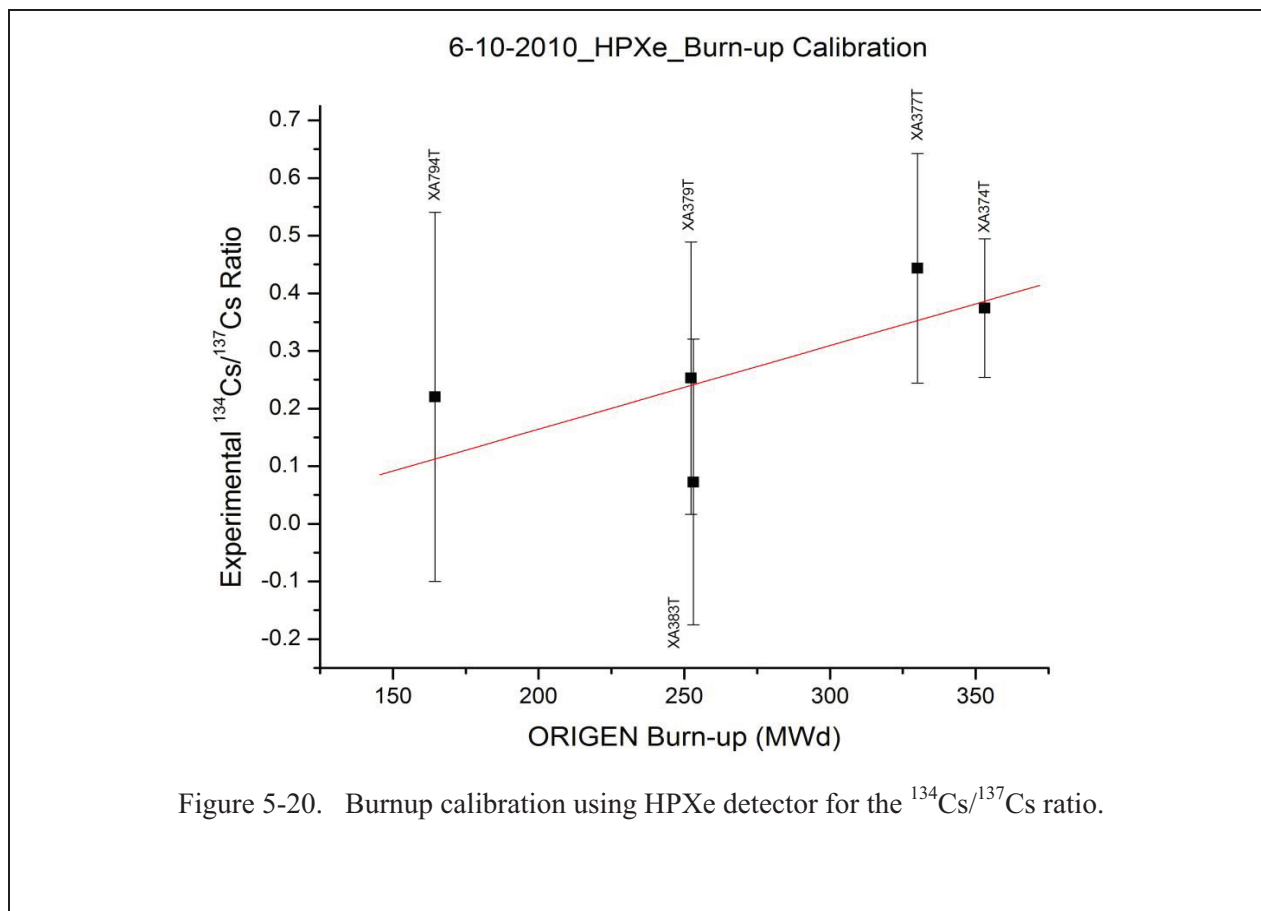


Figure 5-19. Spectrum taken with the HPXe gas detector above the water.



## 5.6 Conclusions

We have established the burnup calibrations for LaBr<sub>3</sub>, HPGe and HPXe detectors. The results show the linear relationship between the  $^{134}\text{Cs}/^{137}\text{Cs}$  ratio and the burnup as expected for all three detectors. For the first time, we found a new activity ratio of  $^{134}\text{Cs}/^{144}\text{Ce}$  to show a linear relationship with the burnup. Although, our detection system was not setup for absolute activity measurement, we looked at the activity of some fission products. Among them  $^{134}\text{Cs}$  and  $^{137}\text{Cs}$  isotopes found to have linear relationship with the burnup and therefore they can be used as burnup monitors for the ATR fuel. We also investigated to see which other isotopic ratios or absolute activities can be used to determine the fuel element cooling time. The  $^{144}\text{Ce}/^{137}\text{Cs}$  ratio,  $^{144}\text{Ce}$ ,  $^{95}\text{Zr}$ , and  $^{95}\text{Nb}$  showed a linear relationship as a function of cooling time. The comprehensive data analysis of these data are still under way but so far the results are impressive indicating the detection system is performing very well and using the above the water configuration is the right way to design the permanent system. This also makes the design simpler and less expensive. We strongly believe that our designed permanent system would improve the quality of data tremendously with much smaller uncertainty and therefore would be able produce better results to be compared with the results of calculations from the ORIGEN code as well as other codes that are currently being developed at the INL. However, if the results are insufficiently conclusive, some destructive fuel analysis may be needed to resolve the discrepancies and to validate the results.

## 5.7 Proposed Permanent system and experimental plans for FY-11

A conceptual design for a permanent ATR Fuel Burnup Measurement System (FBUMS) is shown in Figure 5-21

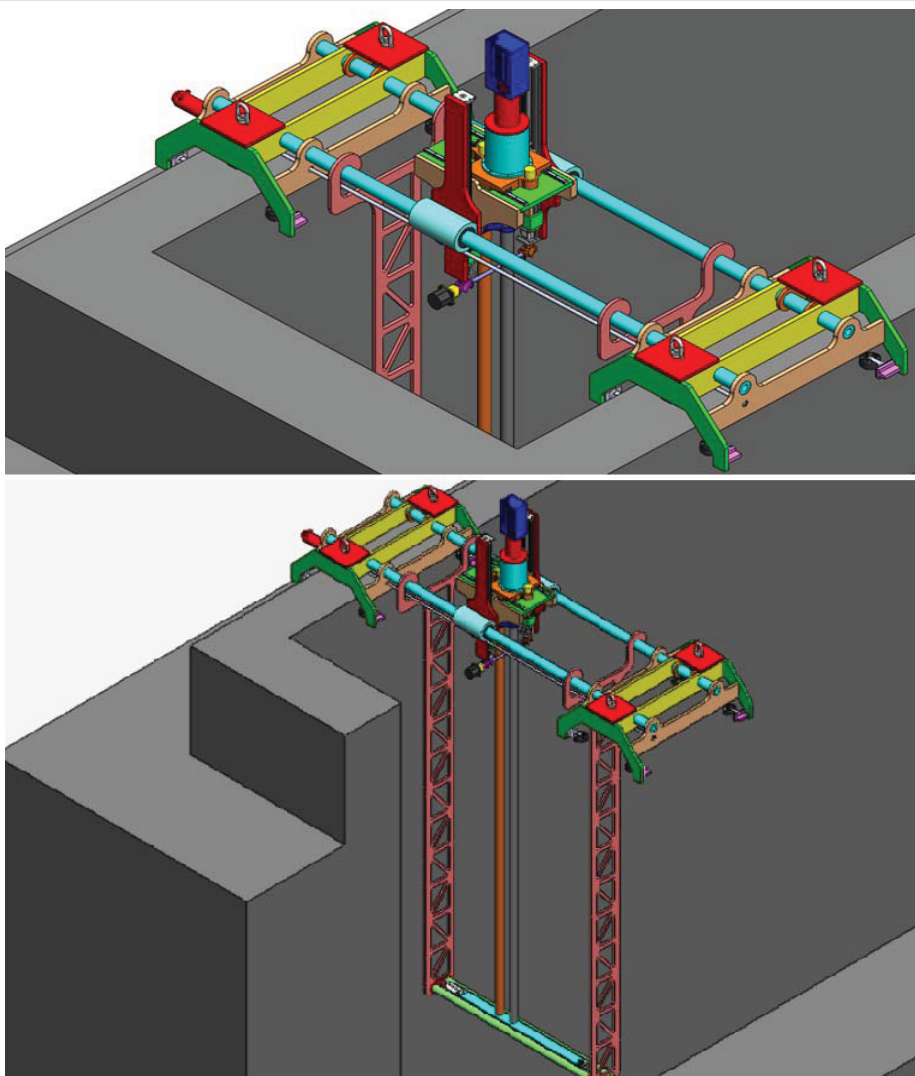


Figure 5.21. Conceptual design of a Permanent system



This system consists of the following major subsystems:

- X Scan Axis
- Lead Screw Trolley
- Detector Housing
- Two Down Pipes
- Fuel Element Carriage
- Computer Control System

It is capable moving the detection system and placing it exactly at desired spot with accuracy of 1/1000". The tower structure will be placed on the east side of canal. The system includes parallel rods to hold the detection system above the water and a U-shape structural frame in the water with the Fuel Element Carriage (FEC) at the bottom to hold a fuel assembly. Measurements will be done with detection system above the water and with the 14' collimated pipe attached to it. This makes the design simpler and less expensive. This is because outside the water and less expensive motors can be used to move the detection system in "X" and "Z" directions. By looking at the data analyzed so far we believe the existing housing collimator can be utilized for the permanent system.

FBUMS is configured as a two axis (X-Z) computer controlled scanning system. Two parallel 3" diameter stainless steel shafts form the X axis which spans the width of the ATR canal. Each end is mounted on a set of wheeled trucks with locks that will retain the FBUMS in position over the canal. A Lead Screw Trolley (LST) moves the detector system along the X axis. The trolley, positioned between the shafts, is incrementally driven back and forth. This movement is parallel and directly above the length of the fuel element suspended below. The X axis provides a trolley parking area at one end to accommodate fuel element loading in the Fuel Element Carriage (FEC) below. The ATR fuel element to be inspected will be supported horizontally in the FEC suspended approximately 14 feet below the canal water level. The FEC will automatically position and center the fuel element in the same position relative to the detector before every inspection cycle.

The Detector Housing Assembly (DHA) is mounted on two short horizontal slides on the X Scan Carriage (XSC) for manual positioning of the assembly over either Down Pipe Assembly (DPA). The DPAs are approximately 14 feet long, air filled pipes with different sized bismuth collimators located at the bottom end of the tubes. Shielding on the DPA insures both down pipes are covered at all times to prevent streaming radiation during inspection of the fuel elements, especially for the pipe that is not used.

The Z axis lifts the XSC, DHA and DPAs vertically, a maximum of 24 inches to increase the distance between the end of the pipe and consequently the HPGe Detector and the fuel element under inspection. A computer system will control the mechanical operation of the scanning system and also collect the spectral data from the detector system.

This system also allows us to do measurements along the fuel element to obtain the radiation profile for investigating the fuel burnup uniformity.

Plans for the first quarter of FY11 are to complete the data analysis and to develop a proposal for construction and calibration of a permanent system. In the experimental plan for the calibration measurements, three fresh fuel assemblies will be selected to put in the reactor. After the first cycle these fuels will be characterized using the detector systems. Next, we put two of the fuel elements back in the reactor for the second cycle. During this cycle, we perform measurements on the other fuel element not in the reactor. After the second discharge we characterize all three fuel elements and put one of the 2-cycle fuel back in the reactor for the third cycle irradiation. During this cycle, we continuously monitor and perform measurements on the other two fuels not in the reactor every week. Finally, after the third

discharge we continue our measurements every week. A combination of these three fuel elements and two other fuel elements that were set aside for us last year should establish burnup calibrations using absolute and ratio methods. The results will be compared with the results of calculation code ORIGEN and the new modeling calculations if available. If the results are insufficiently conclusive, some destructive fuel analysis may be needed to resolve the discrepancies and to validate the results.

## 6.0 REFERENCES

Bowman, S. M. (Ed.), *SCALE: A Modular Code System for Performing Standardized Computer Analyses for Licensing Evaluation*, ORNL/TM-2005/39, Version 6, Vols. I–III, Oak Ridge National Laboratory, Oak Ridge, Tennessee, January 2009. Available from Radiation Safety Information Computational Center at Oak Ridge National Laboratory as CCC-750.

Breismeister J.F., 1999, "MCNP – A General Monte Carlo N-Particle Transport Code, Version 4C, LA-13709-M, Los Alamos National Laboratory, USA (1999).

Briggs, 2010 - Briggs, J. B. (Ed.), *International Handbook of Evaluated Criticality Safety Benchmark Experiments*, NEA/NSC/DOC(95)03/I-IX, Organization for Economic Co-operation and Development - Nuclear Energy Agency (OECD-NEA), May 2010 Edition.

Broadhead, B. L., Rearden, B. T., Hopper, C. M., Wagschal, J. J. and Parks, C. V., "Sensitivity- and Uncertainty-Based Criticality Safety Validation Techniques," *Nucl. Sci. Eng.* **146**, 340–366 (2004).

Croff, A.J. "ORIGEN2 -- A Revised and Updated Version of the Oak Ridge Isotope Generation and Depletion Code," ORNL-5621, July 1980.

DeHart, M. D., Advancements in Generalized-Geometry Discrete Ordinates Transport for Lattice Physics Calculations, A154.pdf in Proc. of PHYSOR–2006, American Nuclear Society Topical Meeting on Reactor Physics: Advances in Nuclear Analysis and Simulation, September 10–14, 2006, Vancouver, British Columbia, Canada.

Draper Jr., E.L., Integral Reaction Rate Determinations - Part I: Tailored Reactor Spectrum Preparation and Measurement, Nuclear Science and Engineering, **48**:22-30 (1971).

Failla, G., "Private Communication D. S. Lucas & D. Nigg," August, 2010.

Goorley, T. Bull, J., Brown, F. et. al., Release of MCNP5\_RSICC\_1.30, MCNP Monte Carlo Team X-5, LA-UR-04-4519, Los Alamos National Laboratory, November 2004 and, X-5 Monte Carlo Team, MCNP—A General Monte Carlo N-Particle Transport Code, Version 5, Volume I, LA-UR-03-1987, Los Alamos National Laboratory, April 24, 2003 (Revised 6/30/2004) and Volume II, LA-CP-0245, Los

Harker, Y.D., Anderl, R.A., Becker, G.K., Miller, L.G., Spectral Characterization of the Epithermal Neutron Beam at the Brookhaven Medical Research Reactor, Nuclear Science and Engineering **110**:355-368 (1992).

Hollenbach, D.F., Petrie, L.M., Landers, N.F., KENO-VI: A General Quadratic Version of the KENO Program, ORNL/TM-13011, Lockheed Martin Energy Research Corp., Oak Ridge National Laboratory, 1996.

Kim, S. S. and Schnitzler, B. G., Advanced Test Reactor: Serpentine Arrangement of Highly Enriched Water-Moderated Uranium-Aluminide Fuel Plates Reflected by Beryllium” HEU-SOLTherm-022, *International Handbook of Evaluated Criticality Safety Benchmark Experiments*, NEA/NSC/DOC(95)03, OECD-NEA (2008).

Lebrun, A. and Bignan, G. Nondestructive Assay of Nuclear Low-Enriched Uranium Spent fuels for Burnup Credit, *Nuclear Technology*, Vol. 135, p. 216-228 (Sept. 2001)

McClure, J. A., 1991. Results of Outer and Neck Shim Calibration Studies, TRA-ATR-542, EG&G Idaho, Inc., September 1991.

McCracken, R. T., Loret, L. S., 1994, Results of ATR Critical Facility Core Reconfiguration and Requalification Testing for Post-Core Internals Changeout Operation, Report No. PG-T-94-006, EG&G Idaho, Inc., June 1994.

McElroy, W.N. and Berg, S., SAND-II Neutron Flux Spectra Determination by Multiple Foil Activation Iterative Method”, AWR-TR-67-41, Vol 1-4 (1967).

McGhee, J.M., Wareing, T.A., Barnett, D.J., ATTILA Version 5: User Manual, Transpire Inc., Gig Harbour WA, USA (2006).

Nigg, D.W., Wemple, C.A., Risler, R., Hartwell, J.K., Harker, Y.D., Laramore, G.E., Modification of the University of Washington Neutron Radiography Facility for Optimization of Neutron Capture Enhanced Fast-Neutron Therapy, *Medical Physics* **27**:359-367 (2000).

Nigg, D.W. and Steuhm, K.A., Project Plan for the ATR Core Modeling Update, PLN-2852, Revision 1, Idaho National Laboratory, 2010.

Pautz, S., VERIFICATION OF TRANSPORT CODES BY THE METHOD OF MANUFACTURED SOLUTIONS: THE ATTILA EXPERIENCE, LA-UR-01-1487.

Pfeifer, C.J., PDQ Reference Manual II, WaPD-TM-947(L), 1971.

Phillips, J.R., et al., Application of Nondestructive Gamma-ray and Neutron Techniques for the Safeguarding of Irradiated Fuel Materials” LA-8212 (May 1980)

Radiation Safety Information Computational Center, NJOY99- Code System for Producing Pointwise and Multigroup Neutron and Photon Cross Sections from ENDF/B Data and AMPX77- Modular Code System for Generating Coupled Multigroup Neutron-Gamma Libraries from ENDF/B, Oak Ridge National Laboratory (<http://www.rsicc.ornl.gov>), 2010.

A. J. G. Ramalho and W. E. Payne, Spent Fuel Measurements using High Resolution Gamma Systems, *Nuclear Materials Management*, p. 76-82, Fall 1979.

D. Reilly, N. Ensslin, H. Smith, Jr., and S. Kreiner, Passive Nondestructive Assay of Nuclear Materials, NUREG/CR-5550 (LA-UR-90-732), March 1991.

Rempe, J.L., Nigg, D.W., Imel, G. R., Unruh, T., FY-10 Irradiation Experiment Plan for the ATR National Scientific User Facility – Idaho State University Project Evaluating Flux Sensors, PLN-3351, Revision 0, Idaho National Laboratory, 2010.

Roache, P., Code Verification by the Method of Manufactured Solutions, J. Fluids Eng., March 2002, Volume 124, Issue 1, 4.

Rogers, JW and Anderl, R.A., ATR Neutron Spectral Characterization, INEL-95/0494, November 1995.

Roth, P. A., 2010, Evaluation of ATR Cycle 145B Physics Analysis Inaccuracy, TEV-765, Idaho National Laboratory, March 2010.

Stallmann, F.W., LSL-M2: A Computer Program for Least Squares Logarithmic Adjustment of Neutron Spectra, NUREG/CR-4349, ORNL/TM-9933, Oak Ridge National Laboratory, USA (1986).

Studsvik Scandpower, HELIOS Methods (Version 1.10), 2008.

Transpire, Inc. ATTILA Tutorial Package, Variance Reduction for MCNP & MCNPX.

Wachs, 2010 - Wachs, D. M., *Demonstration Control Plan for the RERTR Full-size Element*, PLN-2946, Rev. 0, Idaho National Laboratory, May 10, 2010

Wheeler, F.J., Parsons, D.K., Rushton, B.L., Nigg, D.W., Epithermal Neutron Beam Design for Neutron Capture Therapy at the PBF and BMRR Reactor Facilities, Nuclear Technology, **92**:106-118 (1990)

Williams, M.L., Rearden, B.T., SCALE 6 Sensitivity/Uncertainty Methods and Covariance Data, *Nucl. Data Sheets* **109** (2008), p. 2796.

Wilson, P., et. Al, State of the Art 3D Radiation Transport Methods for Fusion Energy Systems, Fusion Engineering and Design, Vol. 83, pgs. 824-833 (2008).